国立公害研究所研究報告　第12号
Research Report from the National Institute for Environmental Studies NO. 12, 1980

R-12-'80

Multielement analysis studies by flame and inductively coupled plasma spectroscopy utilizing computer-controlled instrumentation

Naoki FURUTA

THE NATIONAL INSTITUTE FOR ENVIRONMENTAL STUDIES
環境庁　国立公害研究所

MULTIELEMENT ANALYSIS STUDIES BY FLAME AND INDUCTIVELY COUPLED PLASMA SPECTROSCOPY UTILIZING COMPUTER-CONTROLLED INSTRUMENTATION

Naoki FURUTA

Division of Chemistry and Physics
The National Institute for Environmental Studies

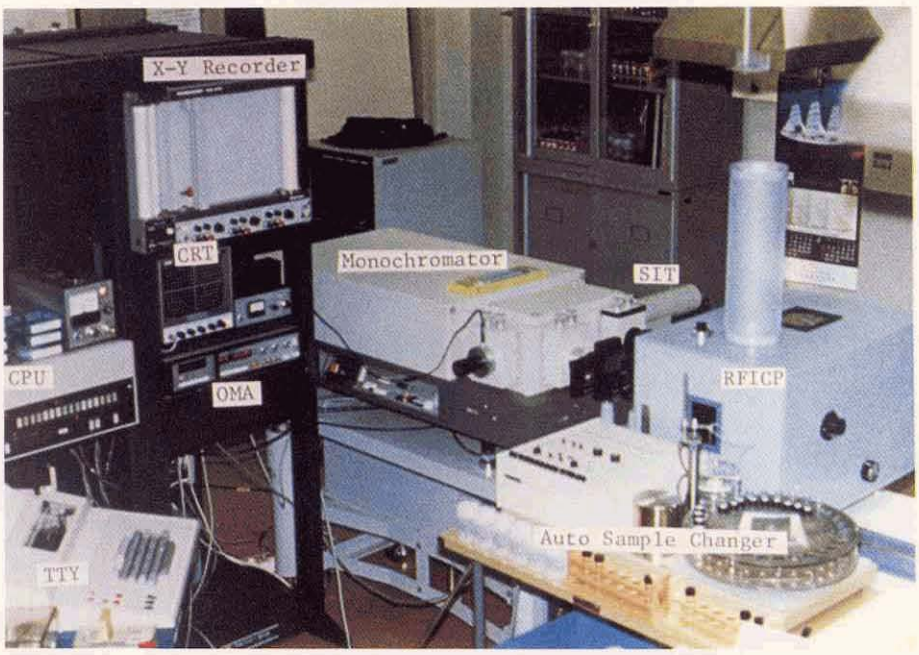

COMPUTER CONTROLLED INSTRUMENT
FOR MULTIELEMENT ANALYSIS

PREFACE

When the National Institute for Environmental Studies commenced research activities in 1974, it had been discussed most seriously what research projects should be initiated in the newly-established institute. The simultaneous multielement analysis field was one of those selected by the Chemistry and Physics Division of the institute. The reason for the choice is briefly described in the following:

1. Atomic absorption spectrometry which has been developed since 1955, is a sensitive method of analyses for all metallic elements, but one of the major drawbacks is that only one element can be determined at a time as the technique requires the light source of the specific element of interest. Consequently, scientific efforts were directed at attaining methods having high sensitivity but at the same time providing the simultaneous multielement capability.
2. In the environmental field, the demand on analytical techniques was naturally coincidental. Namely, the method for individual inorganic elements such as mercury, cadmium or chromium was more or less satisfied by atomic absorption, but the inability to provide multielement information was lacking. The situation was quite similar to total organic materials, which were rather conveniently expressed by such terms as COD or BOD instead of identifying and quantifying each specific pollutant.
3. Not only in the environmental field but also in other scientific areas such as medicine, agriculture and industry, a simultaneous multielement capability is required.

The project was undertaken from the first fiscal year, 1974, by members of the division, Drs. N. Otsuki, H. Haraguchi and N. Furuta. Multielement atomic absorption with a continuous light source such as a Xenon lamp was first investigated with a chemical flame as the atomisation source. The method was found useful for ten to twelve elements with moderate sensitivity. While the work was carried out, a silicon intensified target (SIT) together with an optical multichannel analyzer (OMA) was built into the system, and this enabled further developments to be possible.

Meanwhile instrumentation for inductively coupled plasma (ICP) emission spectrometry made remarkable progress in both the U.S.A. and Europe, and it has reached the stage where the emission sensitivity of many elements is almost equal to or better than that of atomic absorption. We have, therefore, adapted the new plasma light source for multielement analyses. The main part of this report deals with the results for plasma emission.

At present, commercially available ICP systems of polychrometer design have become popular and have been replacing atomic absorption spectrometry in various

fields including the environmental sciences. In our institute, the computerized Jarrell-Ash ICP was introduced a year ago, and is being fully utilized for the simultaneous determination of 15 – 20 elements on a routine basis. The system reported here, however, has the unique characteristic of simultaneous wavelength coverage in contrast to the photomultiplier-based polychrometer, and allows us to investigate the spectra of both the signal and background, and to check for erroneous values which are sometimes inevitable with commercial apparatus presently available.

At the occasion of the publication of this particular issue, I must express my sincere appreciation to former and present directors of the institute, Drs. Y. Oyama, M. Sasa and J. Kondo for their continued encouragement and unlimited support for the project. Thanks are also due to colleages of the institute, particularly those of the Chemistry and Physics Division for their valuable contributions. I wish to express my gratitude for the efforts displayed by persons of the Information and Administration divisions who made the publication of the issue possible.

Keiichiro FUWA, D. Sc.
Director,
Chemistry and Physics
Division

March 1980

CONTENTS

ERRATA

Research Report from The National Institute for Environmental Studies NO.12

Multielement analysis studies by flame and inductively coupled plasma spectroscopy utilizing computer-controlled instrumentation

Naoki FURUTA

Page	Line	Read	Corrected
2	15	elements accumulated$^{2-4}$	elements were accumulated $^{2-4}$
7	3	been	be
8		Insert the following after line 27:	
		analytes are desolvated, vaporized, atomized, ionized and excited by the thermal energy and the	
11		Table 1-7	
		[1975–1976]	[1975 – 1977]
12	1*	CH (350 – 422 *nm*),	CN (350 – 422nm),
17		Table 2-1, column 2.	
		4.0 m*l*/min	3.6 m*l*/min
18		Table 2-1 (Continued)	
		Software Basic Control System.	Basic Control System software.
19	22*	(150 mm widthh	(150 mm width
19	19*	(Figure 2-6)	(Figure 2-5(2))
23	15	and rather	a rather
25	8	vidicontarget	vidicon target
26	28	around	across
33	18	A break	A pause
36	8*	measurement oscilloscope.	measurement of the [A] spectrum the spectrum can be visualized on the oscilloscope.
37	4	236 (or 260)	240 (or 260)
39	19	(20303)	(2-3-3)

Page	Line	Read	Corrected
46	13	Hamamatsu TV Co., R919)	(Hamamatsu TV Co., R919)
50	4	atomised	atomized
53	6	analysis[26,30,31,116-118]	analysis[26,30,31,114,116-118]
53	10*	(optical multichannel analyzer	(Optical Multichannel Analyzer
54	3	(Radiofrequency	(radiofrequency
55	21	N_1^+	N_2^+
55	23	cargon	carbon
66	11*	samples (Chapter 5).	samples.
66	7*	(A)	(a)
66	6*	(B)	(b)
67		Notes to Table 4-2	
		(3) a. (A – B)	(3) a. (A – B);
		b. (A – B) – Side	b. (A – B) – side;
68	6*	380 nm[133]	380 nm[113]
70	2*	high	low
72	5	high	low
75	8	(1965:	(1965):
75	14*	1533.	1533-1545.
75	11*	273.	273-275.
75	2*	27.	27-37.
76	1	42.	42-48.
76	3	2534.	2534-2535.
76	14	111.	111-113.
77	22	in press.	34, 211-216.
77	35	629-635.	629-635, (In Japanese).
79	9	82.	82-88.
79	19	624.	624-631.
80	13	181-	181-208.
80	38	394.	394-398.
82	11*	Seguential	Sequential

* from bottom

ABSTRACT

The report describes analytical studies which are concerned with multielement analysis by atomic spectoscopic methods. The introductory chapter outlines the significance of multielement analysis, and includes classification of the analytical techniques, the excitation sources and the measurement system. Chapter 2 provides details of the developed instrument whose photograph is shown on the first page of this report. The instrument consists of an ICP source, programmable monochromator, and SIT-OMA detector. In Chapter 3, the analytical performance of the SIT-OMA detector is considered when combined with the programmable monochromator by using nitrous oxide-acetylene flame as an excitation source. The analytical performance was improved in Chapter 4 by replacing the nitrous oxide-acetylene flame with an ICP source. ICP emission spectrometry is a most promising method for multielement analysis. Although the interference is very small in comparison to other techniques, major constituents of samples can cause background shifts which result in analytical errors. The developed instrument can correct for such background changes.

CHAPTER 1 General Introduction

1-1 Significance of multielement analysis

The present environmental laws adopt a specific concentration range for each element (metals and nonmetals) as a criterion of pollution, and appropriate analytical methods for each element are established[1]. If we measure each element by a different procedure (flame photometric method, atomic absorption spectrophotometric method, gravimetric method, colorimetric method, flameless atomic absorption method, electrode method, and so on) as proposed in the regulations, it is time consuming and is rather laborious. Therefore, there has been in the last decades an increasing demand for rapid multielement analysis of environmental samples, where simultaneous information on a large number of elements is desired. The demand is given not only from the environmental field, but also from other fields, such as industry, geology, agriculture, medicine, and ecology.

When edible plants were grown on a soil which contained municipal sewage sludge, where large amounts of trace elements accumulated[2-4], the following twelve elements, B, Br, Ca, Cd, Cu, Fe, Mg, Mn, Na, Ni, Se, and Zn were found at high concentrations in the plants as compared to the control[5]. The amount of Fe and Cd that a plant takes up is dependent on the P concentration in the soil[6]. Phosphorus competes with Fe in the uptake process, and phosphorus deficiency in the soil is often a prominent symptom of Al toxicity[7]. Interestingly, when cadmium reaches a very high concentration in a plant, zinc is also high in concentration in the plant[5,6,8]. Zinc is known to have a marked protective effect on cadmium toxicity[9,10]. If the plant grown on the sludge-soil was fed to guinea pigs, elevated concentrations of several elements found in the plant also appeared at higher levels in certain of the animal tissues[11]. These included antimony in adrenal, cadmium in kidney, manganese in liver tissue and tin in kidney, muscle, and spleen. Although, as mentioned above, the zinc content was very high in plant materials in which appreciable levels of cadmium were present, elevated levels of zinc in the animal tissues were not found. This is not surprising since zinc is absorbed poorly from the gastrointestinal tract in humans and variably in animals[11].

Interelement synergism and antagonism during plant and animal absorption is complex, and knowledge is limited to only a few substances. Other examples are selenium against the toxicity of cadmium[12] and mercury[13-15]. At present such an interelement interaction is known to play an important role in environmental and biological problems[16]. Therefore, the need for multielement anlysis is strikingly clear.

1-2 Analytical techniques for multielement analysis

Analytical techniques for multielement analysis such as neutron activation analysis (NAA), spark source mass spectrometry (SSMS), anodic stripping voltammetry (ASV), X-ray fluorescence spectroscopy (XRF) and optical spectroscopy (OS) have been employed. This section presents a brief summary of each analytical technique and compares their features. As each technique has unique advantages and disadvantages, the choice of the technique is based on the requirement of the analysis. So far, Bush and

Morrison have compared these techniques with regard to scope, analysis time, sample type, and precision[17]. Also Dulka and Risby have summarized the detection limits for such techniques[16]. Winefordner has also summarized multielement techniques in a theoretical presentation[18].

1-2-1 Neutron activation analysis (NAA)

NAA (neutron activated gamma-ray spectometry) offers excellent sensitivity for many elements as shown in Table 1-1[16], but it is often necessary to carry out a separation step after irradiation because of interferences from elements such as sodium, chlorine, and bromine. Lead cannot be routinely determined by NAA nor can elements with atomic numbers less than 11. Recently, the prompt radiation method (α particle-induced prompt gamma-ray spectometry) has been developing for measuring elements of atomic numbers less than 11[19]. Multichannel analyzers and minicomputers are usually used for data reduction and spectral interpretation. The big drawback is that the instrumentation cost for NAA is very expensive, and precision of the method is not so good (5 – 10%). Therefore it appears that NAA will be limited to the use in the universities or big laboratories.

Table 1-1 Sensitivities for elements by Neutron Activation Analysis (Cited from Ref. 16)

Sensitivity, g	Elements
$10^{-13} - 10^{-12}$	Dy, Eu
$10^{-12} - 10^{-11}$	Au, In, Mn
$10^{-11} - 10^{-10}$	Hf, Ho, Ir, La, Re, Rh, Sm, V
$10^{-10} - 10^{-9}$	Ag, Al, As, Ba, Co, Cu, Er, Ga, Hg, Lu, Na, Pd, Pr, Sb, Sc, U, W, Yb
$10^{-9} - 10^{-8}$	Cd, Ce, Cs, Gd, Ge, Mo, Nd, Os, Pt, Ru, Sr, Ta, Tb, Th, Tm
$10^{-8} - 10^{-7}$	Bi, Ca, Cr, Mg, Ni, Rb, Se, Te, Ti, Tl, Zn, Zr
$10^{-7} - 10^{-6}$	Pb
$10^{-6} - 10^{-5}$	Fe

Sensitivity based on irradiation period of 0.5 $T_{1/2}$ or 10 h; whichever is less at a flux of 10^{13} neutrons cm^{-2} s^{-1}. Activity measured by NaI (Ti) gamma spectrometry.

1-2-2 Spark source mass spectrometry (SSMS)

A spark source is required for the ionization source of solid sample. The elemental spectra from a mass spectrometer are relatively sample, and moreover this method has the feasibility to measure isotope ratios. The detection limits of this method are shown in Table 1-2[20]. When SSMS is applied, however, to liquids, the sample preparation time is lengthy because of the need for evaporation to dryness and subsequent preparation of the sample electrodes. The big disadvantage is that precision of this method is not so good (5 – 25%%). Recently a mass spectrometric method combined with a plasma source has been developed[21]. The liquid sample is nebulized directly into the plasma without pretreatment. This procedure is much faster, and furthermore most molecular species are completely dissociated and interference is very small. The plasma source will improve the precision in the near future.

Table 1-2 Detection limits (ng) for elements by Spark Source Mass Spectrometry (Cited from Ref. 20)

Element		Element		Element	
Ag	0.2	Hg	0.6	Rh	0.09
Al	0.02	Ho	0.1	Ru	0.03
As	0.05	In	0.1	Sc	0.04
Au	0.2	Ir	0.3	Sm	0.5
Ba	0.2	K	0.03	Sn	0.3
Be	0.008	La	0.1	Sr	0.09
Bi	0.2	Li	0.0006	Ta	0.2
Ca	0.03	Lu	0.1	Tb	0.1
Cd	0.3	Mg	0.03	Th	0.2
Ce	0.1	Mn	0.05	Ti	0.05
Co	0.05	Mo	0.3	Tl	0.2
Cr	0.05	Na	0.02	Tm	0.1
Cs	0.1	Nb	0.08	V	0.04
Cu	0.08	Nd	0.4	W	0.5
Dy	0.5	Os	0.4	Yb	0.5
Er	0.5	Pb	0.3	Zn	0.1
Eu	0.2	Pd	0.3	Zr	0.1
Fe	0.05	Pr	0.1		
Ga	0.09	Pt	0.5		
Gd	0.5	Re	0.2		

1-2-3 Anodic stripping voltammetry (ASV)

ASV has particularly high sensitivity for lead and cadmium. This method can only be applied to a liquid sample. ASV is a two-step process in which a portion of the metal ions in solution is first deposited and reduced at a mercury-containing electrode. In the second step, the reduced metals in the amalgam are reoxidized to the component ions by applying an increasingly positive potential to the electrode. Preconcentration by electrode-deposition allows the determination of metals in the 10^{-9} M range (Table 1-3)[16]. For the differential pulse anodic stripping (DPAS) technique[22], a pulse voltage is superimposed upon the linearly increasing voltage in the second step. Sensitivities can thus be improved to $10^{-10}-10^{-11}$ M. Deposition times for ASV and DPAS are generally in the order of $5-30$ and $1-10$ minutes, respectively. At maximum, six elements (Zn, Cd, Tl, Pb, Cu, and Bi) can be determined simultaneously and a sample volume of about 10 m*l* is usually adequate. The cost of such instruments is modest. The main drawback of this method is that these voltammetric methods cannot determine the large number of metals that other techniques can; thus it would be expected that they would be used to complement other techniques, in paticular for the determination of lead and cadmium. The relative standard deviation of this method is less than 1%.

1-2-4 X-ray fluorescence spectroscopy (XRF)

XRF is well suited for solid samples although elements with atomic numbers less than 11 cannot normally be determined (Table 1-4)[23,24]. Proton-induced X-ray fluorescence (PXF) is now being developed for measuring elements with atomic numbers less

Table 1-3 Detection limits with Anodic Stripping Voltammetry (Cited from Ref. 16)

Element	Detection limits
Ag	0.25 ng/m*l*
Au	1.0 ng/m*l*
Bi	0.01 ng/m*l*
Cd	0.005 ng/m*l*
Cu	0.005 ng/m*l*
Ga	0.4 ng/m*l*
Hg	4.0×10^{-9} M
In	0.1 ng/m*l*
K	1×10^{-5} M
Ni	0.1 g/m*l*
Pd	0.01 ng/m*l*
Pt	1×10^{-9} M
Rh	0.1 ng/m*l*
Sn	2.0 ng/m*l*
Tl	0.01 ng/m*l*
Zn	0.04 ng/m*l*

Table 1-4 Detection limits (μg) for X-Ray Fluorescence Spectroscopy (Cited from Refs 23 and 24)

Element		Element	
Ag	1.2	Nd	0.30
Al	5.0	Ni	0.06
As	0.11	P	0.001
Au	0.001 /cm^2	Pb	0.0003
Ba	0.12	Rb	0.0075
Bi	0.61	Rh	103 /m*l*
Ca	0.100	Sc	0.38
Cd	0.40	Se	0.020 /cm^2
Ce	0.17	Si	170 /m*l*
Co	0.05	Sm	4.1 /m*l*
Cr	0.00006	Sn	3.9 /m*l*
Cs	0.15	Sr	0.00007
Cu	0.00002	Tb	159 /m*l*
Eu	0.66	Te	0.12
Fe	0.0085	Th	6.5 /m*l*
Ga	0.01	Ti	0.001
Hg	0.24	U (as UO_2)	
In	1.1		0.72
K	0.52	U	0.00002
La	0.12	Y	0.22
Mn	0.00015	Yb	6.8 /m*l*
Mo	0.072	Zn	0.00004
		Zr	0.00002

Not available: Be, Dy, Er, Gd, Ge, Hf, Ir, Li, Lu, Mg, Na, Nb, Np, Os, Pa, Pd, Pr, Pu, Re, Sb, Ta, Tm, and W.

than 11[25]. Computational techniques have been coupled with multichannel analyzers to minimize interelement effects. Sample can often be analyzed without pretreatment. The main drawback to use this method is the lack of sensitivity for liquid analysis. The deterction limit is generally in the μg/ml range. Preconcentration of samples utilizing ion-exchange, evaporation, and precipitation techniques has to be performed prior to analysis. Precision of the method rarely exceeds 1%.

1-2-5 Optical spectroscopy (OS)

Emission spectroscopy utilizing Arc or Spark has been used extensively. This method has been rather suitable for solid sample. Though sample preparation has been time-consuming and matrix effects have sometimes been troublesome, the ability to determine many elements simultaneously has been a major. The main drawback has been poor precision (25%). When the Inductively Coupled Plasma combined with the emission spectrograph, the instrument can determine liquid sample directly since the liquid sample is nebulized into the plasma. The detection limits are comparable to those by atomic absorption as shown in Table 1-5[26]. The precision is also improved to less than 1%, and

Table 1-5 Detection limits (μg/ml) for Inductively Coupled Plasma – Atomic Emission Spectroscopy (Cited from Ref. 26)

Element		Element	
Ag	0.004	Na	0.0002
Al	0.002	Nb	0.01
Au	0.04	Nd	0.05
Ba	0.001	Ni	0.006
Be	0.005	Pb	0.008
Bi	0.05	Pd	0.007
Ca	0.00007	Pr	0.06
Cd	0.002	Pt	0.08
Ce	0.007	Rh	0.003
Co	0.003	Sc	0.003
Cr	0.001	Sm	0.02
Cu	0.001	Sn	0.3
Dy	0.004	Sr	0.00002
Er	0.001	Ta	0.07
Eu	0.001	Tb	0.2
Fe	0.005	Th	0.003
Ga	0.014	Ti	0.003
Gd	0.007	Tl	0.2
Hf	0.01	Tm	0.007
Hg	0.2	U	0.03
Ho	0.01	V	0.006
In	0.03	W	0.002
La	0.003	Y	0.002
Lu	0.008	Yb	0.00009
Mg	0.0007	Zn	0.002
Mn	0.0007	Zr	0.005
Mo	0.005		

interelement interference is minimal.

1-3 Excitation sources for optical spectroscopy

Excitation sources for optical spectroscopy can been classified into two types as shown in Table 1-6, namely the electrical discharge and thermal excitation.

Table 1-6 Classification of excitation sources for optical spectroscopy

Thermal Excitation		Electrical Discharge
Combustion Flame		Hollow Cathode
Ar-H_2	427 – 1727 °C	Electrodeless Discharge
Ar-C_2H_2	627 – 2077 °C	Lasers
Air-H_2	1527 – 2107 °C	Grimm Glow
Air-C_2H_2	1927 – 2327 °C	Arc
N_2O-C_2H_2	1927 – 2927 °C	Spark
High Temperature Furnaces		Inductively Coupled Plasma
		Microwave Frequency
		LMD 2.45 G Hz, <100 W
		(Low-wattage Microwave Discharge)
		MTD 2.45 G Hz, 200 – 500 W
		(Microwave Torch Discharge)
		Radio Frequency
		RFICP 4 – 50 M Hz, 10 – 0.5 K W
		(Radio-Frequency Inductively Coupled Plasma)

1-3-1 Electrical discharge

The first three sources indicated in Table 1-6, Hollow cathode, Electrodeless discharge, and Lasers, are usually used as excitation sources for atomic absorption and fluorescence spectrometry, while the Grimm glow, Arc, Spark, and Inductively Coupled Plasma (ICP) are used for excitation sources for atomic emission spectrometry. As mentioned in section 1-2-5, emission spectroscopy utilizing Arc or Spark has been used for simultaneous multielement analysis. In particular the D.C. Arc plasma has been used extensively because it is applicable not only to solid samples but also liquid samples. Although the D.C. plasma sustains a high temperature (10000K), there is contamination from the carbon or tungsten electrodes. Precision is also poorer when compared to the ICP source.

By definition, plasmas are gases in which a significant fraction of the atoms or molecules is ionized, so that magnetic fields may readily interact with plasmas. One of these interactions is an inductive coupling of time-varying magnetic fields with the plasma. A detailed discussion of the theory, formation, and properties of ICP's is given by Eckert[27]. The ICP can be classified into two types according to the frequency used, i.e. a microwave plasma and a radio frequency plasma.

The microwave plasma has been produced at reduced pressure for argon or helium and at atmospheric pressure for only argon[28] so far. Recently it was suggested to operate the plasma at atmospheric pressure with helium[29]. As the energy transfer of microwave energy to the helium plasma gas is efficient, it is possible to produce a stable plasma at

low power. As the electron temperature is high and the energies of helium meta-stable states are also very high (19.73 and 20.52 eV; cf. Argon meta-stable states, 11.5 and 11.67 eV), the microwave plasma is suitable for excitation of nonmetals, such as carbon, hydrogen, sulphur, fluorine, chlorine, bromine, and iodine. However, in the case of the microwave plasma, there are limitations in the amount of sample which can be tolerated. Generally liquid samples cannot be aspirated directly (microliter samples can be injected). The microwave plasma has been used as a detector for gas chromatography[28,29], where the analyte is in the gaseous phase. In this study, the radio frequency plasma was chosen for an excitation source for a variety of elements which enables multielement analysis to be performed (Chapters 2 and 4).

In analytical spectroscopic equipment a typical RFICP excitation source consists of a quartz tube inserted within a copper coil to which is connected a high-frequency generator operating in the 4 – 50 M Hz range with respective generator output powers in the 10 – 0.5 K W range (inverse relation between frequency and power). When argon flows of the proper configuration and magnitude pass through the tube, an adequate seed of electrons is initially provided with a Tesla coil. When the generator power is turned on, the high-frequency currents flowing in the induction coil generate oscillating magnetic fields whose lines of force are axially oriented inside the coil. The induced axial magnetic fields induce the seed of electrons and the produced argon ions to flow in closed annular paths inside the tube space as shown schematically in Figure 1-1[30]. This electron flow is called the eddy current. As the magnetic fields are time varying in their direction and strength, the electrons and ions are accelerated on each half cycle and Joule heating occurs. The sample aerosols, which are produced by pneumatic nebulization, travel upstream in a narrow axial channel of the eddy current as illustrated in Figure 1-2[30]. By the time the sample species reach the observation height of 17 mm above the coil, they have experienced a residence time of ca. 2 ms at temperatures ranging from 5000 K to 8000 K. Figure 1-3 shows the distribution of the temperature[31]. The energy transfer of argon meta-stable states (11.5 and 11.67 eV)[32–34].

The inventor of this ICP is Babat. He discovered in 1942 that an eddy electrodeless discharge, once established, can be maintained while the pressure is raised up to atmospheric level[35]. However, major interest developed only after Reed has shown in 1961 that, with an open tube and streaming gas, "Induction-Coupled Plasma Torch" can be

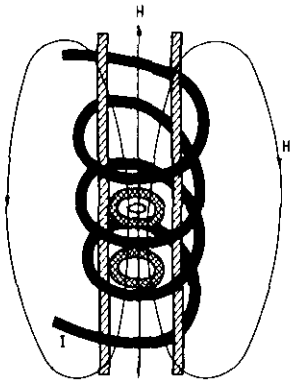

Fig. 1-1 Magnetic fields (H) and eddy currents (shaded) generated by high frequency currents (I) flowing through coil. (Cited from Ref. 30)

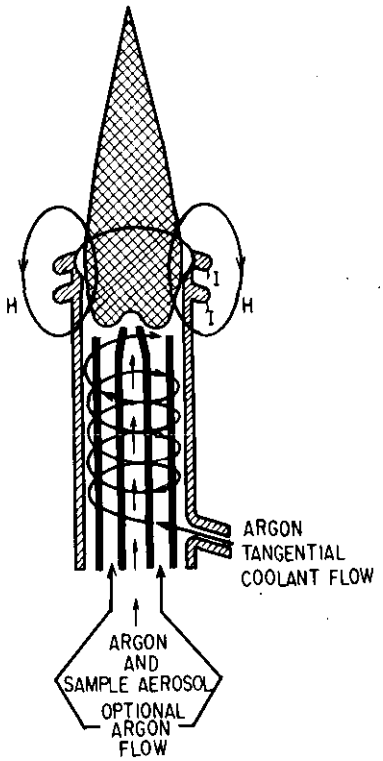

Fig. 1-2 Typical inductively coupled plasma configuration (Cited from Ref. 30)

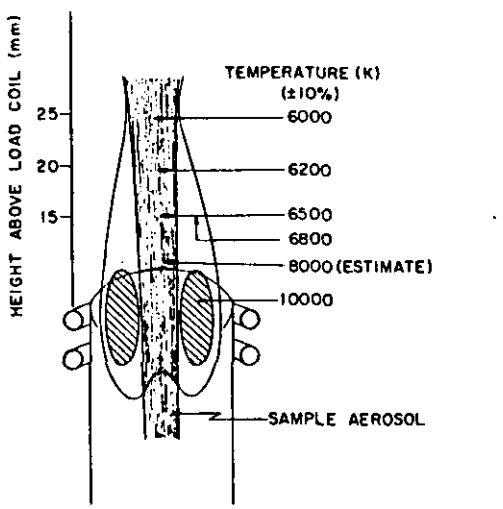

Fig. 1-3 Schematic diagram of sample flow through the plasma and the temperatures experienced (Cited from Ref. 31)

used as a heat source[36] as shown in Figure 1-4[37]. He operated the plasma at atmospheric pressure on argon alone or mixed with other gases. The power was 10 K W at a frequency of 4 M Hz. The application demonstrated by Reed is the growing of crystal of refractory materials[38]. The use of the ICP as an excitation source for optical spectroscopy was first reported by Greenfield et al. in 1964[39]. Shortly afterwards, Wendt and Fassel reported their independent works using the ICP in 1965[40]. Since 1964 a rapid increasing volume of papers has appeared dealing with investigations into the ICP. Initially the detection performance of trace elements was poorer than that of atomic absorption spectroscopy. Progressive refinements in

i. the impedance matching between the high frequency generator and the plasma,
ii. forward power reguration,
iii. shape of the plasma torch,
iv. techniques for generating aerosols of solutions, and
v. the introduction efficiency of aerosols into the ICP resulted in lowering the detection limits by approximately one order of magnetude every two years. The striking improvements in the ICP values during the past twelve years is shown by the data summarized in Table 1-7[39-45] Compromised conditions for multielement analysis were proposed by Fassel et al.[41], and Bouman and de Boer[42]. Since 1974 the RFICP coupled with a direct reading spectrometer and having fully automated sequential sampling, exposure, and read-out, became available commercially. ICP emission spectrometry has been applied to many fields and it has been identified that the ICP emission spectrometry has many advantages for multielement analysis. The ICP method meets the requirements of selectivity, sensitivity, and speed for the determination of multielements in a large number of samples on a routine basis. Under a single set of compromise plasma operating conditions, major, minor, trace, and ultratrace elements can be measured simultaneously. In the ICP the inert argon environment, the high temperature experienced by the sample, and the relatively long residence time of the sample in the high temperature regions overcome to a high degree the inter-element and matrix effects commonly observed in

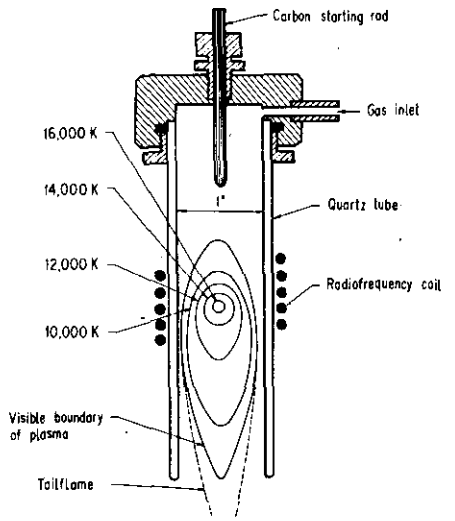

Fig. 1-4 Initial plasma torch produced by Reed (Cited from Ref. 37)
Carbon rod is needed only for starting.

Table 1-7 Inductively coupled plasma detection limits (μg/ml)

	[1964] Ref. 39 Greenfield et al.	[1965] Ref. 40 Wendt Fassel	[1965] Ref. 43 Greenfield et al.	[1969] Ref. 44 Dickinson Fassel	[1974] Ref. 26 Fassel Kniseley	[1975–1976] Refs 42, 45 Boumans, de Boer Olson, Haas, Fassel*
Al	50	3	0.5	0.002	0.002	0.0004*
As	–	25	–	0.1	0.04	0.002*
Ca	1	0.2	0.005	–	0.00007	0.0000001
Cd	–	20	–	0.03	0.002	0.00007*
Co	–	–	0.2	0.003	0.003	0.0001*
Cr	20	0.3	–	0.001	0.001	0.00008*
Cu	10	0.2	0.01	–	0.001	0.00004*
Fe	–	3	0.05	0.005	0.005	0.00009
La	–	50	–	0.003	0.003	0.0001
Mg	5	2	0.03	–	0.0007	0.000003
Mn	10	1	0.05	–	0.0007	0.00001*
Ni	5	1	–	0.006	0.006	0.0002
P	–	10	0.8	0.1	0.04	0.015
Pb	–	–	–	0.008	0.008	0.001*
Si	–	3	–	–	0.01	–
Sn	–	50	4	–	0.3	0.003
Sr	–	0.09	–	0.00002	0.00002	0.000003
Ta	–	16	–	0.07	–	–
Th	–	40	–	0.003	–	–
V	–	–	0.1	0.006	–	0.00006
W	–	3	–	0.002	–	0.0008
Zn	–	30	4	0.009	0.002	0.0001*
Zr	–	15	–	0.005	–	0.06

combustion flames and arc and spark discharges.

1-3-2 Thermal excitation

When energy is supplied to a gas, the temperature rises proportionally as long as all the energy is used only to heat the molecules (atoms for monotomic gases). At higher temperatures in the 3000 – 6000 K range, molecules are dissociated into atoms. Further energy input causes the dissociated atoms to ionize. The relationship between the energy of a gas and its temperature is shown in Figure 1-5[37]. The temperature of the flames, which depends on the combustion heat of the fuel, cannot correspond to a high degree of molecular dissociation. In fact the flame temperature is stabilized at the toe of the molecular dissociation curve shown in Figure 1-5. In the case of furnaces, the temperature is dictated by the electrical current, but 3000 K is about the maximum temperature which can be obtained. The nitrous oxide-acetylene flame

$$2\,N_2O + C_2H_2 \rightarrow 2\,N_2 + 2\,CO + H_2 + 179\ \text{Kcal/mole}$$

has the highest heat of reaction for commonly used flames. The combustion heat is not enough to dissociate N_2 and CO molecules; N_2 has a dissociation energy of 225 Kcal/mole, CO, 257 Kcal/mole[46]. The flame temperature is restricted by the stability of the combustion products. As the atoms in a flame are stabilized by the formation of oxide,

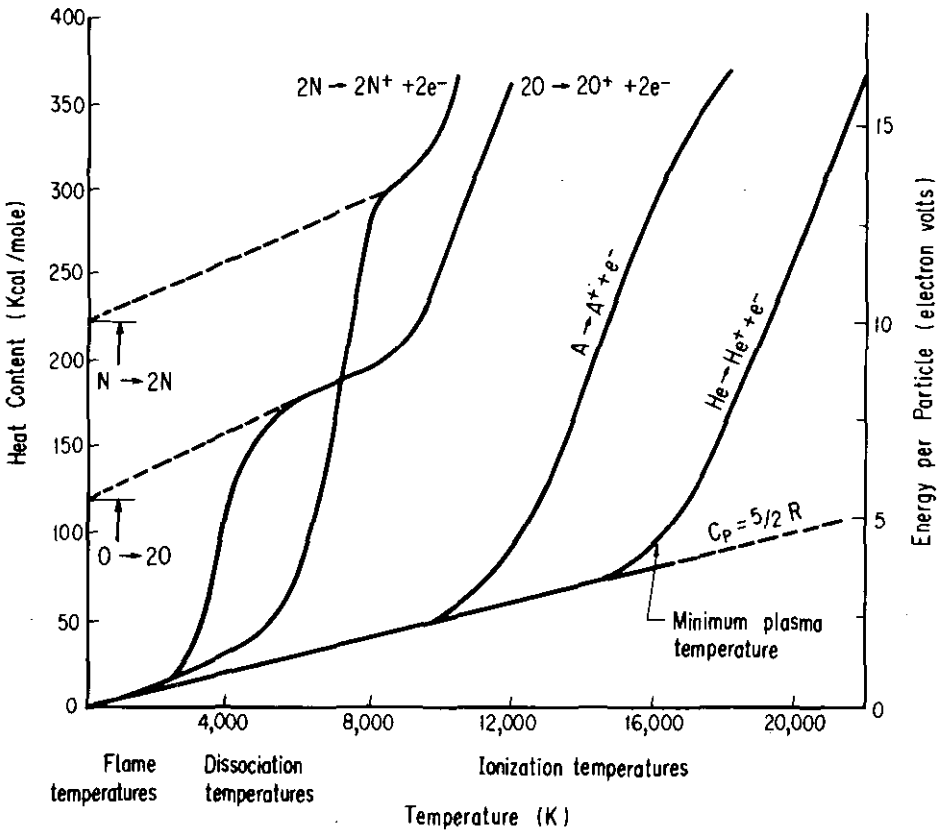

Fig. 1-5 Energy content of gases as a function of temperature. Chemical flames are limited to below dissociation temperature of their combustion products (Cited from Ref. 37)

the reducing atomsphere in addition to the temperature plays an important role in the atomization process. The temperature and reducing atmosphere vary according to the flame operating conditions. The optimum conditions in the flame are usually quite different for the elements.

Usually the Air-C_2H_2 flame is used for atomic absorption spectrometry utilizing the HCL or EDL. The respective molecular emissions of HPO and S_2 in the cool reducing H_2 flame are used as the detector of the gas chromatography[47]. Some workers have used N_2^2O-C_2H_2 *flame as an excitation source for atomic emission spectrometry*[48-51,62]. However, the spread in the optimum flame operating conditions for each element constitutes a major problem in utilizing the N_2O-C_2H_2 source for multielement analysis since fixed conditions would be desirable for rapid analysis (Chapter 3).

1-3-3 Emission spectra of plasma and flame

Figure 1-6 shows the emission spectra for the RFICP, the N_2O-C_2H_2, and the Air-C_2H_2 flame. The major flame constituents are OH (280 – 330 nm), CH (387 – 431 nm), and C_2 (437 – 600 nm) for Air-C_2H_2 and NO (200 – 280 nm), OH (280 – 330 nm), CH (350 – 422 nm), CH (387 – 431 nm), and C_2 (437 – 600 nm) for N_2O-C_2H_2. The

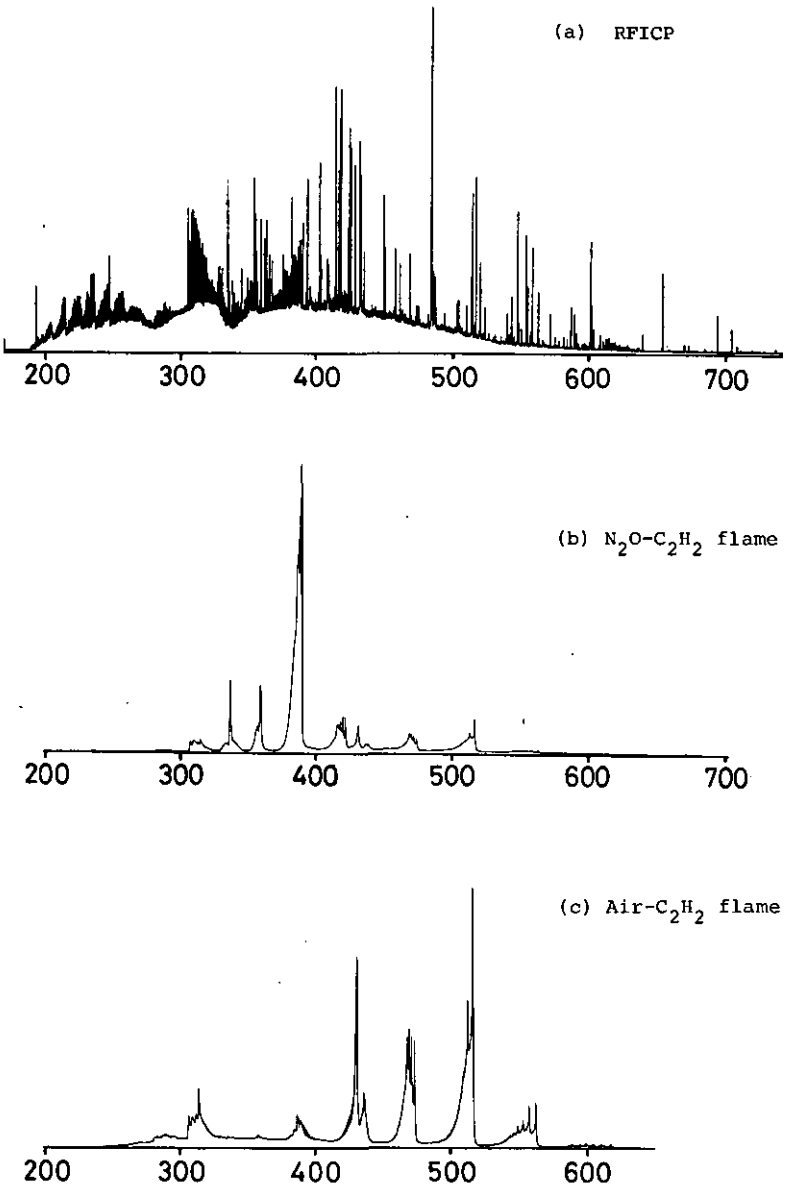

Fig. 1-6 Comparison of emission spectra of excitation sources
(a) RFICP, (b) N_2O-C_2H_2 flame, (c) Air-C_2H_2 flame

ICP major constituents are argon, NO (200 – 280 nm), OH (280 – 330 nm), NH (336 nm), N_2^+ and CN (350 – 430 nm). The temperature of the ICP is approximately twice that of the N_2O-C_2H_2 flame and is about three times that of the Air-C_2H_2 flame, and as shown in Figure 1-6 the ICP background spectrum is very complex.

1-4 Measurement systems for optical spectroscopy

In the optical region of the electromagnetic spectrum, spectral information is often required over a wide spectral range (200 – 800 nm). A systematic grouping of several methods used to obtain this information is given in Table 1-8. The methods have been classified into two types, namely a single channel detector and a multichannel detector[18,52-54]

Table 1-8 Classification of measurement system for optical spectroscopy

Single Channel Detector		Multichannel Detector
Time Domain	Frequency Domain	Image Device
Sequential	Fourier Transform	Electron Beam
Linear Scan	Spectrometry	Image dissector
(SLS)	(FTS)	Vidicon
		SIT
Sequential	Hadamard Transform	(Silicon Intensified Target)
Slew Scan	Spectrometry	Solid State
(SSS)	(HTS)	Photodiode Array
		Direct Reader

1-4-1 Single channel detector

When using a single channel detector the spectral information is encoded before the detector and subsequently decoded or transformed[55]. The most common method is that of encoding in the time-domain, i.e. only one spectral conponent falls on the detector at any given time. For the sequential linear scan (SLS) system, a single slit spectrometer scans the wavelength region of interest at a uniform rate. Johnson, Plankey and Winefordner applied the SLS to atomic fluorescence spectrometry with a continuum source[56]. The author also applied the SLS to atomic absorption spectrometry with a continuum source[57]. This method is useful, when the elemental composition of the sample is not known. However, the grating is continuously moving when the measurement is carried out, so that the sensitivity is poor. Furthermore, much time is lost, if there are spectral regions where no spectral components are present. For the sequential slew scan (SSS) system, only the spectral elements of interest are examined for any appreciable period of time, with the spectrometer rapidly changing (slewing) to a new spectral element. Malmstadt et al. developed the computer-controlled programmable monochromator for the SSS type[58,59]. Johnson, Plankey, and Winefordner proposed multielement atomic fluorescence spectrometry using the SSS system, which was really useful for analysis of many elements in a short time[60]. Kawaguchi et al. used the SSS system for emission spectrometry with a microwave induced argon plasma as a light source[61]. The author also applied the SSS system for emission spectrometry utilizing the nitrous oxide-acetylene flame (Chapter 3)[62] and the radio frequency inductively coupled plasma (Chapter 4)[63] as excitation sources. Details of the programmable monochromator are described in section 2-2-1.

The multiplex methods encode the spectral information in the frequency domain. In these methods, more than one spectral component may fall on the detector at any

given time, and the frequency, with which they vary, requires an appropriate transform to give spectral information[64]. For Fourier transform spectrometry (FTS), in which a Michelson interferometer is used, optical signals are encoded by a moving[65-67] or rotating[68] mirror in one of the arms of the interferometer. Another type of FTS instrument includes the polarization interferometer (a monochromator is not needed)[69]. The encoded multiplex signal is decoded by Fourier transform to retrieve the original spectrum. For Hadamard transform spectrometry (HTS), a multislit cyclic mask, which is constructed according to Hadamard matrices, is placed at the exit slit of the monochromator to allow certain spectral components to either reach or not reach the detector. If the detector receives a series of signals by moving the multislit mask or the grating, it is possible by means of a Hadamard transform to decode the resulting complex array of signals and to retrieve the original spectrum[70-72]. The multiplex advantage can be realized only if the noise is detector limited, and not when the noise is source limited. Examples in which the noise is detector limited include infrared, microwave, nuclear magnetic resonance, and ion cyclotron resonance spectroscopic experiments. Examples in which the noise is source limited include optical (UV and Vis.) and charge-particle (photoelectron, ESCA, electron impact) spectroscopy. Therefore, in the case of optical (UV and Vis.) spectroscopy, the multiplex advantage cannot be expected.

1-4-2 Multichannel detector

The multichannel detector system, in which the spectral information from more than one spectral component is acquired simultaneously and independently, is divided into two methods, namely an image device and direct reading methods.

An image device looks at a continuous wavelength region as a camera[73,74]. There are two types of image devices, i.e. an electron beam type and a solid state type. An electron beam type includes the image dissector[75-79], the vidicon[80-82], and the Silicon Intensified Target (SIT)[83,84] [references are cited in Chapters 3 and 4]. Examples of the solid state type devices are the silicon photodiode arrays[34,85-91], charge coupled devices (CCD). Limitations of the currently available image devices are their low sensitivity in the UV and Vis. region. For example, a high-quality photomultipler tube (PMT) will have a sensitivity in the range of 10^8 μA/lumen. Silicon diode devices have sensitivities in the range of 10^3 to 10^4 μA/lumen. Image intensifiers can be used to increase the sensitivity, and the SIT can yield a sensitivity from 10^4 μA/lumen up through values which are comparable with photomultipliers in the visible region (2-2-2, 3-3-3, and 4-3-4). Recently, intensified photodiode arrays have been reported[92].

A direct reader looks only at selected spectral components, i.e. a polychromator with a single entrance slit and a multiple exit slit-detector combination at the exit focal plane[93,94]. Instruments which adopt this method are commercially available. The method has found widespread use on a routine basis. However, the instrument is expensive because individual photomultiplier tubes are required for each element. Moreover, such a method lacks flexibility, since measurements are generally performed only at fixed wavelengths of the desired elements. In this study, the SIT image device which was combined with the sequential slew scan measurement system was adopted (Chapter 2).

CHAPTER 2 Computer-Controlled Instrumentation

2-1 Introduction

Figure 2-1 shows the total system which combines the ICP source, the programmable monochromator and the SIT detector. The monochromator was set on a vertically adjustable table and the optical axis, the Z axis, was adjusted with the He-Ne laser, installed behind ICP source, by maximizing the laser light which passed through the center of the monochromator entrance and exit slits. The ICP source was imaged on the entrance slit with a magnification of 1/2 by setting a spherical lens (diffused quartz, diameter 26 mm, focal length 118 mm), and was attenuated whenever necessary by a sequentially adjustable fitter. At the other entrance slit a mercury pen ray lamp was set. One of the exit slits was removed and an adaptor was inserted for setting the SIT detector. At the upper side of the adaptor a plate was inserted to obstruct a half of the light which reached the SIT detector (2-2-2). Behind the other exit slit a photomultiplier was posi-

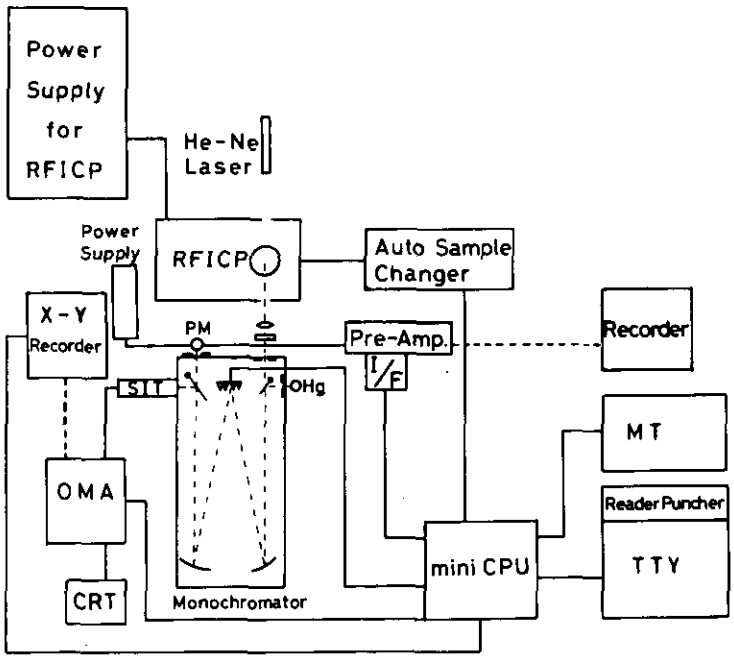

Fig. 2-1 Schematic diagram of computer-controlled instrumentation

RFICP	Radio Frequency Inductively Coupled Plasma
SIT	Silicon Intensified Target
OMA	Optical Multichannel Analyzer
CRT	Cathode Ray Tube
PM	Photomultiplier
I/F	Interface for peak sensor
CPU	Central Processing Unit
TTY	*Teletype*
MT	Magnetic Tape

tioned. Between the photomultiplier and the computer a DC amplifier (laboratory-constructed) and an interface was installed to detect mercury atomic emission. The interface transmitted Transistor-Transistor Logic (TTL) level signal (+5V) to the computer when the photomultiplier "caught" the signal above the level set in advance. Independently, the signal measured by the photomultiplier was fed to a recorder through the DC amplifier. Between the monochromator and the computer an interface was installed to control the position of the lateral mirror and the angle of the grating. Auto sample changer was equipped to introduce the sample and distilled water to ICP source alternatively, and it was controlled by the computer. The spectra obtained by the SIT detector were accumulated and memorized in the OMA and displayed on the oscilloscope. After accumulation (accumulation time is selected by preset dials on the OMA console) was finished, the digitalized spectrum was transferred to the computer and data processing was performed. The spectra measured by the SIT were transferred from the computer to the X-Y recorder through the D/A converter. Alternatively, the spectra were also recorded manually on the X-Y recorder. It was also possible to store the digitalized spectra on paper tape or magnetic tape. The stored spectra were processed by the host computer and plotted by the X-Y plotter. Table 2-1 summarizes the instrumental features.

Table 2-1 Instrumental Facilities

(1) Computer-controlled Instrumentation	
ICP source (Figure 1-2):	
Shimadzu Seisakusho Ltd. (Japan)	Inductively Coupled Argon Plasma
Plasma generator;	1600 W forward power
Model ICPQ-2H	< 3 W reflected power
	27.12 MHz
Plasma torch;	10.5 *l*/min coolant Ar flow
All quartz	1.5 *l*/min plasma Ar flow
	1.0 *l*/min aerosol carrier Ar flow
Pneumatic nebulizer system;	4.0 ml/min sample uptake rate
Teflon and glass	
Auto sample changer:	
Shimadzu Seisakusho Ltd. (Japan)	
Model ASC-2	
Monochromator:	1-m Czerny-Turner spectrograph,
Jobin Yvon	f 5.4; holographic grating,
(France)	2400 grooves/mm
Model HR 1000	reciprocal linear dispersion
	0.4 nm/mm in the first order
	at 200 nm.
Filter;	Sequentially adjustable filter
Matsuzaki Vacuum Evaporation Corp.	
(Japan)	
Rectangular slide type	
Mercury pen ray lamp;	
Ultra-Violet Corp. (U.S.A.)	

Table 2-1 (Continued)

Model 11SC-1

Detector:	
SIT detector;	Ultraviolet sensitized
Princeton Applied Research Corp.	silicon intensified target
(U.S.A.)	vidicon tube assembly with
Model 1205D	optional-01 scintillator screen.
PMT detector;	Sensitive to ultraviolet and
Hamamatsu TV Corp.	visible radiation;
(Japan)	multi-alkali cathode.
Power supply for PMT;	Power 0 – 1500 V
Japan Electronic Measuring Instrument Corp.	
(Japan)	
Model PH-7A	
OMA:	Optical Multichannel Analyzer
Princeton Applied Research Corp.	with 5 binary coded decimal memory
(U.S.A.)	
Model 1205A	
Real time readout:	
CRT;	Monitor scope, Cathode Ray Tube
National Electronic Measuring Instruments	
(Japan)	
Model VP-3834A	
X-Y recorder:	for SIT cetector
Yokogawa Electric Works, Ltd. (Japan)	
Model 3078	
Computer:	Minicomputer with 16 bit 24 K
Hewlett Packard	word memory.
(U.S.A.)	Software Basic Control System.
Model 2108	
I/O Interface 12531D;	Input/Output for TTY
I/O Interface 12566B;	Input/Output for monochromator, OMA, auto sample changer, X-Y recorder, and MT
8 bit D/A converter 12555B;	for X-Y recorder
Peripheral devices:	
TTY;	Teletype
Casio Calculation Corp.	33.3 words/sec print
(Japan)	61 words/sec read
Model 501	30 words/sec punch
MT;	9 tracks, 800 BPI Magnetic Tape
Hewlett Packard (U.S.A.)	32 K bite/sec read
Model 12970A	

Table 2-1 (Continued)

He-Ne laser: *Coherent (U.S.A.)* Model CR136 class IIIb	for adjustment of optical axis
Recorder: Shimadzu Seisakusho Ltd. (Japan) Model U-125MN	for PMT detector
(2) Additional Facilities	
Host computer: Hitachi Seisakusho Ltd. (Japan) Model HITAC 8450	524 K bite memory
X-Y plotter: Fujitsu Corp. (Japan) Model B02L-9019-B002A	

2-2 Instrumentation

2-2-1 Programmable monochromator

This monochromator has two entrance slits and two exit slits enabling the measurement of two different sources with two detectors by changing the direction of lateral mirrors. It is suitable for use with an image detector as it has a large collimating mirror (150 mm widthh x 130 mm height) and forcusing mirror (200 mm width x 130 mm height). In addition, a large holographic grating (140 mm width x 120 mm height) provides a very high luminosity[95]. As the effective width of the SIT detector is 12.5 mm (Figure 2-6) and the reciprocal linear dispersion of the monochromator is 0.4 nm/mm at 200 nm, a spectral window of 5 nm is achieved. The reciprocal linear dispersion is better at longer wavelengths so that the spectral window decreases to about 2.5 nm at 750 nm. The SIT detector has 500 channels, so that 1 channel corresponds to 0.01 nm at 200 nm and 0.005 nm at 750 nm.

To shows the performance of this monochromator, the mercury emission lines (313.183 nm and 313.155 nm) were measured by both photomultiplier and SIT detector. These two emission lines were resolved perfectly by the photomultiplier (Figure 2-2(1)), but in the case of the SIT the resolution was relatively rather poor (Figure 2-2(2)). One channel of the SIT detector is only 25 μm width, but channel spreading results in poorer resolution. In the case of the photomultiplier, the exit slit width is 10 μm. The resolution power measured by a photomultiplier is 0.0048 nm and that measured by a SIT detector is 0.0325 nm, that is about 7 times worse.

The grating drive is controlled by the stepping motor. The linkage of the mother screw and the stepping motor was assured by means of 2 reducers. High scanning (0.0125 nm/pulse) and low scanning (0.0005 nm/pulse) are selected by the reducers, whose clutches are changed by electromagnetic switches. One of the advantages of this monochromator is that a remote control capability is also provided. When the stepping motor is controlled by an external pulse, the maximum frequency for initiation is 200 Hz, and

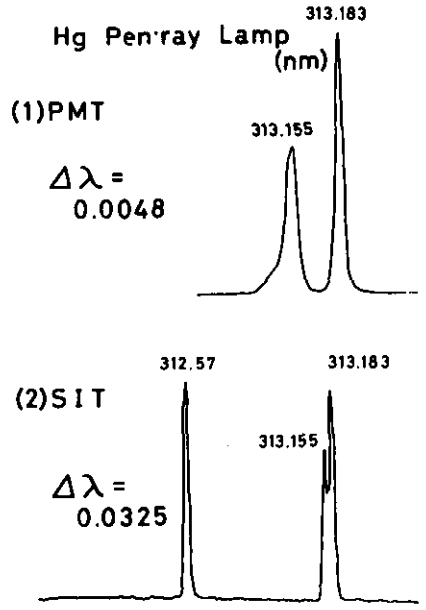

Fig. 2-2 Resolution power of the HR 1000 monochromator
(1) Photomultiplier both entrance and exit slit width 10 μm, slit height 5 mm
(2) SIT detector entrance
slit width 10μm, slit height 2 mm, exit slit was removed.

during moving the frequency is elevated up to 500 Hz. But in that case it is necessary to generate a frequency slope from 200 Hz to 500 Hz in 1 second.

a. Interface

Table 2-2 gives the directions necessary for an external control. Wavelength scanning is performed by transferring the TTL level pulse (+5V) from bit 4 of the CPU to pin number 8 of the monochromator. On the contrary, the confirming signal returns from the monochromator to the CPU. The directions are shown in Table 2-3. Table 2-3 includes the connection of a photomultiplier and the CPU. During the calibration procedure pin number 1 of the photomultiplier emits a signal to bit 15 of the CPU when it "catches" the mercury atomic emission.

b. Sequential slew scan method

It is necessary to slew the monochromator from the present analytical wavelength (RNOW) to the next one (RNEXT) in a very rapid and precise manner. Therefore the monochromator is slewed rapidly between wavelengths, and its slew speed is reduced as it approaches the desired wavelength. By the motor step select and frequency select the slew mechanism is controlled through three different slewing speeds. These include a slow (0.1 nm/s), a medium (2.5 nm/s), and a fast (6.25 nm/s) speed. The motor step select has a slow scanning mode (0.0005 nm/pulse) and a fast scanning mode (0.125 nm/pulse) and the frequency select is 200 Hz and 500 Hz. The changeover from 200 Hz to 500 Hz is performed in 1 second by using software, and that of the slow and fast scanning mode is done in about 300 msec by changing the electromagnetic clutches. Before slew scanning it is necessary for the computer to calculate how many pulses will produce a 0.1 nm wavelength change. For that purpose under computer control the mercury emission line at 253.65 nm and the second order line corresponding to 507.30 nm are searched by a

Table 2-2 Commutating signal from CPU to monochromator

Bit of CPU	Function	Pin number of monochromator
0	scanning direction increasing wavelength decreasing wavelength	2
1	motor step selection 0.0005 nm/pulse 0.0125 nm/pulse	4
2	clock selection external clock internal clock	6
3	control motor forward –validiating the clock forward stop	7
4	external clock	8
5	*(not used)*	
6	lateral entrance selection lateral entrance axial entrance	20
7	lateral exit selection lateral exit axial exit	21
8-15	(not used)	

Table 2-3 Confirming signal from monochromator and photomultiplier to CPU

Bit of CPU	Function	Pin number of monochromator
0	scanning direction increasing wavelength decreasing wavelength	13
1	motor step selection 0.0005 nm/pulse 0.0125 nm/pulse	15
2	indication of stop position	34
3	control motor forward –validiating the clock forward stop	18
4	external clock	19
5	(not used)	
6	lateral exit selection lateral exit axial exit	16
7	lateral entrance selection lateral entrance axial entrance	17
8	indication of minimum wavelength	35
9	indication of maximum wavelength	36
10-14	(not used)	
		Pin number of photomultiplier
15	detection of mercury atomic emission	1

photomultiplier, and the computer calculates the pulse counts for moving 0.1 nm wavelength from the used pulses (Calibration procedure in 2-3). From the difference of RNOW and RNEXT wavelengths and the pulse counts for moving 0.1 nm wavelength, the pulse counts which are required to slew between two analytical lines are calculated as follows.

$$PCNT = (RNEXT - RNOW)\ [\text{Å}] \times \text{Pulses/Angstrom}$$

According to the magnitude of PCNT, one of the following three slewing modes are chosen.

(1) PCNT$<$25
(less than 0.0125 nm between wavelengths)
Slew scanning performed by slow scanning mode 0.0005 nm/pulse at the frequency of 200 Hz.

(2) $1 \leqslant PCNT/25 \leqslant 700$
(less than 8.75 nm between wavelengths)
Slew scanning performed by fast scanning mode 0.0125 nm/pulse at the frequency of 200 Hz. When the monochromator closes to within 0.0125 nm of the next wavelength, the remainder is performed by slow scanning mode 0.0005 nm/pulse at the frequency of 200 Hz.

(3) 700$<$PCNT/25
(larger than 8.75 nm between wavelengths)
Slew scanning is performed by fast scanning mode 0.0125 nm/pulse at the frequency of 500 Hz. When the monochromator closes to within 0.0125 nm of the next wavelength, the rest is performed by slow scanning mode 0.0005 nm/pulse at the frequency of 200 Hz.

The flowchart for these procedures is shown in Figure 2-3. Then the monochromator is sequentially slewed to what should be exactly the desired wavelength.

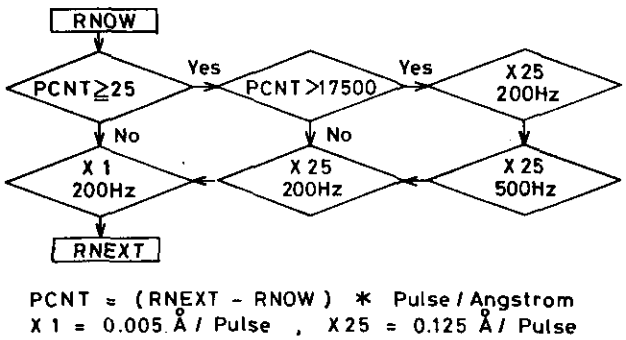

Fig. 2-3 Motor speed contol between RNOW and RNEXT
Three different slewing speeds are employed so that the wavelength selection is both rapid and precise.
(1) x 1,200 Hz; slewing speed 0.1 nm/s
(2) x 25,200 Hz; slewing speed 2.5 nm/s
(3) x 25,500 Hz; slewing speed 6.25 nm/s

c. Accuracy of sequential slew scan

To check the accuracy of the slew mechanism, the mercury atomic emission lines of a mercury pen ray lamp were measured with the photomultiplier and SIT detectors.

Fourteen mercury emission lines at 253.65, 313.16, 313.18, 365.02, 365.48, 366.33, 404.66, 407.78, 434-75, 435.84, 491.60, 546.07, 576.96, and 579.07 nm were sequentially monitored by both detectors. The degree of deviation was shown in Figure 2-4. Detecting the mercury emission with a photomultiplier, the peak was searched manually. When the monochromator found the peak, the counter number was read to check the monochromator wavelength accuracy. After that, the emission line was detected with the SIT detector by switching the exit lateral mirror. The mercury emission line was located exactly at the central channel of the SIT detector if the line peak was detected with a photomultiplier. This procedure was repeated three times, and the results are plotted in Figure 2-4(1). The results indicates the error of the reading counter was within 0.025 nm.

Input of the mercury emission lines by the teletype was performed in advance. After the monochromator was calibrated, the error of the counter set under computer control and the deviation from the OMA central channel (No. 250) were checked during sequential slew scanning. As shown in Figure 2-4(2), and rather large error occured when the monochromator slewed to the first mercury emission line after the calibration and when the monochromator returned from the longest mercury emission line to the previous wavelength. This error is due to the backlash of gears when the scanning direction changes. If only forward scanning is used for analysis, the accuracy is within 0.01 nm. If both forward and backward scannings are taken into consideration, wavelength setting is possible within 0.025 nm. This accuracy is however not enough for the photomultiplier to detect atomic emission with a 0.001 nm linewidth.

If the photomultiplier is used for the detection of the atomic line, a quartz plate is set in the optical axis and the deviation is corrected by rotating the plate. H. V. Malmstadt and his co-workers reported it was possible to set at a preselected wavelength

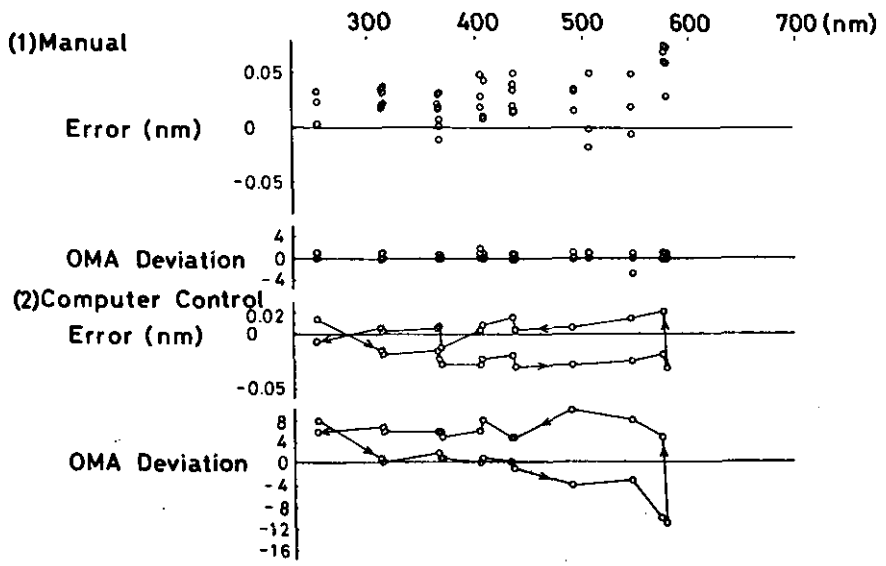

Fig. 2-4 Monochromator wavelength accuracy and deviation from OMA central channel (No. 250)

(1) Manual

(2) Computer-control

within an accuracy of 0.02 nm by using a DC motor and an encoder[58]. Rotating a quartz plate by a stepping motor to detect the emission line improved the situation slightly and accuracy was within 0.017 nm[59], but if the SIT detector is used instead of a photomultiplier, accurate monochromator wavelength setting is not required since a 5 nm spectral window is obtained. This accuracy (within 0.025 nm) of the slew scanning without a quartz plate is enough. In addition it is a laborious process to find emission peaks by rotating a quartz plate. For the system being discussed, it takes only 1 minute to slew the monochromator between 20 analytical lines.

2-2-2 Silicon Intensified Target (SIT) and Optical Multichannel Analyzer (OMA)

Figure 2-5(1) illustrates a cross section of the Silicon Intensified Target (SIT) detector[96]. An image is focused on a scintillator and converted to visible light if the radiation is ultraviolet. The incident visible light generates photoelectrons at the photocathode. The photoelectrons are accelerated to strike the silicon target by a high voltage (typically −10 KV), and ion pairs are created on the surface, typically 1500 pairs per electron. The surface of the silicon target is made of a n-type semiconductor. Although light also produces ion pairs on the target, an accelerated electron is much more efficient. On the reverse side of the silicon target, p-type semiconductors are buried as a mosaic pattern in a silicon dioxide insulator. When the electron beam scans the p-type semiconductors from the reverse side and charges them negatively, the positive ions of the ion pairs

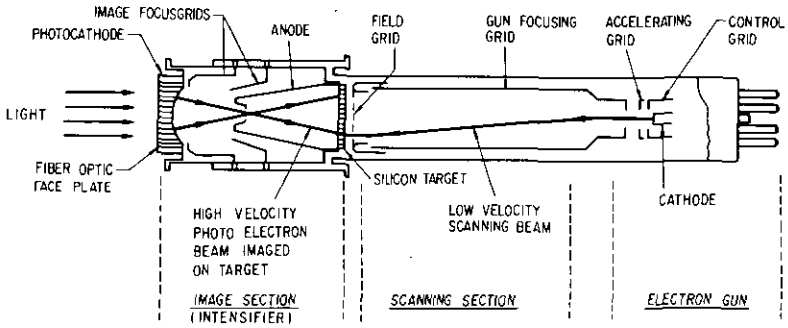

Fig. 2-5 (1) Cross section of a SIT detector (Ref. 96)

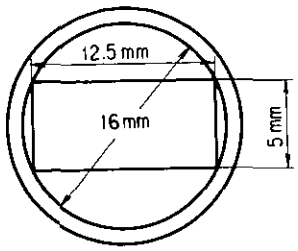

Fig. 2-5 (2) Silicon Target (Ref. 96)

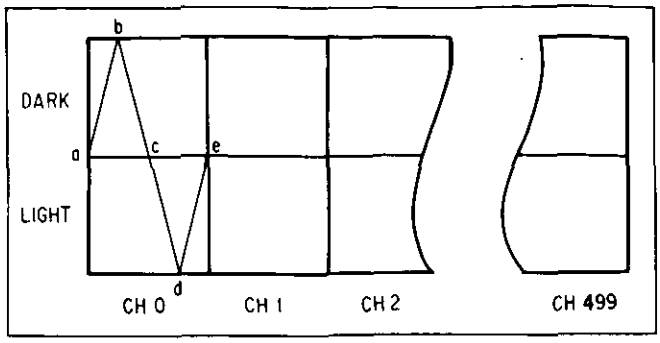

Fig. 2-5 (3) Scanning pattern showing light-dark correction (Ref. 96)

produced previously on the n-type semiconductor flow to the p-type semiconductor to neutralize the negative charge. This current, which is proportional to the ion pairs, is read by the OMA amplifiers as the vidicon signal[54,73,74,85,97,98].

The silicon target is 16 mm in diameter, and the effective area is divided into 500 channels as shown in Figure 2-5(2). To correct for the dark current of the SIT detector, each channel is also divided into a light and a dark half as shown in Figure 2-5(3). One half of the vidicontarget must be kept dark by inserting a plate in front of the target. Each channel scan pattern is divided into two parts. The scan from a to b to c reads dark current, while the scan from c to d to e reads the signal plus the dark current. The two parts are electronically subtracted and integrated to obtain a voltage proportional to exposure. The silicon target can integrate the ion pairs until scanning by the electron beam occurs, and moreover the repetition of the scan enables signals to be accumulated. The vidicon signal obtained with the SIT detector is digitalized by an analog-to-digital converter and memorized in the Optical Multichannel Anlyzer (OMA). The analog to digital converter counts the charge at about 2500 electrons per count. The resulting minimum detectable signal is about 15 photons:

$$S_{SIT}(\lambda) = \frac{2500}{G_{SIT} \times Q_{SIT}(\lambda)} = 15 \text{ photons/count}$$

where

$S_{SIT}(\lambda)$ is the number of photons per count

S_{SIT} is the gain of the intensifier stage (typically 1500)

$Q_{SIT}(\lambda)$ is the quantum efficiency for the intensifier photocathode (17% at peak).

The maximum integration per one scanning is 750 counts, while accumulation up to 100000 counts is possible for each channel. The OMA has two memory areas for storing spectra obtained by the SIT detector [A] and [B] and a subtracted spectrum is obtained by use of the arithmetic logic in the OMA console [A-B]. It is possible to transfer the memorized [A] and [B] spectra and the subtracted [A – B] spectrum to computer in digital form, and are also to display the spectra on the monitor scope or record on the X-Y recorder by utilizing the conversion facility.

a. Interface

The OMA has signal inputs and outputs available on its back panel to present measurement data in both analog and digital form and allow remote programming of most OMA functions. Analog output signals are designed to display all 500 channels in graphic

form on CRT displays and X-Y recorders. Digital outputs present a single channel of data with 20 bit, 5-digit Binary Coded Decimal (BCD) word. Table 2-4 shows the directions necessary for an external control. For example, accumulation of OMA [A] memory area starts by emitting the TTL level pulse from bit 6 of the CPU to pin number 50 of the OMA PROGRAM. After that, digital data are transferred from the OMA to the CPU as shown in Table 2-5. Table 2-5 includes the confirming signal which returns from the OMA to the CPU.

b. Features of Silicon Intensified Target and Optical Multichannel Analyzer for sequential slew scan multielement analysis

The sequential multielement analysis procedure by a rapid slew scan method with a programmable monochromator has been developed by other workers[58-61,99,100]. The slew scan method is convenient for rapid sequential multielement analysis and has more inherent flexibility for multielement detection than the well-established direct reading method where only fixed wavelengths of the desired elements are available. However, this technique lacks the necessary precision to measure atomic emission with linewidth 0.001 nm using the conventional exit slit-based photomultiplier detection system. The precision of wavelength measurement is limited to 0.02 nm, even if accurate wavelength setting is achieved by a stepping motor[60] or a DC motor with an encoder[58]. If the exit slit-based photomultiplier is used for the detection of the atomic line, a quartz plate is necessary to accurately locate the atomic line. After the signal is found out by rotating the plate, the intensity of the signal is measured over a certain period of time. When the signal is buried in many sharp background emissions, it is possible that the background peak may be mistaken for the signal. This is so especially when the signal is weak. To discriminate the signal from the background, the following two ways, which obtain the profile around the wavelength, are designed so far.

(1) The grating is stopped temporarily before the monochromator arrives at a preselected wavelength, and data acquisition is performed while the monochromator is scanning gradually narrow wavelength region around the wavelength.

(2) The grating remains at a preselected wavelength, and a quartz plate inserted into an optical path scans repetitively narrow wavelength region around the wavelength. Data acquisition is synchronized with the vibration of the plate[61,100,101]. The maximum

Table 2-4 Commutating signal from CPU to OMA

Bit of CPU	Function	Pin number of OMA	
		OMA PROGRAM	OMA OUTPUT
0-2	(not used)		
3	[B] elase	49	
4	[A] elase	48	
5	[B] accumulation	24	
6	[A] accumulation	50	
7-8	(not used)		
9	request data		22
10	set cursor zero ←⊖		49
11	move cursor ⟶		23
12	real switch	47	
13	[A − B] switch		38
14	[B] switch		13
15	[A] switch		14

Table 2-5 Transferring digital data and confirming signal from OMA to CPU

Bit of CPU	Function	Pin number of OMA OMA PROGRAM	Pin number of OMA OMA OUTPUT
0	DIG 01		1
1	DIG 02		2
2	DIG 04		26
3	DIG 08		27
4	DIG 11		3
5	DIG 12		4
6	DIG 14		28
7	DIG 18		29
8	DIG 21		5
9	DIG 22		6
10	DIG 24		30
11	DIG 28		31
12	real switch	47	
13	[A – B] switch		38
14	[B] switch		13
15	[A] switch		14
0	DIG 31		7
1	DIG 32		8
2	DIG 34		32
3	DIG 38		33
4	DIG 41		9
5	DIG 42		10
6	DIG 44		34
7	DIG 48		35
8	sign	11	
9	data ready		39
10	input busy	29	
11-15	(not used)		

scanning speed to produce an exact trace of a spectrum is equal to the bandpass divided by the response time. Roughly four time constants are required to achieve a 98% response for the peak height[102].

$$\text{Maximum scan speed} = \text{bandpass} / \text{response time} = \text{bandpass} / (4 \times \text{time constant})$$

For example, when the peak is measured using a bandpass of 0.03 nm and a time constant of 2 s, the maximum scan speed is 0.22 nm/min. According to the former (1) way, it will take at least one minute to measure the profile of 0.22 nm wavelength region. As the real time to use for measuring the signal is very short, sensitivity is also poor. In the case of the latter (2) way, the consumption of time goes down and sensitivity is improved by accumulation. However, it is rather difficult to discriminate the signal from the background by the information of the narrow profile (maximum 0.3 nm). As the background spectrum of ICP source is very complex, this problem becomes all the more severe.

Even if the wavelength setting was attempted as accurately as possible by a small wavelength change of 0.0005 nm per pulse, an error within 0.025 nm would be inevitable (2-2-1c.). In this study, to avoid the error it was decided to adopt the SIT image detector in the slewing system instead of the PMT detector. The spectral window of 5 nm is obtained simultaneously. The application of the SIT detector to the sequential slew scan technique has not been done yet.

In order to take advantage of the SIT image detector for simultaneous miltielement analysis, relatively low dispersion monochromators which provide a spectral window generally greater than 20 nm have been preferred (Table 2-6). As the channel number of

Table 2-6 Comparison of a spectral window and a dispersing instrument

	K. M. Aldous[a)] D. G. Mitchell K. W. Jackson	F. L. Fricke[b)] O. Rose, Jr. J. A. Caruso	T. L. Chester[c)] H. Haraguchi J. D. Messman J. D. Winefordner	K. W. Busch[d)] N. G. Howell G. H. Morrison	This Study
Reciprocal Linear Dispersion (nm/mm)	13.2	5.5	3.1	1.6	0.4
Spectral Window (nm)	165	69	39	20	5
Resolution (nm/channel)	0.33	0.14	0.08	0.04	0.01
Grating (grooves/mm)	295	590	590	1180	2400
Focal Length (mm)	250	300	350	500	1000

a) Ref. 83, 103, 104
b) Ref. 105, 106
c) Ref. 107
d) Ref. 17, 108–113

the SIT is restricted to 500 channels, enlarging the spectral window sacrifices the resolution. To get sufficient resolution for atomic spectroscopy, the spectral window was limited to 5 nm in this study. The signals obtained by the SIT detector are processed in the OMA, and are designed to be presented in both analog and digital forms. The OMA has two memory areas, that is, [A] memory and [B] memory. The spectrum obtained by the SIT for the sample plus background is accumulated and stored in [A] memory. Next, the spectrum obtained by the SIT for only the background is accumulated and stored in [B] memory. Noise can be reduced by integration and accumulation. As is shown in Figure 2-6, signal over noise is improved in proportion to the square root of the accumulation times. By subtracting the two spectra memorized in [A] and [B] memories, the spectrum for only the sample is obtained. As these three different spectra are displayed on an oscilloscope, the interpretation of the signal and the background is possible. Data in digital form can be readily processed by a computer. So far, from [A] spectrum that is due to the sample plus background, the signal was seeked by measuring the profile[61,100,101]. In this paper the background corrected [A – B] spectrum, that is only due to the sample, is used to perform analysis. Adding one step to subtract the background is extremely helpful to get the net signal. Although a high resolution monochromator reduces the spectral window, some spectroscopic element lines, which are within

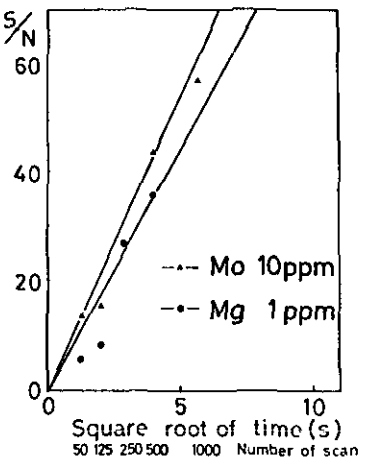

Fig. 2-6 S/N improvement by accumulation (integration time is fixed to 32.8 ms)

a 5 nm range, are observed simultaneously and the important capability of simultaneous multielement analysis is retained.

c. Comparison of responsivity of Silicon Intensified Target and Photomultiplier Tube

Comparison of responsivity between the Silicon Intensified Target (SIT) and the Photomultiplier Tube (PMT) requires conversion of the appropriate mathematical expressions to the equivalent format[113]. Assuming the PMT signal conversion from amperes to counts is made by the OMA circuit, an expression for the responsivity of the PMT can be derived in digital form. The digital responsivity for a PMT (R_{PMT}) *is given by:*

$$R_{PMT} = Q_{PMT}(\lambda)\ G_{PMT}\ e\ D\ [1/t_0] \quad \text{counts/photon}$$

where

$Q_{PMT}(\lambda)$ is quantum efficiency of the photocathode of PMT

Q_{PMT} is the gain of the dynode chain (2.5×10^6)

e is the charge of electron (1.6×10^{-19} coulombs)

D is conversion factor (8.0×10^{10} counts/ampere)
((1 count/2500 electron) x (1 electron/ 1.6×10^{-19} coulombs)
x (3.2×10^{-5} s for conversion))

t_0 is the time of observation.
The time equivalent to a vidicon frame scan period is given as 3.28 $\times 10^{-2}$ s.

Numerical substitutions for the variable reduces to:

$$R_{PMT} = Q_{PMT}(\lambda) \times (0.98) \qquad \text{Eq. 1}$$

The responsivity for a SIT (R_{SIT}) is given by:

$$R_{SIT} = \frac{Q_{SIT}(\lambda)\ G_{SIT}}{2500}\ [t_e / t_r] \quad \text{counts/photon}$$

where

$Q_{SIT}(\lambda)$ is quantum efficiency of the intensifier photocathode

G_{SIT} is the gain of the intensifier stage (Typically 1500)

t_e is exposure time of a channel (3.28×10^{-2} s)

t_r is signal readout time for a channel (3.2×10^{-5} s).

By substituting the variables, the SIT vidicon responsivity (R_{SIT}) expression reduces to:

$$R_{SIT} = Q_{SIT}(\lambda) \times (0.6 \times 10^3) \qquad \text{Eq. 2}$$

The quantum efficiency of the SIT is dependent on the characteristics of the photocathode, the fiberoptic faceplate, and the scintillator screen. A plot of the two digital responsivity expressions Eq. 1 and Eq. 2 vs. wavelength yields the curves shown in Figure 2-7[113].

In the ultraviolet region (below 380 nm) the quantum efficiency of the PMT is better than that of the SIT due to rapid decrease of SIT responsivity with decreasing wavelength. Further improvements in SIT UV response may alter the situation. The PMT's quantum efficiency decreases in the visible region where the SIT reaches the optimum spectral responsivity. The responsivity of the SIT is nearly equivalent or better than that of the PMT over the visible wavelength range (above 380 nm). It is of course possible to choose a PMT more sensitive to visible radiation at the expense of UV responsivity.

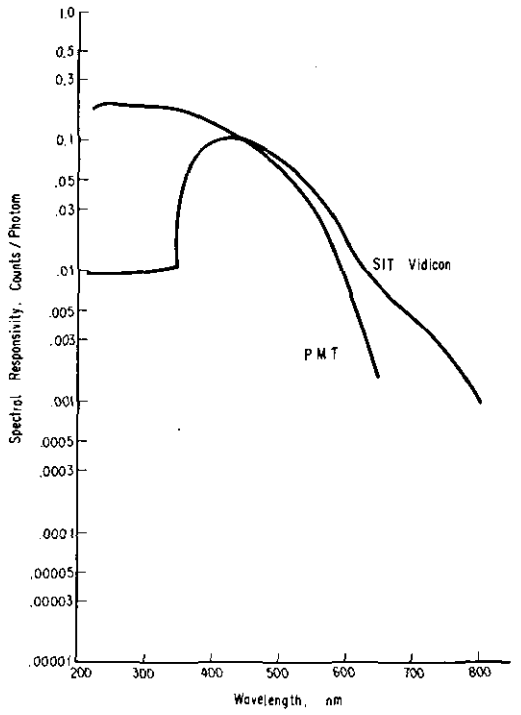

Fig. 2-7 The comparison of the spectral responsivity between PMT and SIT detectors (Ref. 113)

PMT; Photomultiplier RCA 1P28 (This charactaristic is similar to Hamamatsu R919, which is used in this study.)

SIT; Silicon Intensified Target PAR 1205D/01

2-2-3 Sample introduction system

To introduce a sample automatically into the ICP source, an autosampler was employed. The autosampler introduces the sample and distilled water alternatively. In this study two procedures for quantitative analysis were selected namely 3 point standardization and 2 point standardization. The 3 point standardized method is primary designed for accurate single element analysis, whereas the 2 point standardized method is used for multielement analysis in conjunction with the slew scan technique. According to the quantitative method, the samples are arranged in advance.

(1) 3 point standardization

The setting for 3 point standardization is illustrated in Figure 2-8. Standard solutions at three different concentrations are used to construct the analytical curve for analysis of test samples (n) and blank samples (k). A check sample is set at the head of the sequence to obtain the desired light intensity by the sequentially adjustable filter. Standard solutions are arranged with the higher concentrated solution coming first. If necessary, blank solutions follow the samples. Analytical curves are obtained by the least squares method for three data points. The average intensity of the blank samples can be subtracted from the intensity of the test samples.

(2) 2 point standardization

The setting of samples for 2 point standardization is illustrated in Figure 2-9. One standard solution and the origin of the coordinated system are used to prepare the calibration curve. The test sample is measured before the standard solution in order to set the sequentially adjustable filter at a position to obtain adequate light for detection.

The procedure, by which the autosampler alternates between the sample and distilled water, is shown in Figure 2-10. There are four choices in rinse time, i.e. 3, 6, 15, and 30 seconds according to sample requirements.

2-2-4 Recording system

The analog signal detected by the SIT is converted to a digital signal in the OMA. The spectra memorized in the OMA are transferred to and averaged in the CPU. The

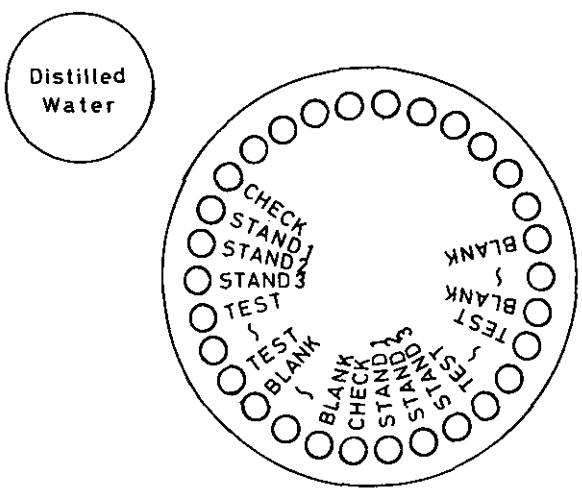

Fig. 2-8 Autosampler positions for the 3 point standardized method

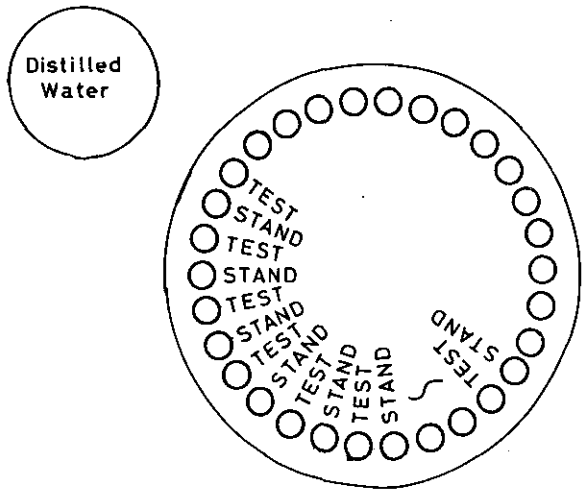

Fig. 2-9 Autosampler positions for the 2 point standardized method

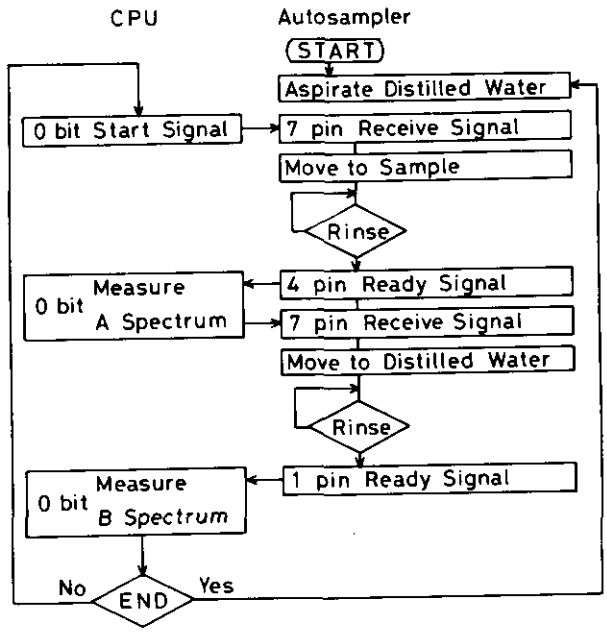

Fig. 2-10 Computer-controlled movement of autosampler

maximum number of OMA spectra that can be transferred is 50 and the time required is about 200 seconds. The averaged spectra are recorded on a X-Y recorder through a D/A converter. Output of the X-axis voltages enters pin numbers 12 and 24 and output of the Y-axis voltage enters pin numbers 10 and 22 of the X-Y recorder. In addition to the spectrum, the scale factor is printed out on the head of the spectrum. Pen up and down are controlled by emitting a TTL level signal (+5V) from bit 2 of the CPU to pin numbers 1 and 13 of the X-Y recorder. Paper feed is also controlled by emitting a TTL level signal

(+5V) from bit 1 of the CPU to pin numbers 3 and 15 of the X-Y recorder. On the contrary, a confirming signal of the paper feed end returns from pin numbers 3 and 15 of the X-Y recorder to bit 1 of the CPU.

If necessary, the spectrum obtained by the SIT is recorder off line, and the analog signal detected by PMT is monitored by a recorder after DC amplification.

2-2-5 Data storage

[A] and [B] spectra obtained by the SIT detector are stored on paper tape or magnetic tape. Parameters are also stored for each preset wavelength before spectral data are obtained. Real parameters such as wavelength, standard solution concentrations, and specified intensity level are expressed by two words or four bites (32 bits, since 1 word is 16 bits and 1 bite is 8 bits). Integral parameters such as the name of the element, method of treatment of data, and the number of samples are expressed by one word or two bites (16 bits). A spectral datum for one channel is expressed by two words (32 bits) as a real number. Total 500 channels occupy 1K words or 2K bites. As [A] and [B] spectra are recorded at the same time, 2K words or 4K bites are necessary for one sample and distilled water. One record is formed by the maximum 59 words and the record length is recorded on the head. Therefore, [A] and [B] spectra consist of 34 records (2000/59 = 33.9). Paper tape is punched by binary format shown in Figure 2-11. A break of the records is revealed by four feed holes.

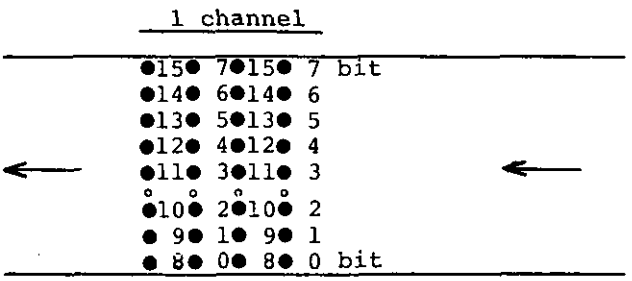

Fig. 2-11 Punch out format of a spectral datum for one channel. It is expressed by two words (32 bits)

After a part of the software format is modified for reception by the host computer, digitalized data for 500 channels are printed out and plotted. Subtracted [A-B] spectral data are also printed out and plotted together with [A] and [B] spectral data. The digitalized data are useful for various arithmetic calculations.

2-3 Analytical procedures

FORTRAN (formula translation) and ASSEMBLER are used for the program language. Figure 2-12 shows the flow chart of the analytical procedure. There are six commands such as CALIBRATE, SET, LIST, RUN(A), RUN(B) and END. After monochromator scanning is calibrated using the Hg emission lines, various parameters are set and confirmed by listing. For quantitative analysis two alternative standardized methods have been prepared. Three point standardized method [RUN(A)] requires three standard solutions at different concentrations. This method is primary designed for single element

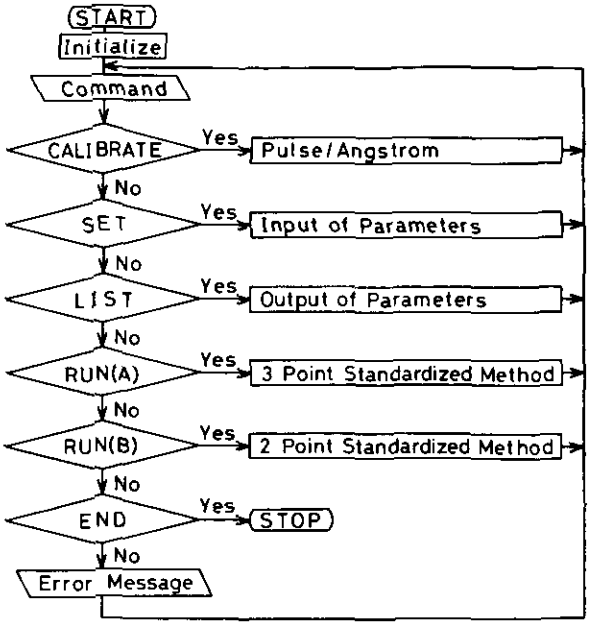

Fig. 2-12 Flow chart for analytical procedure

analysis of many samples. This method requires a longer time but is more reliable than the two point standardized method. The two point standardized method [RUN(B)] is more convenient for rapid multielement analysis in conjunction with the slew scan technique.

Before input of a command, preliminary steps are necessary. Samples are arranged in the autosampler as shown in Figures 2−8 and 2−9 according to the quantitative method, and the rinse time is selected (3, 6, 15 and 30 seconds) by a dial. The level of the peak sensor is set so that the sensor can detect the 253.65 nm mercury emission line in the second order (507.30 nm)using the PMT. The intensity of the second order line is weaker than that of the first order. If the level is set for the second order line, the first order line can also be detected. The level is used for calibration of monochromator scanning. After the level is set, the monochromator returns to around 253.00 nm wavelength (below 253.65 nm within 3 nm) and is connected to the CPU. The delay and preset switches of the OMA console are selected to 0 and 125, respectively. This setting provides 32.8 ms integration and 125 times accumlation. It takes 4.1 s to obtain one spectrum [(delay+1) x preset x 32.8 ms]. Both X and Y input ranges of the X-Y recorder are preset at 0.5 mV/cm. The following explains each command briefly.

2-3-1 Calibration of the monochromator wavelength scanning

Under computer control the mercury emission line at 253.65 nm and the second order line corresponding to 507.30 nm are searched by a photomultiplier. Between the photomultiplier and the computer an interface is installed to monitor the mercury emission lines. The interface transmits a TTL level signal to the computer when the photomultiplier receives the signal above the level set in the initialization step. The computer calculates the pulse counts for moving 0.1 nm wavelength and prints out the pulse counts on the teletype.

2-3-2 Input and output of parameters

After monochromator scanning is calibrated, the following parameters are set for each wavelength from the teletype.

Item 1 is measuring number: The maximum number is 10.

Item 2 is the name of the element: The sequence terminates by the input of END mark.

Item 3 is the wavelength at the central channel of the SIT detecator: It is variable from 1500 to 7000 in angstrom unit.

Items 4-6 are the three different concentrations of standard solutions with the higher concentration coming first for 3 point standardization.

Item 4 is the single concentration of a standard solution for 2 point standardization.

Items 7-8 determine whether the outputs of the X-Y recorder are necessary or not for standard solutions and samples respectively: It is possible to select the following eight parameters.

0; without spectra	4; only [A − B] spectrum
1; only [A] spectrum	5; [A] and [A − B] spectra
2; only [B] spectrum	6; [B] and [A − B] spectra
3; [A] and [B] spectra	7; [A], [B] and [A − B] spectra

Item 9 decides whether storage on PT (paper tape) or MT (magnetic tape) is necessary or not:

0; without storage

4; stored on PT

8; stored on MT

Item 10 designates the number of times spectra obtained by the SIT are transferred from the OMA to the CPU for accumulation: The maximum number is 50.

Item 11 identifies the side background which can be subtracted from the peak [A − B] signal to obtain the real intensity:

1; longer wavelength side
[from central channel-14 (usually 236) to central channel-10 (usually 240)]

2; shorter wavelength side
[from central channel+10 (usually 260) to central channel+14 (usually 264)]

3; both wavelength sides

Items 12-13 are the numbers of test and blank samples respectively: The variable range is is from 1 to 20 for test sample and from 0 to 20 for blank sample.

Item 14 is the minimum intensity level used to judge whether the peak in the spectrum obtained by the SIT detector is registered or not in the CPU: The maximum figure is 98000.

Items 15-16 designate whether the side background defined by item 11 is corrected or not in calculating the concentration.

1; Net intensity is used to calculate the concentration without side-background correction.

2; Real intensity is used to calculate the concentration with side-background correction.

In order to confirm the input of paramterrs a complete list of parameters is possible.

2-3-3 3 point standardized method

The analytical procedure for 3 point standardized method is shown in Figure 2-13. Once the run(A) "command RA" is entered from the teletype, the monochromator slews

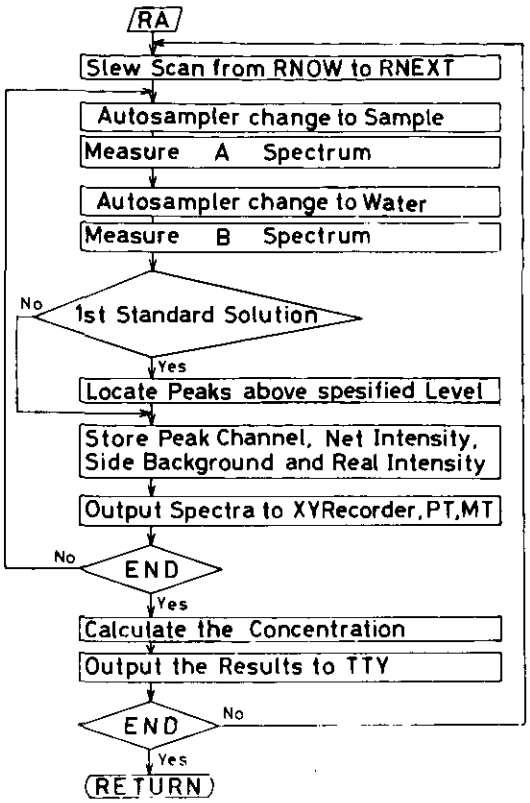

Fig. 2-13 Flow chart for the 3 point standardized method

sequentially to preselected wavelengths. The slew scanning continues automatically until the wavelength setting command reaches END (Parameter of item 2). When the monochromator stops at a certain preselected wavelength, only parameters at the wavelength are stored on paper tape or magnetic tape (Parameter of item 9). The CPU activates the real display switch of the OMA and changes the autosampler to a check sample. The highest concentrated standard solution or test sample is used for the check sample. While the check sample's spectrum obtained by the SIT is monitored on the oscilloscope, the sequentially adjustable filter is set to obtain adequate light for detection. After the adjustment of the filter is completed, the autosampler changes to distilled water by input of an arbitrary character (ex. GO) on the teletype. After the preset rinse time has passed, the autosampler changes to the first standard solution and [A] spectra measured by the SIT are transferred to and averaged in the CPU (Parameter of item 10). During the measurement oscilloscope. Next, the autosampler changes to distilled water and [B] spectra are measured in the same way. Figure 2-14 shows how to transfer the SIT data to the CPU. The highest concentrated standard solution in three standard solutions is measured at first to locate peaks above the specified level (Parameter of item 14) from [A-B] spectrum. At this stage channel numbers to locate peaks are determined and hereafter other channels are ignored even if large peaks are observed at different channels. Net intensity, side background and real intensity at the determined channel are stored in the CPU. Net intensity is the peak value in the [A – B] spectrum, and the side back-

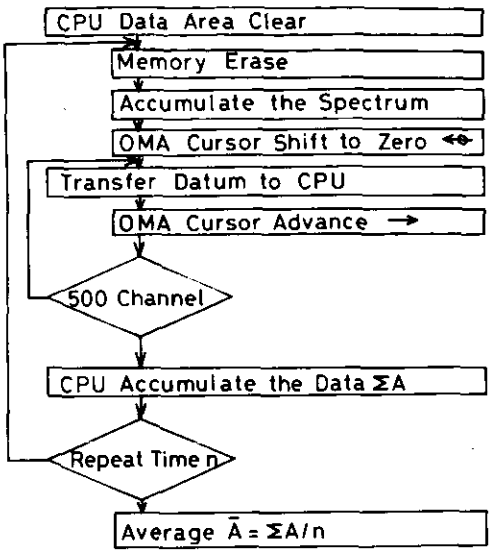

Fig. 2-14 Flow chart for transfer of SIT data to CPU

ground in the [A – B] spectrum is the average value for 5 channels located on either side of the central channel. Usually channel numbers are 236–240 and 260–264. Wavelength separation between the central channel (250) and channel 236 (or 260) is 0.1 nm and for channels 236–240 (or 260–264) is 0.05 nm. The real intensity requires subtraction of the side background from the net intensity. The side background can be selected from the longer wavelength side, the shorter wavelength side or both sides in advance (Parameter of item 11). To save memory area, [A] and [B] spectra obtained by the SIT detector are stored in the same area as the previous [A] and [B] spectra, and the previous spectra are erased. In order to preserve [A] and [B] spectra storage on paper tape or magnetic tape is possible as described in 2-2-5 (Parameters of items 7 and 8). When [A] and [B] spectra are recorded on the X-Y recorder, the full scale factor is always 100,000 counts, but the full scale factor for the [A – B] spectrum is determined by the maximum peak counts of the highest concentrated standard solution, which is measured at first, in three standard solutions. The scale factor is also recorded on the head of the spectrum in addition to the [A – B] spectrum. During output of the spectra to PT, MT or the X-Y recorder, the [A – B] spectrum is visualized on the oscilloscope automatically and [A] and [B] spectra can also be displayed by pushing the desired button of the OMA console. The measurements of [A] spectrum (sample) and [B] spectrum (distilled water) are repeated for three standard solutions, test samples, and blank samples (Parameters of items 12 and 13). Net intensity, side background, and real intensity are obtained and memorized for each peak channel number. In this case, the channel number to locate peaks is determined by the highest concentrated standard solution. The peak channel is chosen from the [A – B] spectrum within ±1 channel. After all samples are measured at the preselected wavelength, the following calculations are performed for each peak channel: the concentration of the standard solution divided by the intensity, analytical curves obtained by the least squares method for three standard solutions, and the average intensity of blank samples. The selection of peak intensity

and real intensity during calculation is conducted when the parameters are set (Parameters of items 15 and 16). The concentration of the test sample for each peak channel is calculated from the analytical curve by using the subtracted intensity of the average value of the blank samples. All results are printed out of the teletype along with the memorized data in the CPU.

2-3-4 2 point standardized method

The analytical procedure for the 2 point standardized method is shown in Figure 2-15. Once the run(B) "command RB" is entered from the teletype, the monochromator slews to preselected wavelengths and the autosampler introduces the test sample to the plasma. While the sample's spectrum obtained by the SIT is monitored on the oscilloscope, the sequentially adjustable filter is set to obtain adequate light for detection. After adjustment of the filter is completed, the measurement of [A] spectrum starts by input of an arbitrary character (ex. GO) on the teletype. In the case of the 2 point standardized method, the test sample is measured at first and doubles as a check sample unlike the 3 point standardized method (2-3-3). The [A] spectrum measured by the SIT is transferred to and averaged in the CPU (Parameter of item 10). During the measure-

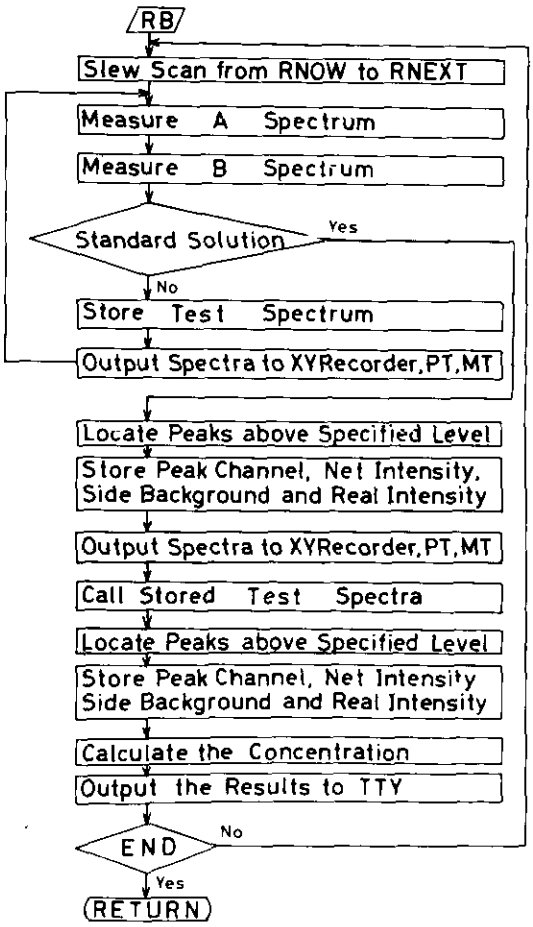

Fig. 2-15 Flow chart for the 2 point standardized method

ment of the [A] spectrum, the spectrum can be visualized on the oscilloscope. Next, the autosampler changes to distilled water and the [B] spectrum is measured in the same way. Figure 2-14 shows how to transfer the SIT data to the CPU. As only one standard solution is used for measuring one test sample, the total number of spectra is less than that of the 3 point standardized method. This enables the [A] and [B] spectra for the test sample to be memorized using different memory areas. Independently, storage of the [A] and [B] spectra on paper tape or magnetic tape is possible as described in 2-2-5 (Parameter of item 9). The X-Y recorder can be used for records of the [A], [B], and [A − B] spectra as described in 2-2-4 (Parameters of items 7 and 8). When the [A] and [B] spectra are recorded on the X-Y recorder, the full scale factor is always 100,000 counts, but the full scale factor for the [A − B] spectrum is determined by the maximum peak counts of the sample. In the case of the 3 point standardized method, the full scale factor of the [A − B] spectra for the test samples is determined by the highest concentrated standard solution (1-3-3). Whereas, in the case of the 2 point standardized method, different full scale factors of the [A − B] spectra for the test sample and the standard solution are determined by the maximum peak counts, respectively. During output of the spectra to the PT, MT, or the X-Y recorder, the [A], [B], and [A − B] spectra can be displayed on the oscilloscope in the same way as for the 3 point standardized method (20303). The measurements of the [A] and [B] spectra are repeated for the standard solution. From the [A − B] spectrum, peaks above a specified level (Parameter of item 14) are located. At this stage channel numbers of the peaks are determined. The net intensity, side background and real intensity at the appropriate channels are stored in the CPU. Output of the spectra for the standard solution to the PT, MT, or the X-Y recorder is possible in the same way as for the test sample. The [A] and [B] spectra for the test sample, which are stored at different memory areas, are recalled and the peak channels are chosen from the [A − B] spectrum (peak channel within ±1). The net intensity, the side background and the real intensity at the channels are stored in the CPU. In this case, other peaks, whose intensities are greater than the specified level, but were not observed in the standard solution, are also registered in the CPU unlike the 3 point standardized method (2-3-3). The channel number, the net intensity, the side background and the real intensity are also stored. After all samples are measured at the preselected wavelengths, the concentration of the test sample is calculated by using the analytical curve which is derived from one standard solution and the origin of the coordinate system. All results are printed out on the teletype along with the memorized data in the CPU. The slew scanning continues automatically until the wavelength command reaches END (Parameter item 2).

2-3-5 Experimental results

This section shows examples of the analytical procedure. Representing the major constituents of a digested plant sample, a synthesized solution containing Ca 200, K 150, Mg 60, P 20, and Zn 1 μg/m*l* was prepared. The test sample was measured by the 3 point standardized method and the 2 point standardized method.

a. 3 point standardized method

Figure 2-16(1) shows a printout of the multielement analysis program. Capital letters represent the input command from the teletype, and small letters the output of the computer. The output "NEXT?" represents the request for a command. CA is the command for calibration (2-3-1). The computer calculates the pulse counts for moving 0.1 nm and prints out the pulse counts on the teletype. As one pulse corresponds to 0.0005 nm,

```
    *** MULTIELEMENT ANALYSIS PROGRAM ***

NEXT?
CA
STEP/ANGSTROM=200.015
NEXT?
ST
01   ZN 2135.00 5 1 0.5 4 4 4 2 3 2 0 6000 2 2
02 END
NEXT?
LI
NO NAME WAVE(A) D1(PPM) D2(PPM) D3(PPM) VS VT DT IN SB NT NB LEVEL FS FT
-- ---- ------- ------- ------- ------- -- -- -- -- -- -- -- ----- -- --
 1   Zn 2135.00 5.00000 1.00000  .50000  4  4  4  2  3  2  0  6000  2  2
NEXT?
RA
```

Fig. 2-16 (1) Example of the 3 point standardized method

the pulse counts for moving 0.1 nm should be 200. However there are slight day to day variations in this count number. ST is the command for setting of the parameters. The parameters set in the examples are explained as follows (2-3-2):

- 01 is the measuring number.
- ZN is the element symbol.
- 2135.00 is the wavelength (Å) at the central channel of the SIT detector.
- 5 1 0.5 are the three different concentrations ($\mu g/ml$) of the standard solutions.
- 4 4 requests the X-Y recorder output for only the [A – B] spectrum.
- 4 decides storage on PT (paper tape).
- 2 designates that the data transfer from the OMA to the CPU is performed twice (i.e. number of accumulation is 2).
- 3 designates that the side background at both the high and low wavelength side of the analytical line is subtracted from the net signal.
- 2 represents the number of test samples.
- 0 corresponds to the number of blank samples.
- 6000 If the intensity in the [A – B] spectrum is above 6,000 counts, the peak is registered in the CPU.
- 2 2 designates that the side background is corrected for in calculating the concentration.

To confirm the input of parameters, the list command LI may be used. Once the run(A) "command RA" is entered from the teletype, the monochromator slews sequentially to preselected wavelengths and analysis is performed. Figure 2-16(2) shows the spectra recorded on the X-Y recorder. Standard solutions at the concentrations of 5, 1, and 0.5 $\mu g/ml$ Zn were used to construct the analytical curve for analysis of Zn in the test sample (2-3-3). The figure recorded on the head of the spectrum represents the full scale factor. This factor was determined by the maximum peak count of the highest concentrated standard solution (Zn 5 $\mu g/ml$). On account of the Ca far scatter light, the background level for the test sample increased. After measurement was completed, the results were printed out on the teletype as shown in Figure 2-16(3). The data included the peak

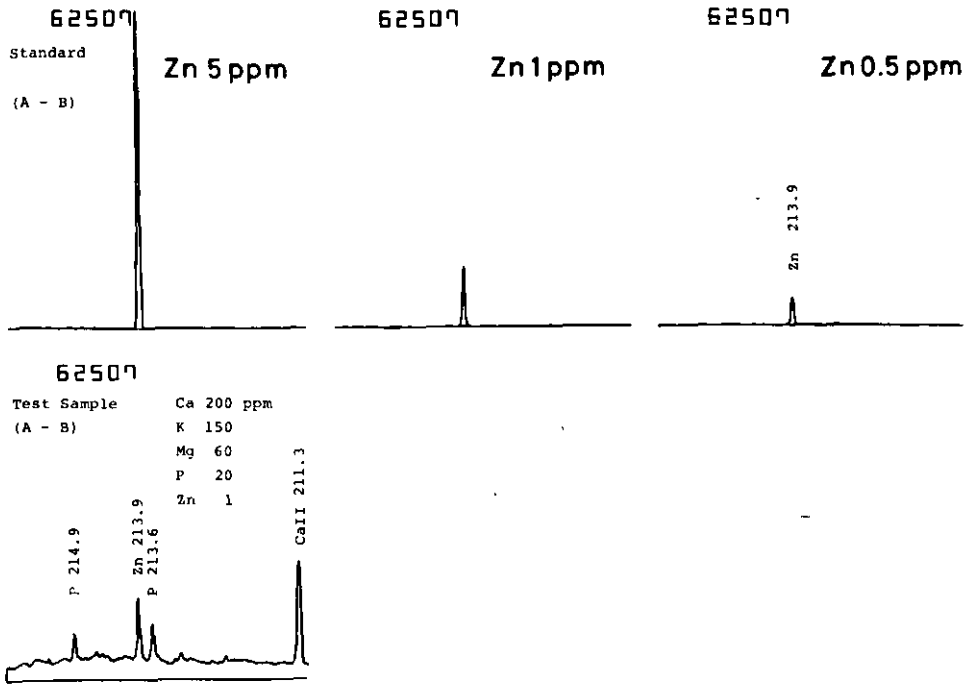

Fig. 2-16 (2) Example of the 3 point standardized method

intensities of the [A], [B], and [A − B] spectra. The [A − B] peaks are referred to here as the net intensity. The side background is the average value for 5 channels located on either side of the central channel (2-3-3). The real intensity requires the subtraction of the side background from the net intensity. The numbers in the last column correspond to the gradient of the straight line which links the measurement point for the particular concentration with the origin of the coordinate system. The values were used for checking linearity. The analytical curve (gradient = $.7926 \times 10^{-4}$, intercept = $.3441 \times 10^{-1}$) is obtained by the least squares method, and the concentration of the test sample is calculated from the analytical curve. Because Ca far scatter light causes the plasma background level to increase at the Zn wavelength the side background for the test sample was rather high (Test sample 1 = 4146, Test sample 2 = 4099), and analytical results would be in error if correction was not performed. Correction for the side background increase may enable accurate analytical results to be obtained.

b. 2 point standardized method

Figure 2-17(1) shows a printout of the multielement analysis program. The format is almost the same as the 3 point standardized method. However, in this case a single standard solution is required (2-3-2). Figure 2-17(2) shows the spectra recorded on the X-Y recorder. The standard solution at the concentration of 1 $\mu g/ml$ Zn was used for analysis of Zn in the test sample (2-3-4). The figure recorded on the head of the spectrum represents the full scale factor. The factors of the test sample and the standard solution were determined by the maximum peak counts, respectively. After the measurement was completed, the results were printed out on the teletype as shown in Figure 2-17(3). One standard solution and the origin of the coordinate system was used to prepare the

```
NEXT?
RA
GO
NAME(  ZN) WAVE(2135.00) LEVEL( 6000) SIDE-BAND(3) MODE(2,2)
STANDARD SAMPLE 1  (5.00000 PPM)
    CHANNEL PEAK(A) PEAK(B) PK(A-B) BACK GD  INTEN      A
    ------- ------- ------- ------- ------- ------- -------
        218   76288   13780   62507    -121   62629  .798E-04
STANDARD SAMPLE 2  (1.00000 PPM)
    CHANNEL PEAK(A) PEAK(B) PK(A-B) BACK GD  INTEN      A
    ------- ------- ------- ------- ------- ------- -------
        218   26085   13746   12339     -60   12399  .798E-04
STANDARD SAMPLE 3  ( .50000 PPM)
    CHANNEL PEAK(A) PEAK(B) PK(A-B) BACK GD  INTEN      A
    ------- ------- ------- ------- ------- ------- -------
        218   19575   13890    5685       1    5684  .880E-04
PEAK CONCENTRATION EQUATION   CONCENTRATION=A*PEAK+B
       A         B
    --------- ---------
    .7926E-04  .3441E-01
TEST SAMPLE 1
    CHANNEL PEAK(A) PEAK(B) PK(A-B) BACK GD  INTEN  TES-BLN CONCENT
    ------- ------- ------- ------- ------- ------- ------- -------
        218   30785   13874   16911    4146   12765   12765  .105E+01
TEST SAMPLE 2
    CHANNEL PEAK(A) PEAK(B) PK(A-B) BACK GD  INTEN  TES-BLN CONCENT
    ------- ------- ------- ------- ------- ------- ------- -------
        218   30593   14075   16517    4099   12418   12418  .102E+01
```

Fig. 2-16 (3) Example of the 3 point standardized method

```
    *** MULTIELEMENT ANALYSIS PROGRAM ***
NEXT?
CA
STEP/ANGSTROM=200.034
NEXT?
01   ZN 2135.00 1 0 0 4 4 4 2 3 1 0 6000 2 2
02 END
NEXT?
LI
NO NAME WAVE(A) D1(PPM) D2(PPM) D3(PPM) VS VT DT IN SB NT NB LEVEL FS FT
-- ---- ------- ------- ------- ------- -- -- -- -- -- -- -- ----- -- --
 1   ZN 2135.00 1.00000   00000   00000  4  4  4  2  3  1  0  6000  2  2
NEXT?
RB
```

Fig. 2-17 (1) Example of the 2 point standardized method

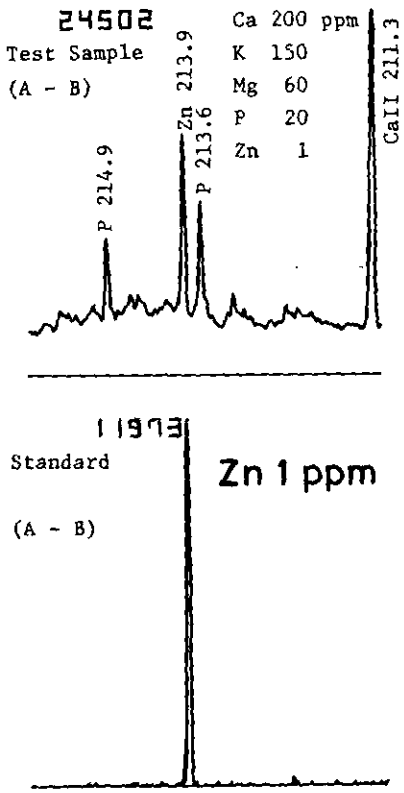

Fig. 2-17 (2) Example of the 2 point standardized method

```
NEXT?
RB
GO
NAME(  ZN) WAVE(2135.00) LEVEL( 6000) SIDE-BAND(3) MODE(2,2)
STANDARD SAMPLE    (1.00000 PPM)
    CHANNEL PEAK(A) PEAK(B) PK(A-B) BACK GD  INTEN      A
    ------- ------- ------- ------- -------  -------  -------
        220   24876   12903   11973     -21    11994  .834E-04
TEST SAMPLE
    CHANNEL PEAK(A) PEAK(B) PK(A-B) BACK GD  INTEN  CONCENT
    ------- ------- ------- ------- -------  -------  -------
        220   29366   12974   16392    4125    12266  .102E+01
OTHER PEAKS
        112   18831    9419    9412    3979     5433
        244   19903    8037   11865    4011     7854
        488   31415    6913   24502 $$$$$$$ $$$$$$$
```

Fig. 2-17 (3) Example of the 2 point standardized method

analytical curve. The printout format was also the same as the 3 point standardized method. However, in this case additional peaks due to the presence of other elements in the test sample could also be monitored. Other peaks at 112, 244, and 488 channels were identified as the P and Ca lines at 214.9, 213.6, and 211.3 nm, respectively.

CHAPTER 3 Studies of Atomic Emission Spectroscopy Using Nitrous Oxide-Acetylene Flame

3-1 Introduction

The silicon intensified target tube (SIT) coupled with an optical multichannel analyser (OMA) has been utilized as a detector system in emission[62,63,105,106,108-113], absorption[83,103,104] and fluorescence[107] spectroscopic studies. Attractive analytical features of the SIT detection system, which have been well documented in the reports from Morrison and his co-workers[108-113] and include the simultaneous multielement analysis capability, the facility to correct for spectral and background interference and detection power equivalent to the photomultiplier tube (PMT) in the visible region, although detection performance is relatively poorer in the ultraviolet. As is well known[73,74], the standard SIT image detector consists of about 500 light sensitive elements (channels) within an area of approximately 62.5 mm^2 (length 12.5 mm, height 5 mm) so that when situated in a dispersing instrument, simultaneous detection of atomic lines is possible. The range of wavelengths which are detected simultaneously is determined primarily by the reciprocal linear dispersion (RLD) of the monochromator. In order to take advantage of the SIT-OMA system for simultaneous multielement analysis, relatively low dispersion monochromators which provide a spectral window generally greater than 20 nm have been preferred (2-2-2b.). The use of the low-dispersion monochromator, however, may result in severe spectral interference in atomic emission spectroscopy in high temperature media, particularly in inductively coupled plasma emission spectroscopy.

In the present study, the SIT-OMA system has been combined with a medium resolution monochromator (focal length, 1 m; RLD, 0.4 nm/mm) to evaluate detectability performance. The use of the medium resolution monochromator reduces the spectral region spatially detected by the SIT-OMA system (5 nm for present instrumentation) and sacrifices to some extent the capability for simultaneous multielement analysis.

We have developed a programmable monochromator controlled by a minicomputer, where a slew scan technique was employed as has been reported by other workers[58-61,99]. The programmable monochromator of the slew scan type is convenient for rapid sequential multielement analysis and has more inherent flexibility for multielement detection than the well-established direct reading system where only fixed wavelengths of the desired elements are available[114]. However, the slew scan technique suffers from the problem of irreproducibility in wavelength setting, precision being limited to ±0.1 nm, as has already been pointed out[60,61]. To avoid the error caused by irreproducible wavelength setting in the slit-based spectrometer, it was decided to adopt the SIT as the spatial detector in the slew scan system. The important capability of simultaneous multielement analysis is still retained provided element lines are within a 5 nm range for the present instrumentation (±2.5 nm from the central OMA channel).

In this study, the analytical performance of the SIT-OMA detector is considered when combined with the programmable monochromator system. The nitrous oxide-acetylene flame was selected as the excitation source for initial studies.

3-2 Experimental

3-2-1 Instrumentation

The experimental system is shown in Figure 3-1. A nitrous oxide-acetylene flame was supported on a burner assembly (5 cm slot burner) of a commercially available spectrophotometer (Shimadzu AA-650). The monochromator (Jobin Yvon HR 1000, focal length, 1 m) has dual entrance and exit slit ports and was equipped with a holographic grating (2400 grooves/mm); the desired optical path was selected by mirrors positioned beside the entrance and exit slits. The entrance slits were used to receive radiation from the flame and a mercury pen lamp, respectively, the latter being used for wavelength calibration of the monochromator scanning system. The flame focused on the entrance slit was imaged down a factor of 2 using a single spherical silica lens (diameter, 60 mm; focal length, 219 mm). The SIT detector tube (Princeton Applied Research Co., SIT 1205D/01) and a standard photomultiplier Hamamatsu TV Co., R 919) sensitive to ultraviolet and visible light were positioned at the exit slit ports. The slit unit was removed in the former case and a plate was equipped on the SIT adaptor to obstruct 50% of the incident light to enable dark current correction. The lateral length of the SIT detecter was 12.5 mm for the monochromator RLD of 0.4 nm/mm and a 5 nm spectral window was obtained. The resolution power for the SIT, 0.032 nm, was about 7 times poorer than that by PMT (2-2-1). The SIT signal after processing in the OMA (Princeton Applied Research Co., OMA 1205A) was displayed on the oscilloscope and/or could be recorded by an external X-Y recorder (Yokogawa Electric Works, Ltd., 3078).

For PMT detection, a pre-amplifier (laboratory constructed), a light chopper and a lock-in-amplifier (Princeton Applied Research Co., 125A and 5203, respectively) were used.

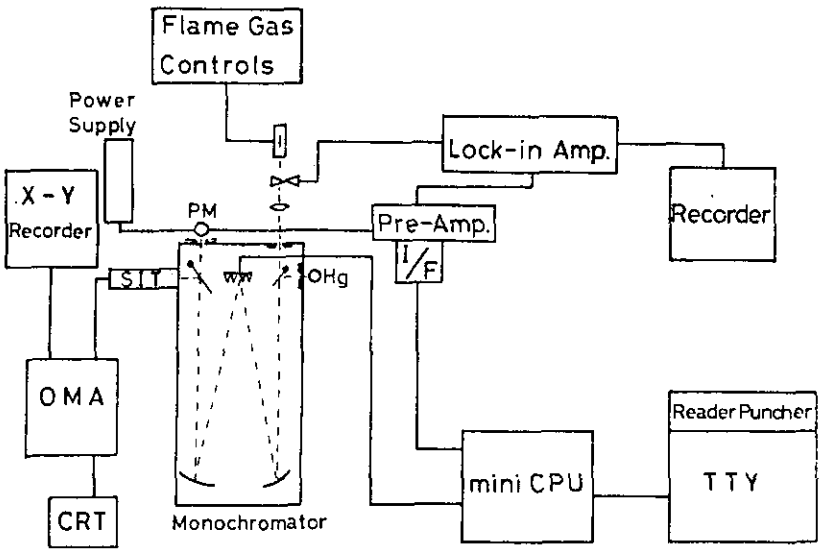

Fig. 3-1 Schematic diagram of computer-controlled instrumentation for multielement analysis utilizing N_2O-C_2H_2 flame as an excitation source

A minicomputer (Hewlett Packard 2108) was employed to control the monochromator wavelength by the slew scanning technique. A mercury lamp (Ultra-Violet Co., 11SC-1) was used for initial wavelength calibration.

3-2-2 Procedures

For wavelength calibration the scanning system was referenced to the mercury lines at 253.65 and 507.30 nm using the Hg pen-ray lamp. This procedure determined the number of steps/wavelength (nm) to be employed in wavelength selection by the stepping motor when controlling the grating angle. After calibration, the wavelengths of the desired atomic lines could be set arbitrarily by command from the computer.

The experimental conditions for the measurement of atomic emission using the nitrous oxide-acetylene flame were optiomized in terms of the flame and slit conditions. Once the conditions had been optiomized, a standard solution was aspirated and the accumulated spectrum was stored in OMA memory [A]. The procedure was repeated for the blank solution using memory [B]. The subtracted spectrum [A-B] provided the emission line(s) of the element. The emission intensity was obtained by noting the peak height and subtracting the average reading of the side background for 10 channels around the peak channel. The background noise level ([A-B] spectrum for the channel range 240–260) was obtained when distilled water was aspirated and subtraction of the [A] and [B] memories was performed. The PMT detection system was used for comparison studies. The signal and background noise were measured from the pen deflection on the chart recorder paper.

The detection limits in Tables 3-1 and 3-2 are defined as the concentrations which represent a signal equivalent to twice the standard deviation of the background noise level. The values were obtained from the standard calibration curve for each element prepared by the least squares method. The optimized conditions determined are also summarized in Table 3-1 with the wavelengths of analytical lines. The chemicals used were of analytical reagent grade and deionized water was used as the blank solution.

3-3 Results and discussion

3-3-1 Flame background correction

The atomic emission of 22 elements in the nitrous oxide-acetylene flame was measured by the SIT-OMA system coupled to the programmable monochromator. Figure 3-2 shows the N_2O-C_2H_2 flame emission spectra recorded by the PMT when only distilled water was aspirated. The upper curve was recorded at a high EHT (−695 V) to indicate the prominent background constituents of the flame. Background species at approximate wavelengths are NO (200–280 nm), OH (280–330), NH (336 nm)' CN (350–422 nm), CH (387–431 nm) and C_2(437–600 nm). The analytical lines of the elements used in the study are indicated by the dotted lines on the lower spectrum.

Flame emission spectra observed by the SIT-OMA system for a 5 nm spectral window are shown in Figures 3-3 and 3-4 for Bi, Mo, Pb, Cr, Sr, and Li, respectively. Since the SIT-OMA system has 2 memories, each memory was used for the emission measurements of the sample solution and the blank solution, respectively. Spectra [A-B] in Figures 3-3 and 3-4 are the corrected spectra calculated from the [A] and [B] memories, and subtraction is automatically performed in the OMA. The background at the Bi wavelength is particularly severe and corresponds to the OH vibrational fine structure. The

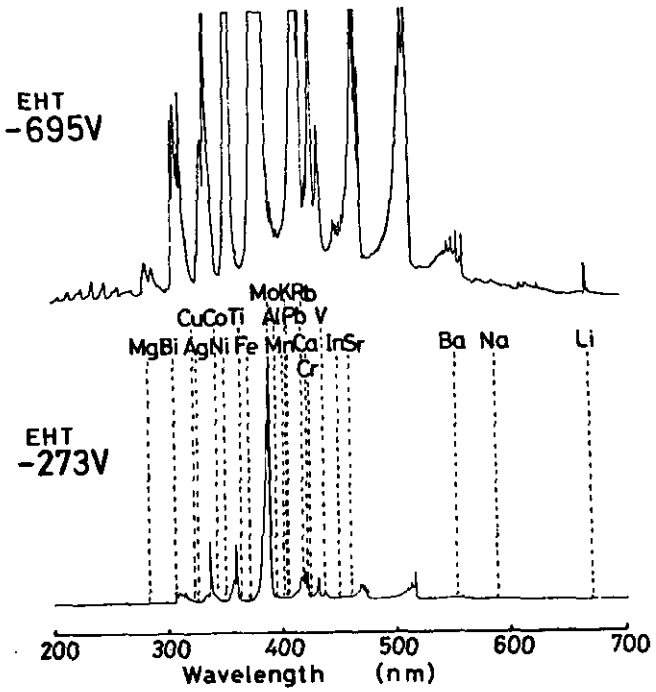

Fig. 3-2 Emission spectra of N_2O-C_2H_2 flame observed at different extra high tension (EHT) applied to a photomultiplier

Upper spectrum : −695 V

Lower spectrum : −273 V

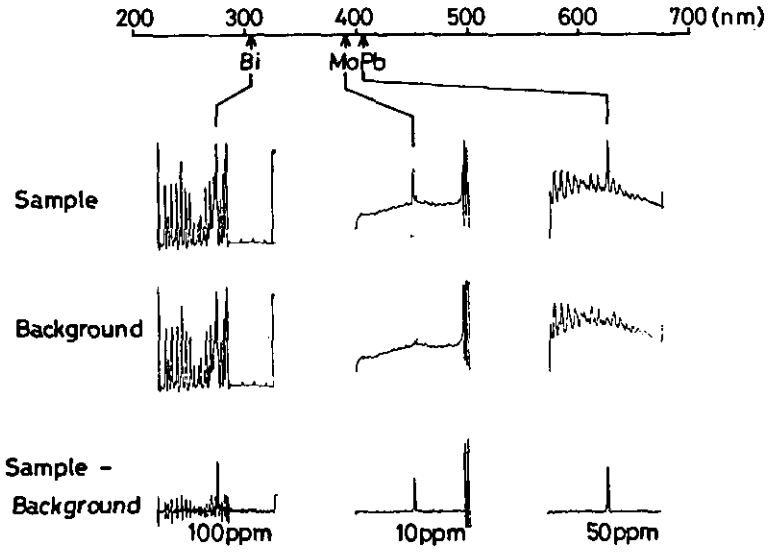

Fig. 3-3 Emission spectra observed by SIT-OMA system for Bi (306.8 nm), Mo (390.3 nm), and Pb (405.8 nm) (Bi 100 μg/ml, Mo 10 μg/ml, Pb 50 μg/ml)

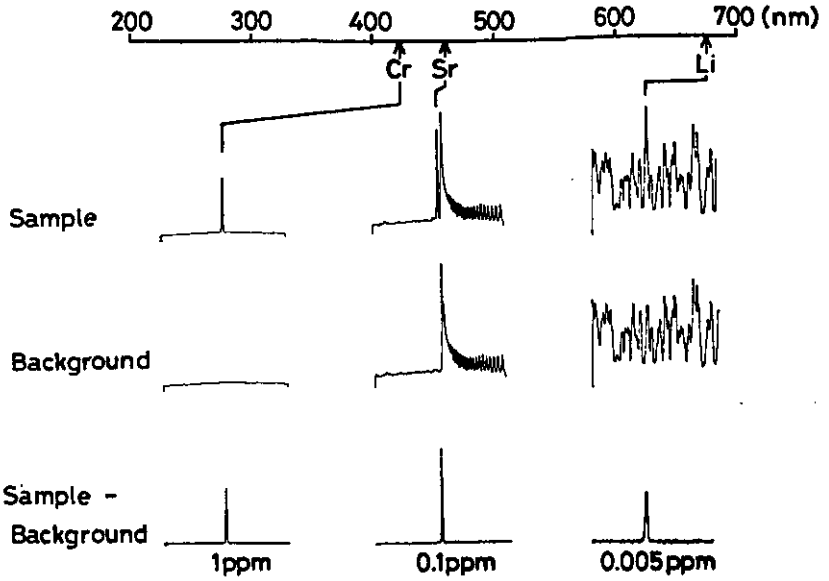

Fig. 3-4 Emission spectra observed by SIT-OMA system for Cr (425.4 nm), Sr (460.7 nm), and Li (670.8 nm) (Cr 1 μg/m*l*, Sr 0.1 μg/m*l*, Li 0.005 μg/m*l*)

predominant background species at the Mo wavelength is OH and CH, while at the Pb wavelength CN is predominant. For Sr and Li the predominant species is C_2, while at the Cr wavelength flame background is negligible. Sequential slew scan measurement of the above 6 elements required approximately 5 minutes disregarding the recording time.

3-3-2 Analytical performance parameters

The analytical performance data summarized in Table 3-1 were obtained by accumulating the signals for 4.1 s. In the SIT-OMA system, the scanning rate of the electron beam over 500 channels was 32.8 ms, and the 4.1 s accumulation time corresponded to 125 times accumulation of the signals at each channel in the SIT detector. The dynamic range of the SIT-OMA system is 10^5 counts and the real-time dynamic range (real-time is a single scan) is about 750 counts for each channel. Therefore, the entrance slit width and slit height were required to be adjusted to obtain the appropriate signal intensities which were within the dynamic range of the SIT-OMA system. Before adjustment of the slit conditions mentioned above, the flame conditions and height above the burner head were optimized for each element using a constant nitrous oxide flow rate of 7.5 *l*/min. Optimized conditions for individual elements are depicted in Figure 3-5. The experimental results obtained through the above procedures are summarized in Table 3-1, along with the analytical lines and other experimental conditions. The detection limit data are similar to those obtained by Howell and Morrison[113] who used a 0.5 m monochromator-SIT combination. The relative standard deviation (RSD) values for the concentrations indicated in parentheses were generally in the 3% range although for some elements of low sensitivity, e.g. Bi, Pb where concentrations were relatively closer to the respective detection limits, higher RSD values were obtained.

Regarding the flame operating conditions, it can be seen from Figure 3-5 that the

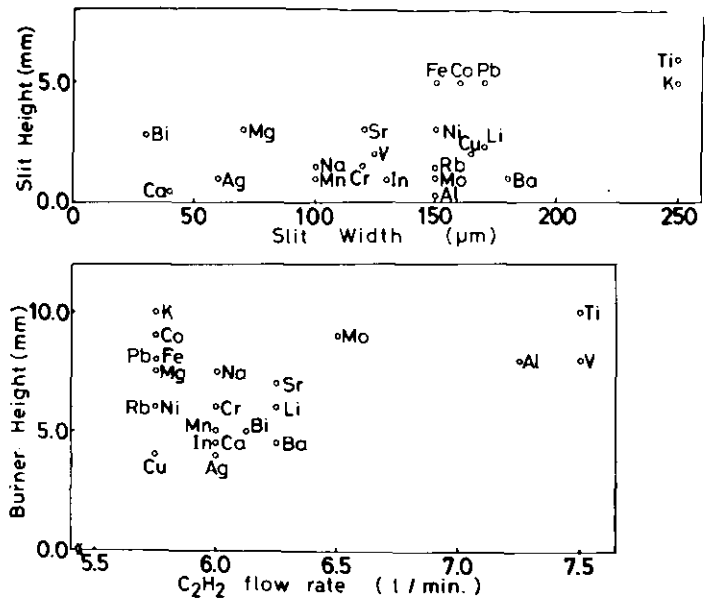

Fig. 3-5 Optimum conditions for individual elements
Upper : Slit height vs. slit width of monochromator
Lower : Burner height vs. C_2H_2 flow rate (N_2O flow rate is fixed at 7.5 l/min.)

elements such as Ti, V, Al and Mo were atomised effectively in the reducing atmosphere of the C_2H_2-rich flame and in the high temperature region corresponding to a high position above the burner head. These conditions are required to prevent formation of the refractory oxide species. In contrast, optimum sensitivity for Co, Pb and Fe was obtained in the oxygenated atmosphere of the C_2H_2-lean flame and at a high position above the burner, and that of Ni, Cu and Ag was obtained in the oxygenated atmosphere of the C_2H_2-lean flame and at a low position above the burner[115]. In this way, the optimum conditions in the N_2O-C_2H_2 flame are very different for the elements. This spread in the optimum values constitutes a major problem in utilizing the N_2O-C_2H_2 source for multi-element analysis since fixed conditions and flame height would be desirable for rapid analysis. The other major drawback, of course, in the N_2O-C_2H_2 excitation source is that elements whose resonance lines are in the UV region are not sufficiently excited to observe atomic emission[48-51,62].

3-3-3 Comparison of Silicon Intensified Target (SIT) and Photomultiplier Tube (PMT)

So far, to evaluate SIT detector performance, the detection limits obtained by the SIT image detector have been compared with those obtained by the photomultiplier tube in separate studies[103-108,110-113]. In the present study, the detection limits of 8 elements were also obtained by a photomultiplier (R919). The experimental conditions for the SIT detector were the same as those shown in Table 3-1 and the conditions for the photomultiplier were independently determined by optimization procedures for each element.

As is shown in Figure 2-7 the photon quantum yield of the SIT in the ultraviolet region is worse by 1 – 2 orders of magnitude when compared to that of the photomulti-

Table 3-1 The detection limits of various elements obtained by the N_2O-C_2H_2 flame emission spectrometry using a SIT detector under optimized conditions

Element	Wavelength nm	C_2H_2 flow rate[a] $l\ min^{-1}$	Flame height[b] mm	Slit width μm	Slit height mm	Detection Limit[c] $\mu g\ ml^{-1}$	RSD[d] %
Mg	285.21	5.75	7.5	70	3	0.22	3.0(1)
Bi	306.77	6.13	5	30	2.8	21	12.6(100)
Cu	324.75	5.75	4	165	2	0.066	5.6(1)
Ag	328.07	6.0	4	60	1	0.11	2.3(5)
Co	345.35	5.75	9	160	5	0.21	8.4(1)
Ni	352.45	5.75	6	150	3	0.61	2.8(10)
Ti	365.35	7.5	10	250	6	0.15	3.8(5)
Fe	371.99	5.75	8	150	5	0.13	7.2(1)
Mo	390.30	6.5	9	150	1	0.17	15.4(1)
Al	396.15	7.25	8	150	0.3	0.32	7.4(0.5)
Mn	403.08	6	5	100	1	0.017	2.1(1)
K	404.41	5.75	10	250	5	7.5	–
Pb	405.78	5.75	8	170	5	0.95	11.4(10)
Rb	420.19	5.75	6	150	1.4	2.2	5.1(50)
Ca	422.67	6	4.5	40	0.4	0.002	2.8(0.1)
Cr	425.43	6	6	120	1.5	0.0028	2.2(0.1)
V	437.92	7.5	8	125	2	0.018	2.4(0.5)
In	451.13	6	4.5	130	0.9	0.0092	1.6(0.5)
Sr	460.73	6.25	7	120	3	0.0008	1.5(0.05)
Ba	553.56	6.25	4.5	180	1	0.064	3.7(1)
Na	589.00	6	7.5	100	1.5	0.00066	–
Li	670.78	6.25	6	170	2.3	0.00013	2.1(0.005)

a) The flow rate of nitrous oxide was measured at 7.5 $l\ min^{-1}$.

b) Height above the burner head.

c) See text.

d) Relative standard deviation calculated from 10 determinations. Value in parenthesis is concentration at which determination was performed.

plier, while it is almost comparable with or better than that of the photomultiplier in the visible region. Although a rigorous comparison of data is ruled out due to fundamental design differences between the SIT and the PMT, for standard measurement conditions, i.e. SIT accumulation time of 4.1 s and a PMT time constant of 2 s, a general trend in the results can be pointed out. Poor SIT detector performance is evident for Mg and Ag where detection limits are about 20 times poorer than the PMT data. The excellent detection power in the visible region is, however, clearly seen from Table 3-2.

Table 3-2 Comparison of detection limits with SIT and PMT

Element	Wavelength nm	SIT $\mu g\ ml^{-1}$	PMT $\mu g\ ml^{-1}$
Mg	285.21	0.24	0.004
Bi	306.77	24	23
Ag	328.07	0.20	0.060
Mo	390.30	0.39	0.87
Pb	405.78	0.35	0.48
Cr	425.44	0.005	0.018
Sr	460.73	0.0005	0.0007
Li	670.78	0.00028	0.0022

CHAPTER 4 Studies of Atomic Emission Spectroscopy Using Radio Frequency Inductively Coupled Argon Plasma (RFICAP)

4-1 Introduction

Inductively coupled plasma (ICP) emission spectometry has in recent years been extensively developed as a new analytical technique for elemental analysis[26,30,31,116-118] ICP emission spectrometry has the advantageous features of high detection limits and wide dynamic ranges (about five orders of magnitude). Furthermore, it is almost free from chemical[119] and ionization[119,120] interferences, and is suitable for multielement analysis. When a direct reading system is employed, simultaneous multielement analysis is easily performed with the ICP excitation source[94]. Usually, conventional photomultipliers are used as the detectors in ICP emission spectrometry.

A silicon intensified target (SIT) tube has received as a spectroscopic detector due to the high detection efficiency and multielement detection capability[83]. Actually, the SIT detector has been applied to flame spectrometry in emission[62,63,105,106,108-113], absorption[83,103,104] and fluorescence[107]. According to the studies, the detectivity of the SIT is worse by one or two orders of magnitude in the UV region than that of a conventional photomultiplier. However, simultaneous multielement analysis capability and the facility of background correction[109] appear to be attractive features for analytical atomic spectrometry. Therefore, it may be interesting to apply the SIT detector for ICP emission spectrometry.

So far, in flame spectrometry, the SIT detector has been preferably used with relatively low-dispersion monochromators in order to take advantage of the SIT for multielement analysis. Generally, a spectral window greater than 20 nm has been provided by those dispersion systems (Table 2-6). However, it has been pointed out that the spectral line interference is a serious problem in ICP emission spectometry[121]. Therefore, the use of the low-dispersion monochromator may result in spectral interference. Hence, in this study, the SIT detector has been combined with a medium-resolution monochromator (1 m focal length monochromator using a grating with 2,400 grooves/mm; reciprocal linear dispersion of 0.4 nm/mm), which provided a 5 nm spectral window on 500 channels of the SIT-OMA (optical multichannel analyzer for data procession) system. The use of the SIT in such a medium resolution monochromator system sacrifices to some extent the simultaneous multielement detection capability, but the spectra measured by the SIT detector provide useful information on plasma background changes which is another serious problem in ICP emission spectrometry[121-123]. On considering these situations, the analytical performance of the SIT image detector in ICP emission spectrometry has been investigated.

4-2 Experimental

4-2-1 Compromised experimental conditions

A schematic diagram of the present experimental system is shown in Figure 2-1

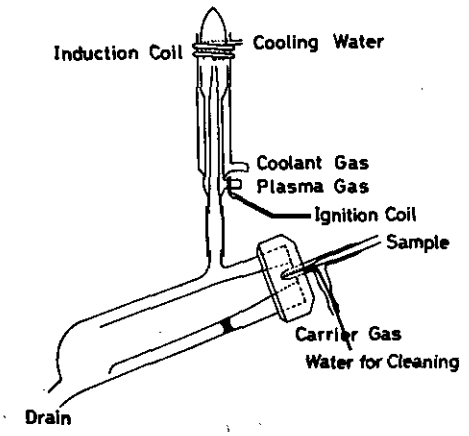

Fig. 4-1 ICP torch and glass concentric nebulizer

(Chapter 2), and its photograph is put on the first page of this report. The instrumentation is explained in detail in Chapter 2. An ICP source (Radiofrequency generator and ICP torch system), Model ICPQ-2H, was purchased from Shimadzu Seisakusho, Japan. A glass concentric nebulizer was used for the solution nebulization. Figure 4-1 shows the ICP torch assembly with the nebulizing system. The ICP was operated with the rf power of 1.6 KW at 27.12 MHz, feeding argon gas at 10.5 *l*/min, 1.5 *l*/min, and 1.0 *l*/min for the coolant, plasma and carrier gases, respectively. The sample uptake rate was ca. 3.6 *ml*/min at the present carrier argon flow rate. An observation height of 17 ± 2 mm above the rf load coil was used for all experiments. The slit height and slit width of the monochromator was usually fixed at 2 mm and 100 μm, respectively. Whenever necessary, the intensity of the ICP emission was attenuated by a sequentially adjustable filter. The emission signals were integrated for 4.1 s in the SIT-OMA system. Since one electronic scanning time in the SIT detector took 32.8 ms, the accumulation time of 4.1 s corresponded to 125 machine scanning cycles. This signal accumulation time was set to enable the comparison of the present data with those obtained by the flame emission-SIT detector system (Chapter 3), although arbitrary accumulation times were possible in the SIT-OMA system.

4-2-2 Analytical performance of the instrument

The sample and blank spectra were stored in memory [A] and memory [B] on the SIT-OMA system, respectively, when the sample solution and the blank solution (deionized water) were nebulized independently into the ICP source. The subtracted spectrum [A-B] provided the emission line(s) of the analyte in the sample solution. The emission intensity was obtained by noting the peak height and subtracting the average reading of the side background for 10 channels around the peak channel. The background noise level ([A-B] spectrum for the channel range 240–260) was obtained when distilled water was aspirated and subtraction of the [A] and [B] memories was performed. The detection limits in Table 4-1 were defined as the concentrations which represented an emission signal equivalent to twice the standard deviation of the background noise level. The values were obtained from the standard calibration curve for each element prepared by the least squares method. All the chemicals used were of analytical reagent grade and deionized water was used as the blank solution.

For comparison with a conventional PMT-based system, an ICP emission spectrometer, the Plasma AtomComp, from Jarrell Ash Division, Fisher Scientific Co., U.S.A. (which employed the direct reading method), was used for the measurements of the detection limits.

4-2-3 Matrix effect

For the study of matrix effects, matrix solutions were prepared by dissolving reagent grade $Ca(NO_3)_2$, $Mg(NO_3)_2$, $NaNO_3$, KNO_3, and $NH_4H_2PO_4$ in 0.1N HNO_3 (concentration 200 $\mu g/ml$). The Zn, V, Mo, Al, and Mn analytes were dissolved in each matrix solution and adjusted to 1 $\mu g/ml$ multielement solution. The multielement solution was analyzed by the 3 point standardized method (2-3-4).

For the study of the effect of various concentrations of Ca on Zn analysis, increasing amounts of Ca were added to the Zn solution. The zinc 1 $\mu g/ml$ solutions, which contained Ca at various concentrations of 100, 200, 300, 400, and, 500 $\mu g/ml$ were analyzed ten times repeatedly by the 3 point standardized method.

4-3 Results and discussion

4-3-1 ICP background correction

The emission spectrum of argon plasma is shown in Figure 4-2. The spectrum was observed at the plasma height of 17 mm above the rf coil with aspirating deionized water, where a photomultiplier was used as the detector. As can be seen in Figure 4-2, the emission spectrum of the argon plasma consists of emission lines of argon, emission bands of NO (200–280 nm), OH (280–330 nm), NH (336 nm), N_1^+ and CN (350–430 nm), and continuum background emission. According to a careful survey of the spectrum, the atomic lines due to cargon at 193.1 and 247.9 nm and hydrogen for the Balmer series at 656.3 nm(H_α), 486.1 nm(H_β), 434.0 nm(H_γ), 410.2 nm(H_δ), and 397.0 nm(H_ϵ) can be identified in Figure 4-2.

With respect to Zn, Cd, Bi, Cu, Mo, Mn, Cr, In, Sr, Ba, Na, and Li, the emission spectra for the sample and blank solutions and the subtracted spectra, which were observed by the SIT detector, are shown in Figures 4-3 – 4-6. The emission spectra for the sample solutions detected by the SIT detector included background line and band emissions caused by the plasma and analyte species, as is seen in the spectra for memory [A] in Figure 4-3 – 4-6. Fortunately, these background line and band emissions could be observed in memory [B], when the blank solution was aspirated. Therefore, in the SIT-OMA system, the emission signals which originated from only the analytes could be easily obtained by subtracting the background spectra in memory [B] from the spectra in memory [A]. This facility of the SIT-OMA system is very useful for the identification of spectral lines for background correction. The background correction procedure has already been described in section 2-2-2 b.

4-3-2 Evaluation of Radio Frequency Inductively Coupled Argon Plasma as an Excitation source for multielement analysis

The detection limits obtained by the present experimental intrumentation are summarized in Table 4-1, where the detection limits obtained by the N_2O-C_2H_2 flame emission-SIT detection system (Chapter 3) are also listed for comparison of the excitation efficiency of the ICP and nitrous oxide-acetylene flame. As was described in Chapter 3,

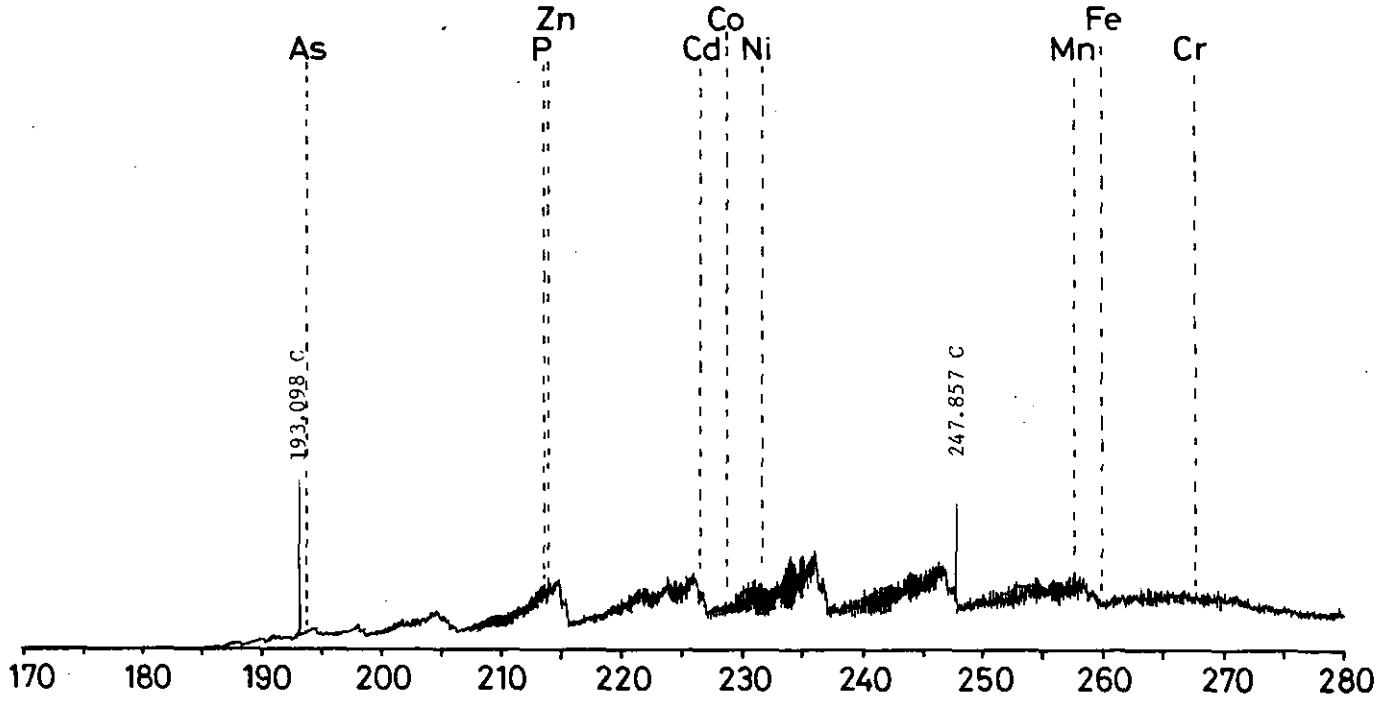

Fig. 4-2 Emission spectra of ICP source obtained by photomultiplier tube
Entrance and Exit slit height 5 mm, Entrance and Exit slit width 10 μm.
Plasma Conditions: Power 1.6 KW, Height 17 mm, Uptake rate 3.6 ml/min.

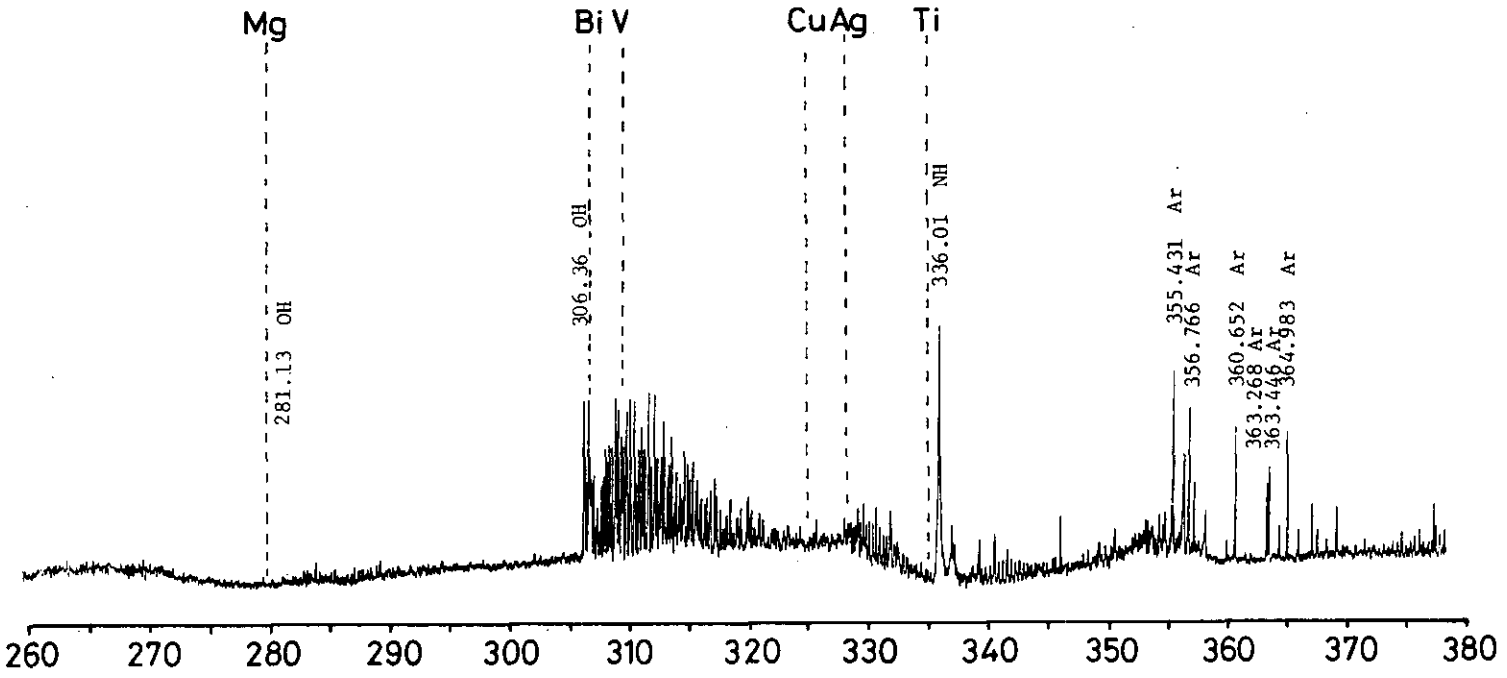

Fig. 4-2 (continued)

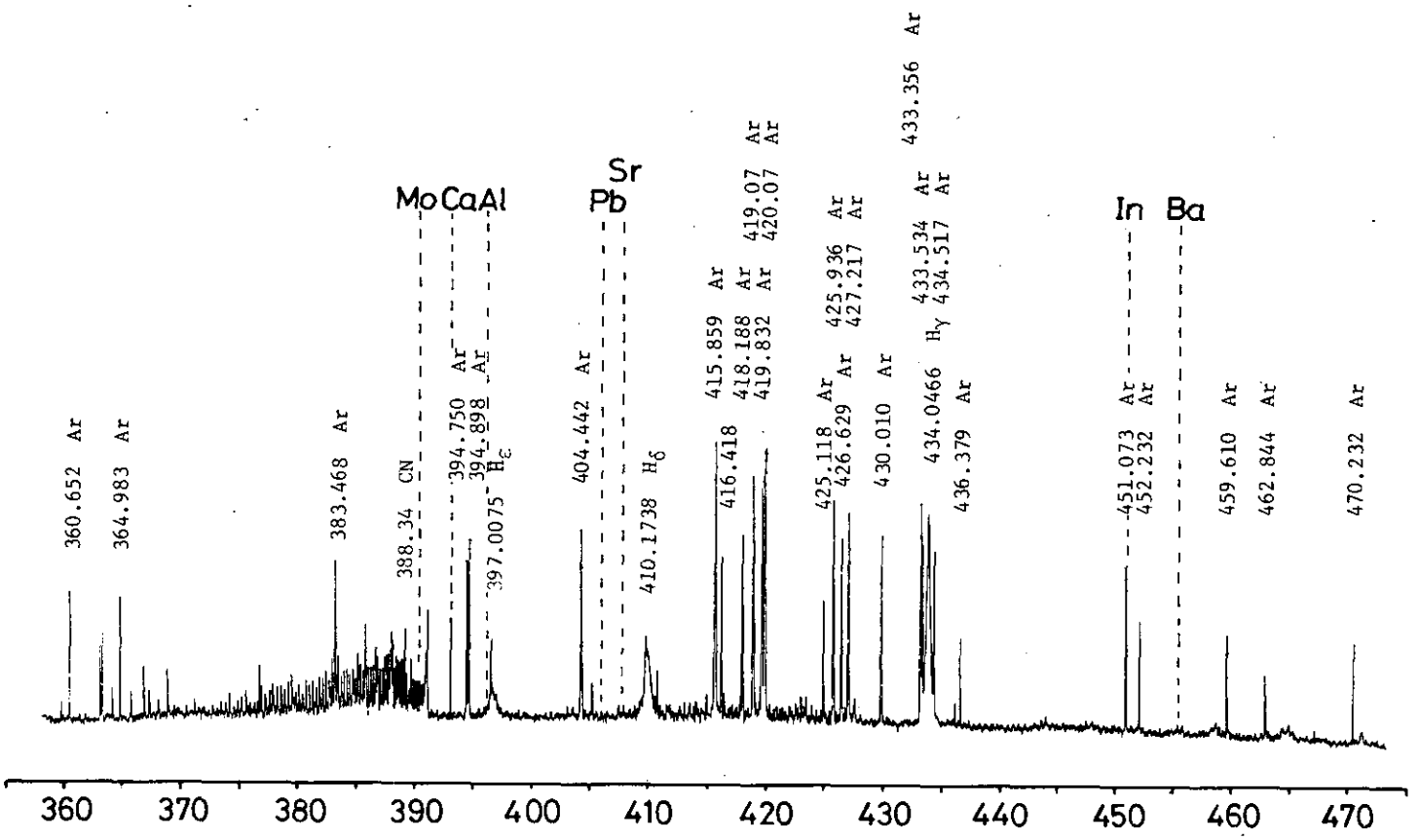

Fig. 4-2 (continued)

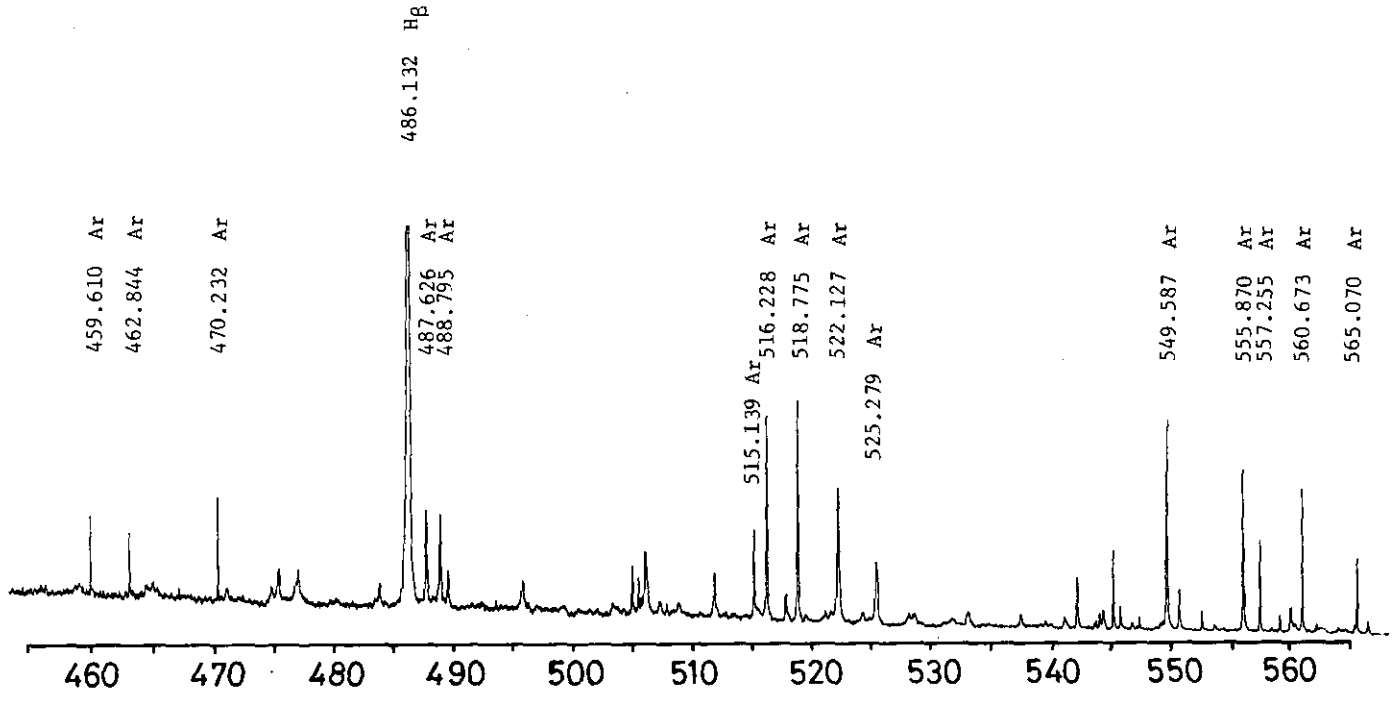

Fig. 4-2 (*continued*)

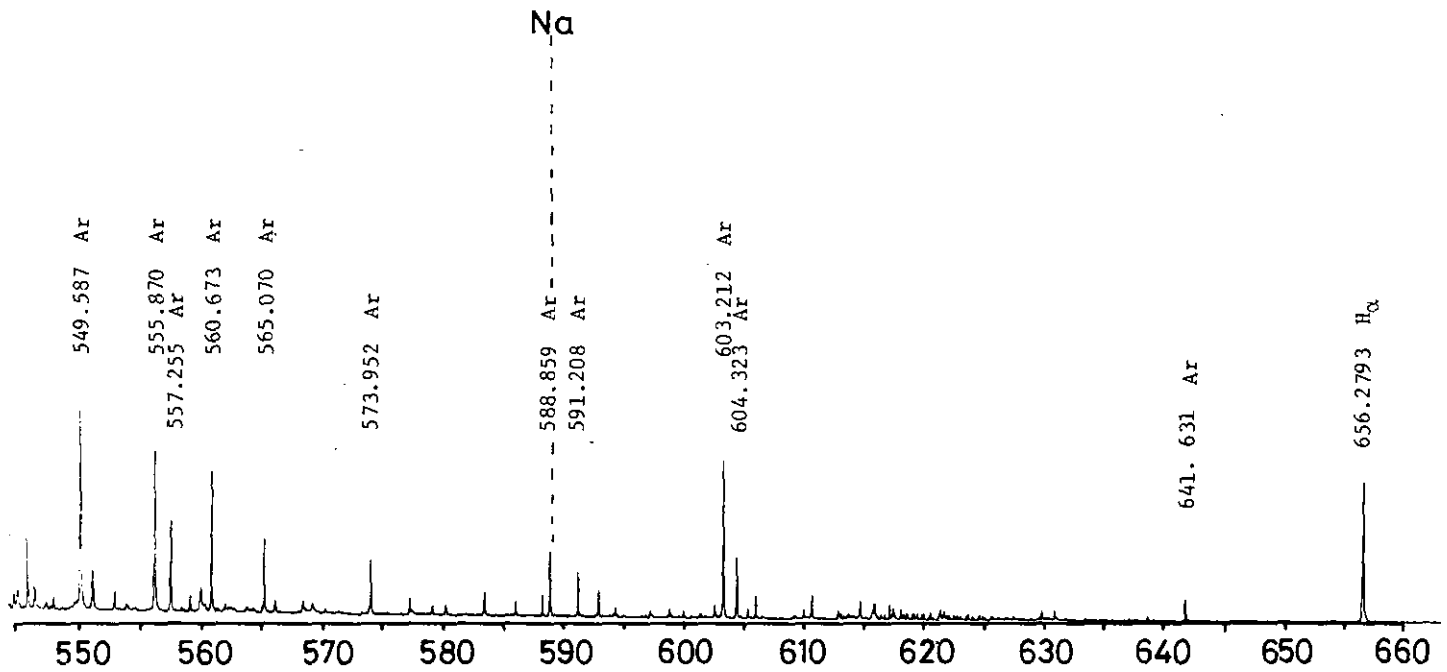

Fig. 4-2 (continued)

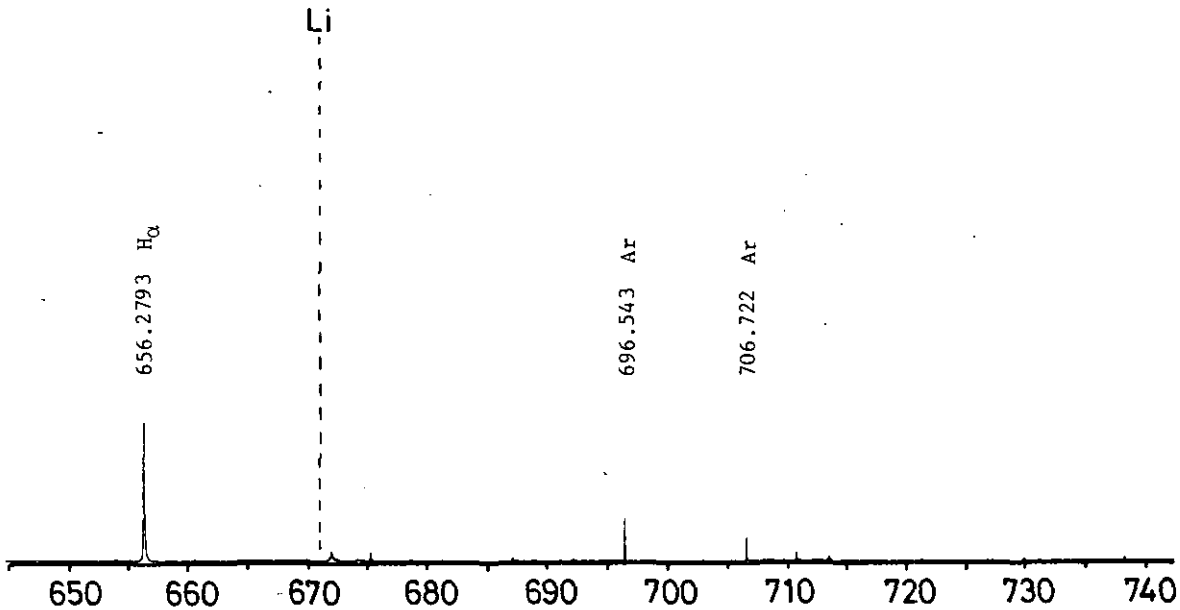

Fig. 4-2 (continued)

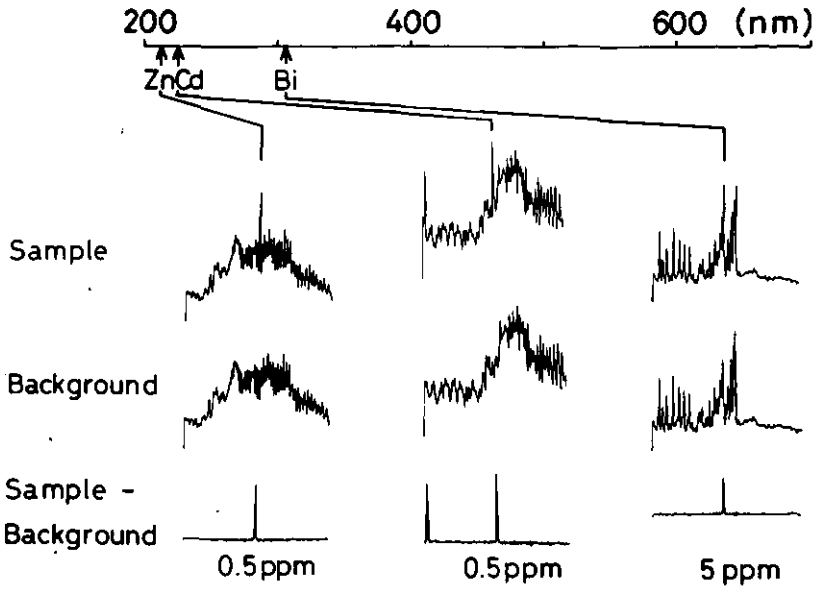

Fig. 4-3 Emission spectra observed by SIT-OMA system for Zn (213.9 nm), Cd (226.5 nm), and Bi (306.8 nm) (Zn 0.5 μg/ml, Cd 0.5 μg/ml, Bi 5 μg/ml)

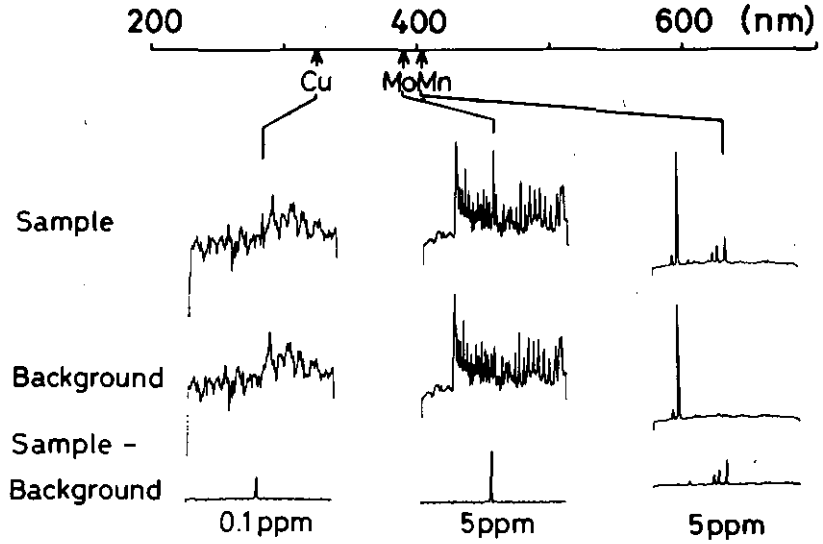

Fig. 4-4 Emission spectra observed by SIT-OMA system for Cu (324.8 nm), Mo (390.3 nm), and Mn (403.1 nm) (Cu 0.1 μg/ml, Mo 5 μg/ml, Mn 5 μg/ml)

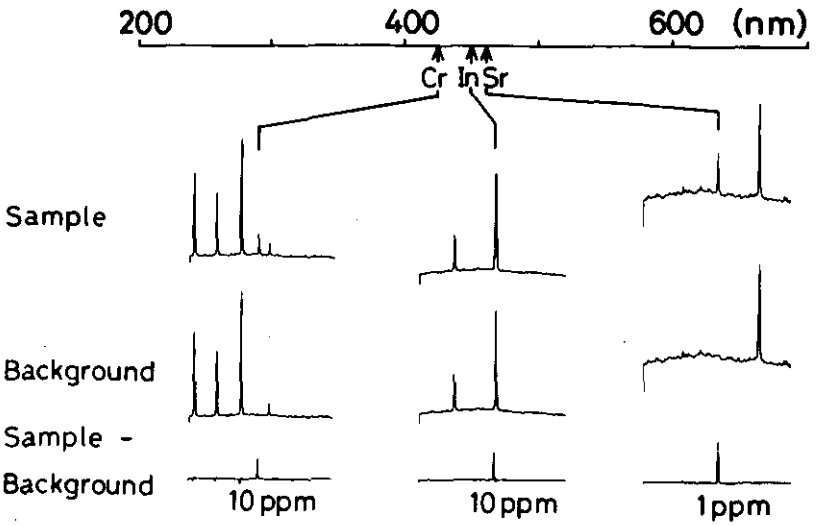

Fig. 4-5 Emission spectra observed by SIT-OMA system for Cr (425.4 nm), In (451.1 nm), and Sr (460.7 nm) (Cr 10 μg/m*l*, In 10 μg/m*l*, Sr 1 μg/m*l*)

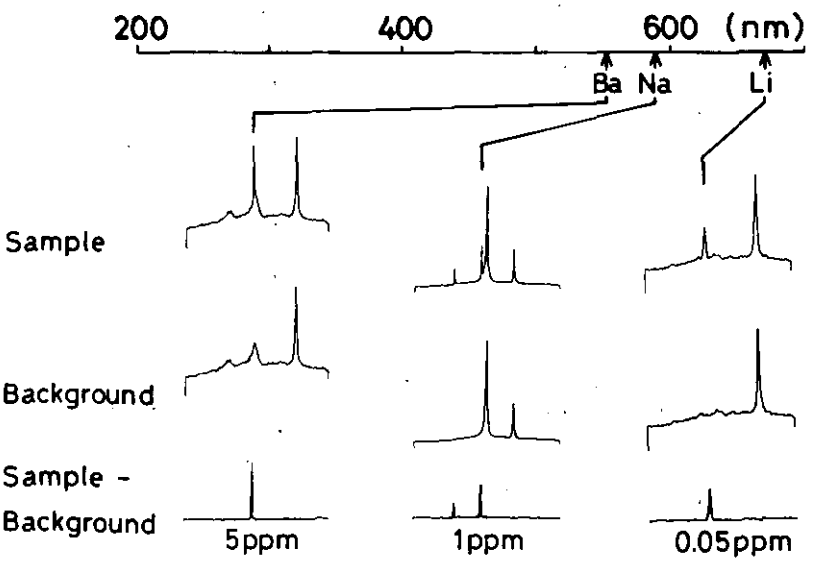

Fig. 4-6 Emission spectra observed by SIT-OMA system for Ba (553.6 nm), Na (589.0 nm), and Li (670.8 nm) (Ba 5 μg/m*l*, Na 1 μg/m*l*, Li 0.05 μg/m*l*)

the flame emission data were obtained under the same instrumental conditions and procedures as those in the present work, i.e., the same optical and detection system, and the same accumulation time (4.1 s). In order to show the difference of the excitation mechanisms in the two sources, for example, the emission spectra (corrected) for titanium observed near 365.4 nm in the nitrous oxcide-acetylene flame and the ICP are shown in Figure 4-7. As is well known, only atomic emission lines (Ti I) are observed in

Table 4-1 The detection limits of various elements obtained by the ICP and Flame emission spectrometry using a SIT detector

Element[a]	Ionization Potential eV	Wavelength nm	ICP[b] Detection Limits ($\mu g/ml$)	RSD[c] % ($\mu g/ml$)	Flame[d] Detection Limits ($\mu g/ml$)	Ratio of Detection Limits (Flame/ICP)
Ag	7.58	328.07	0.008	5.9 (0.5)	0.20	25
Al	5.99	308.22	0.12	–	–	
		396.15	0.036	2.95 (5.0)	0.041	1
As	9.81	193.70	0.63	–	–	–
Ba	5.21	553.56	0.061	–	0.060	
Ba II	10.00	455.40	0.0003	–	–	200
Bi	7.29	306.77	0.35	4.5 (1.0)	24	69
Ca	6.11	422.67	0.007	–	0.004	
Ca II	11.87	393.37	0.00004	–	–	100
Cd	8.99	228.80	0.013	–	–	
Cd II	16.91	226.50	0.008	–	–	–
Co	7.86	345.35	0.038	4.6 (5.0)	0.32	
Co II	17.06	228.62	0.016	7.7 (0.1)	–	20
Cr	6.77	425.43	0.11	3.1 (5.0)	0.005	
Cr II	16.50	267.72	0.010	–	–	0.5
Cu	7.73	324.75	0.005	6.9 (0.1)	0.083	17
Fe	7.87	371.99	0.073	5.8 (3.0)	0.15	
Fe II	16.18	259.94	0.003	8.4 (0.05)	–	50
In	5.79	451.13	0.33	6.6 (10)	0.013	0.04
K	4.34	404.41	45	–	3.8	
		404.72	21	–	–	0.2
Li	5.40	670.78	0.001	–	0.0001	0.1
Mg	7.65	285.21	0.004	3.4 (0.1)	0.24	
Mg II	15.04	279.55	0.0002	5.6 (0.001)	–	1200
Mn	7.44	403.08	0.080	3.3 (1.0)	0.021	
Mn II	15.64	257.61	0.0004	8.0 (0.005)	–	53
Mo	7.10	202.03	0.086	–	–	
		390.30	0.078	6.7 (5.0)	0.39	5
Na	5.14	589.00	0.006	–	0.0007	0.1
Ni	7.64	352.45	0.043	4.8 (1.0)	0.66	
Ni II	18.17	231.60	0.033	3.5 (0.5)	–	20

Table 4-1 (Continued)

Element[a]	Ionization Potential eV	Wavelength nm	ICP [b] Detection Limits ($\mu g/ml$)	RSD [c] % ($\mu g/ml$)	Flame [d] Detection Limits ($\mu g/ml$)	Ratio of Detection Limits (Flame/ICP)
P	10.49	213.62	0.25	–	–	
		214.91	0.40	–		–
Pb	7.42	405.78	0.26	3.0 (10)	0.35	
Pb II	15.03	220.35	0.33	7.6 (1.0)	–	1
Rb	4.18	420.19	59	–	2.0	0.03
Sn	7.34	284.00	0.67	–	–	
Sn II	14.63	189.99	1.40	–	–	–
Sr	5.70	460.73	0.013	–	0.0005	
Sr II	11.03	407.77	0.00009	–	–	6
Ti	6.82	365.35	0.23	6.7 (5.0)	0.30	
Ti II	13.58	334.90	0.002	5.1 (0.1)	–	150
V	6.74	437.92	0.077	3.2 (1.0)	0.025	
V II	14.65	292.40	0.006	–	–	
		309.31	0.005	3.1 (0.5)	–	5
Zn	9.39	213.86	0.015	3.1 (1.0)	–	–

a) II refers to ionic line.

b) This work, see text for definition.

c) Relative standard deviation calculated from 10 determinations.
Value in parenthesis is concentration at which determination was performed.

d) Previous work, nitrous oxide-acetylene flame (62).

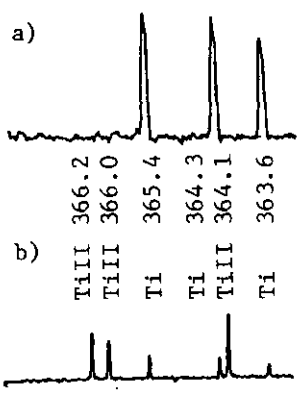

Fig. 4-7 Emission spectra obtained by SIT-OMA system near the Ti line in
(a) N_2O-C_2H_2 Flame
(b) ICP.

the case of flame excitation, while ionic emission lines (Ti II) as well as atomic lines are observed in the case of ICP excitation. In order to compare the emission sensitivities of atomic and ionic lines, the detection limits for both atomic and ionic lines are also shown in Table 4-1, when intense ionic lines are available in the usual UV and visible region. According to the detection limits summarized in Table 4-1, almost all elements, whose ionization potential is less than 9 eV, are ionized in the ICP, and ionic lines, if available, provide better detection limits for all the elements than atomic lines. The ratios of the best detection limits by ICP and flame emission spectrometry are shown in the final column of Table 4-1. It should be stressed here that the detection limits obtained with the ICP under a single set of compromised conditions are much better for most elements than those obtained with the flame under optimised conditions for each element. As the excitation temperature of the ICP is very high (5000–8000 K), Zn, Cd, and P, whose analytical lines are located in the UV region and are barely excited with the flame, can be measured by ICP emission spectrometry. The poorer detection limits for Cr, In, K, Li, Na, and Rb are exceptions, because these elements (except Cr) do not have intense ionic emission. In the case of Cr, intense emission lines of argon exist near the analytical line (Figure 4-5). The emission intensity must be attenuated by the filter to avoid the overflow, so that the detection performance for Cr becomes poor. Whereas, the background of the nitrous oxcide-acetylene flame around the Cr line is negligible as can be seen in Figure 3-4. These results show that the ICP is a more efficient excitation source compared to the nitrous oxide-acetylene flame. Consequently, it has been found that the detection limits at the ng/m*l* level or below can be obtained even with the SIT detector, when the ICP source is used for excitation.

The relative standard deviation (RSD) values were generally in the 3% range for the concentration equivalent to 50 times the detection limits. The RSD values are almost the same as those obtained by the N_2O-C_2H_2 flame. It implies that the detector noise to some extent contributes to the detection limits along with the fluctuation noise in the flame and plasma studies.

For the SIT detector the real-time dynamic range (real-time is a single scan) is about 750 counts for each channel as limited by the analog-to-digital converter of the OMA and this results in a dynamic range of about 3 orders of magnitude. If the output of the SIT was connected with the CPU directly, the dynamic range would be improved to over four orders of magnitude[124,125]

4-3-3 Spectral interference problems

In the past few years ICP emission spectrometry has been developed for simultaneous multielement analysis over wide concentration ranges, and applied to various kinds of samples (Chapter 5). With the progress of studies in ICP emission spectrometry, it has been found that spectral and physical (nebulization) interferences are serious problems in practical analysis by ICP emission spectometry, while chemical and ionization interferences are not serious. The spectral interference is investigated in this section.

The results of matrix effects are summarized in Table 4-2. The (A) column in Table 4-2 represents the data without side background correction and the (B) column represents the data with side background correction. The data should be 1 μg/m*l*. As ionization and chemical interference is not so severe in the ICP, Na, K, and P do not effect the analytical data. However, analytical results for the solution which contained Ca (200 μg/m*l*) and some results for the Mg matrix are high if side background correction is not performed. This is because of the scattered light from calcium and magnesium emission.

Table 4-2 Matrix effects of Ca, Mg, Na, K, and P – data with and without background correction

Matrix (μg/ml)	Zn		V						Mo	
	a	b	a			b			a	b
Ca 200	1.42	0.97	1.09	1.11	1.08	0.97	0.99	1.00	3.26	0.90
Mg 200	0.99	0.95	1.02	0.98	2.01	1.01	0.96	1.98	1.18	1.02
Na 200	0.96	0.93	1.00	0.99	1.00	0.99	0.98	0.99	1.10	0.97
K 200	0.96	0.93	1.03	0.99	1.02	1.02	0.98	1.00	0.97	1.10
P 200	1.02	0.99	1.00	0.99	1.00	0.99	0.98	0.99	1.05	1.03

Matrix (μg/ml)	Al				Mn					
	a		b		a			b		
Ca 200	2.81	3.69	0.87	1.22	3.47	2.54	2.04	0.62	0.91	0.99
Mg 200	0.97	0.90	0.98	0.91	1.45	0.98	2.04	1.00	0.89	1.02
Na 200	0.99	0.92	0.99	0.92	1.09	0.93	1.04	0.81	0.87	1.04
K 200	0.93	0.88	0.94	0.91	1.13	0.85	1.06	0.86	0.82	1.11
P 200	1.01	1.01	0.98	0.98	1.20	0.97	0.98	0.96	0.98	1.05

(1) Analytes (1 μg/ml) are dissolved in matrix solution (200 μg/ml).
(2) Results in μg/ml.
(3) a. (A – B) without side background correction
b. (A – B) – Side with side background correction
(4) Zn I 213.9nm
V II 311.1, 310.2, 309.3nm
Mo I 390.3nm
Al I 396.2, 394.4nm
Mn I 403.5, 403.3, 403.1nm

The degree of the effect is dependent on the wavelength and the sensitivity of the analyte. Figure 4-8 shows an example of the spectral interference. The lower case is the interference due to the stray light caused by the near scatter light of calcium: Standard solutions at the concentration of 5, 1, 0.5 μg/ml Al were used to measure Al 1 μg/ml which contained Ca 200 μg/ml. In Figure 4-8, only the [A-B] spectra are shown. If side background correction is not performed for Al 396.2 nm and Al 394.4 nm, both results become apparently high (2.81 μg/ml for 396.2 nm and 3.69 μg/ml for 394.4 nm). So far, Snellman et al., Skogerboe et al., Koirtyohann et al., and Kawaguchi et al. proposed wavelength scanning or modulation techniques[61,126-128] utilizing a refractor plate to correct the baseline shifts in the background. However, when the background has significant structure, such techniques would have limitations. Adding the further step of subtracting the ICP background in the SIT-based system may be very powerful for these techniques. Recently some attempts to reduce the effect of the enormous Ca emission have been

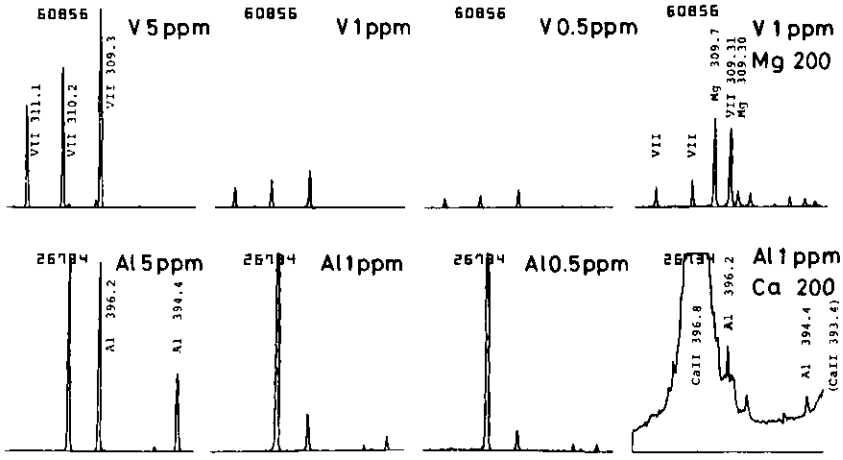

Fig. 4-8 Spectral interference
Upper: Line interference from Mg on V.
Lower: Stray light interference from Ca on Al.

reported. To reduce the calcium emission, band rejection filters[129,130] or an absorption cell[131] are installed between the source and the spectrometer. In the case of the direct reading system, the fitting of broad band pass filter to individual PM tube or the use of solar blind PM tube for the shorter wavelength elements can minimize the stray light[132] However it is difficult to eliminate the strong emission and the stray light selectively and completely with any devices so far used.

As can be seen in Table 4-2, almost all results for vanadium are good after side background correction except the result of the V 309.3 nm line for the sample which contained Mg 200 μg/m*l*. It is due to spectral line interference of the Mg line at 309.30 nm. The spectra obtained by the 3 point standardized method are shown in Figure 4-8 (upper side), where only the [A-B] spectra are shown. By selecting another vanadium line, spectral line interference is avoided.

In Figure 4-9 the effect of increasing Ca concentration on Zn (1 μg/m*l*) is illustrated. If side background correction was not performed, the analytical error would occur as shown in Table 4-3. However side background correction may achieve accurate analysis. Analytical results and standard deviations were not changed remarkably even if the concentration of calcium was increased (Table 4-4).

4-3-4 Comparison of Silicon Intensified Target (SIT) and Photomultiplier Tube (PMT)

These days the direct reading method with PMT has found widespread use on a commercial basis. In general, the response (usually quantum yield) of the SIT detector is almost the same as or better than the PMT above 380 nm and poorer than the PMT below 380 nm[133] (These features of the SIT and PMT are represented in Figure 2-7). In order to compare the spectral responsibity of the SIT and PMT, the detection limits obtained with the PMTs which were measured with a commercial ICP direct reader system, are also shown in Table 4-5. Although the results listed in Table 4-5 cannot be compared directly because the operating conditions are different, the detection limits obtained with the SIT generally reflect the poorer spectral responsibity of the SIT in the UV region. That

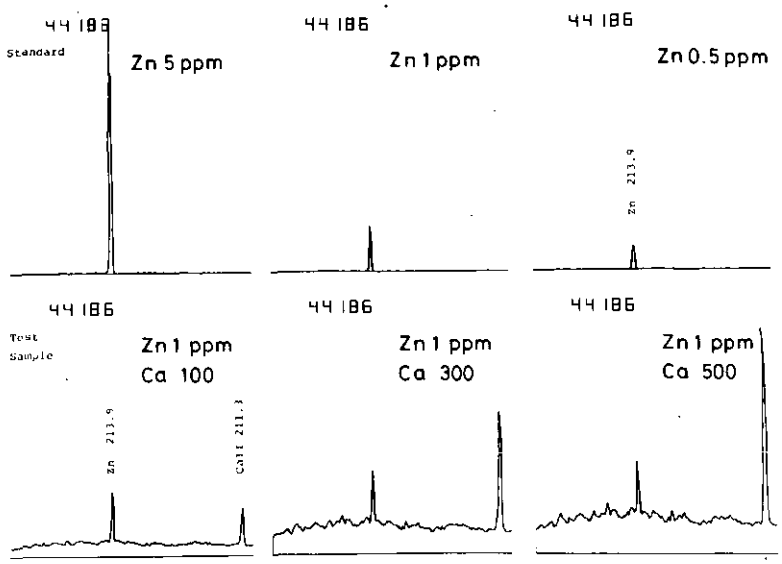

Fig. 4-9 Effect of far scatter light from Ca Emission

Table 4-3 Matrix effect of increasing Ca concentration

Matrix (μg/ml)	Zn	
	a	b
Ca 0	1.00	1.00
Ca 100	1.29	1.00
Ca 200	1.49	0.99
Ca 300	1.67	1.01
Ca 400	1.87	1.11
Ca 500	1.83	1.02

(1) Analyte Zn (1 μg/ml) is dissolved in calcium matrix solutions (0, 100, 200, 300, 400, and 500 μg/ml).
(2) Results in μg/ml.
(3) a. (A – B) without side background correction.
b. (A – B) – Side with side background correction.
(4) Zn I 213.9 nm.

Table 4-4 Effect of calcium matrix on the intensity and precision of Zn analysis

		A	B	A−B	Side	(A−B) −Side	
		1203	1191	12	1	11	−0.03
ICP	off	36	29	15		17	−
		2.95	2.46	−		−	−
Zn	1 ppm	16900	10232	6669	−9	6678	1.00
Ca	0 ppm	214	96	216		210	0.031
		1.27	0.94	3.24		3.15	3.12
Zn	1 ppm	23900	12822	11078	2679	8398	0.97
Ca	100 ppm	292	202	355		350	0.041
		1.22	1.57	3.20		4.16	4.19
Zn	1 ppm	22443	10986	11457	4390	7068	0.97
Ca	200 ppm	302	229	188		183	0.026
		1.35	2.09	1.64		2.59	2.65
Zn	1 ppm	24475	11389	13086	5629	7457	1.00
Ca	300 ppm	179	139	279		260	0.036
		0.73	1.22	2.13		3.48	3.64
Zn	1 ppm	28337	12403	15934	6855	9079	1.10
Ca	400 ppm	437	164	343		293	0.037
		1.54	1.32	2.15		3.48	3.34
Zn	1 ppm	28401	12701	15700	7667	8033	0.94
Ca	500 ppm	223	165	234		196	0.023
		0.79	1.30	1.49		2.40	2.47

Upper: Average of 10 measurements (counts)
Middle: Standard deviation obtained by 10 measurements (counts)
Lower: Relative Standard Deviation (%)

is, by using the SIT, poorer detection limits by about one order of magnitude (maximum) were achieved for the elements with the UV lines, when compared to those achieved by the PMTs. However, since the SIT gives the detection limits at the ng/m*l* level for many elements, as mentioned in 4-3-2, it is quite useful as the detector for ICP emission spectrometry. The spectral responsibity of the SIT may be improved by using a more efficient UV sensitizer which is equipped in the front window of the SIT (2-2-2). Furthermore, the detection limits obtained with the SIT may be improved by reducing the dark current and shot noises of the SIT, which may be realized by cooling the SIT detector. Also signal integration and accumulation times may be used to improve detection limits.

The SIT detector has excellent facility for simultaneous multielement detection as has been reported by many workers. The facility of the SIT to perform side background correction is also helpful to get accurate analytical data by measuring the ICP background subtracted [A-B] spectrum. On considering these additional facilities of the SIT detector as well as high detection limits for many elements, the SIT detector performance is useful in ICP emission spectrometry.

Table 4-5 Comparison of the detection limits obtained with the SIT and PMT in ICP emission spectrometry

Element[a]	Wavelength	Detection Limits[b] (μg/ml)		Ratio of Detection Limits (SIT/PMT)
	nm	SIT	PMT	
Sn II	189.99	1.4	0.021	67
As	193.70	0.63	0.020	32
Mo	202.03	0.086	0.005	17
Zn	213.86	0.015	0.001	15
P	214.91	0.40	0.05*	8
Pb II	220.35	0.33	0.03	11
Co II	228.62	0.016	0.002	8
Cd	228.80	0.013	0.001*	13
Ni II	231.60	0.033	0.006	6
Mn II	257.61	0.0004	0.0006*	1
Fe II	259.94	0.003	0.002	2
Cr II	267.72	0.010	0.003	3
Mg II	279.55	0.0002	0.00007	3
V II	292.40	0.006	0.002	3
Al	308.22	0.12	0.012	10
Cu	324.75	0.005	0.0008	6
Ag	328.07	0.008	0.001	8
Ti II	334.90	0.002	0.0005	4

Operating Conditions:
SIT-based System: Power 1.6 KW, Obs. Ht 17 mm, Sample Uptake Rate 3.6 ml/min.
PMT-based System: Power 1.1 KW, Obs. Ht 19 mm, Sample Uptake Rate 1.0 ml/min.
a) II refers to ionic line.
b) Detection limit definition, see text. PMT integration time, 10 s.
* Measured in second order.

CONCLUSION

The advantages and disadvantages of the developed instrument are summarized as follows:

[Advantages]

1. By employing the ICP source, high detection limits at the ng/m*l* levels can be obtained at a single set of compromised operating conditions. The relative standard deviation is about in the 3% range for the concentration equivalent to 50 times the detection limit.
2. Programmable monochromator of the slew scan type has more flexibility for multielement detection than the well-established direct reading system where only fixed wavelengths of the desired elements are available.
3. Accurate monochromator wavelength setting is not required as in the case of the PMT, since a 5 nm wavelength range is measured simultaneously with the SIT, so that rapid sequential slew scanning is possible. It takes about 2 minutes to analyze for a few elements in 1 spectral window so that for the determination of say 10 elements by the slew scan technique approximately 5 to 10 minutes are required.
4. Simultaneous multielement analysis is possible if the element lines are within a 5 nm wavelength range.
5. The ICP background correction is readily performed and the analysis procedure is performed conveniently by the background corrected spectrum [A − B].
6. Background shifts at the analytical wavelength due to matrix constituents of the sample can be corrected for by side background subtraction.

[Disadvantages]

1. The sequential slew scan method requires a longer time than the direct reading method for multielement analysis.
2. The quantum efficiency of the SIT detector is poorer than that of the PMT in the UV region (below 380 nm).
3. The resolution power of the SIT is poorer than that obtained by the PMT (Figure 2-2).

Detection limits for many elements are compared favorably with PMT values except in the low UV region (<240 nm) where deterioration by one order of magnitude could occur. Although various approaches may be used to improve detection limits, e.g., detector cooling, increased integration and accumulation time, or ultrasonic nebulization, the present detection performance is considered to be satisfactory for trace analysis. The application of the present system (ICP−Programmable monochromator−SIT-OMA detector) to rapid sequential multielement analysis is in progress. Correction for background shifts associated with the major matrix components of real samples is an area in ICP emission spectrometry currently receiving much interesting. The SIT image detector facilitates such a background correction. The results of the study will be reported in the near future.

ACKNOWLEDGEMENTS

I am grateful to Professor K. Fuwa for giving me the opportunity and encouragement to perform this study. I wish to thank Assistant Professor H. Haraguchi and Dr. C. W. McLeod for invaluable suggestions and comments during the programme. Encouragement and support by members of Division of Chemistry and Physics, particularly Dr. A. Otsuki, deserves special mention.

REFERENCES

1. Japan Industrial Standards (1978). Methods for Chemical Analysis of Water and Wastes, Environ. Prot. Agency, Cincinati, Ohio (1979) (EPA-6004-79-020). American Society for Testing and Materials (ASTM) Part 23 (1970).
2. Furr, A.K., A.W. Lawrence, S.S.C. Tong, M.C. Grandolfo, R.A. Hofstader, C.A. Bache, W.H. Gutenmann, and D.J. Lisk (1979): Multielement and Chlorimated Hydrocarbon Analysis of Municipal Sewage Sludges of American Cities. Environ. Sci. Technol., **10**, 683-687.
3. Sommers L.E. (1977): Chemical Composition of Sewage Sludges and Analysis of Their Potential Use as Fertilizers. J.Environ. Qual., **6**, 232-233.
4. Capar, S.G., J.T. Tanner, M.H. Friedman, and K.W. Boyer (1978): Multielement Analysis of Animal Feed, Animal Wastes, and Sewage Sludge. Environ. Sci. Technol., **12**, 785-790.
5. Furr, A.K., W.C. Kelly, C.A. Bache, W.H. Gutenmann, and D.J. Lisk (1976): Multielement Absorption by Crops Grown in Pots on Municipal Sludge-Amended Soil. J. Agric. Food Chem., **24**, 889-892.
6. Kirkham, M.B. (1975): Trace Elements in Corn Grown on Long-Term Sludge Disposal Site. Environ. Sci. Technol., **9**, 765-768.
7. Brown, J.C., J.E. Ambler, R.L. Chaney, and C.D. Foy in Micronutrients in Agriculture. J.J. Mortvedt, P.M. Giordano, W.L. Lindsay, Eds, Soil Sci. Soc. Amer., Inc., Madison, Wis. (1972), pp 389-418.
8. Hinesly, T.D., R.L. Jones, E.L. Ziegler, and J.J. Tyler (1977): Effect of Annual and Accumulative Applications of Sewage Sludge on Assimilation of Zinc and Cadmium by Corn (Zea mays L.). Environ. Sci. Technol., **11**, 182-188.
9. Parizek, J. (1957): The Destructive Effect of Cadmium Ion on Testicular Tissue and Its Prevention by Zinc. J. Endocrinol., **15**, 56-63.
10. Schroeder, H.A. and J. Buckman (1967): Cadmium Hypertension. Its Reversal in Rats by a Zinc Chelate. Arch. Environ. Health, **14**, 693-697.
11. Furr, A.K., G.S. Stowsand, C.A. Bache, and D.J. Lisk (1976): Study of Guinea Pigs Fed Swiss Chard Grown on Municipal Sludge-Amended Soil. Multi-Element Content Tissues. Arch. Environ. Health, **31**, 87-91.
12. Parizek, J., I. Ostadalova, I. Benes, and A. Babicky (1968): Pregnancy and Trace Elements: The Protective Effect of Compounds of an Essential Trace Element-Selenium-Against the Peculiar Toxic Effects of Cadmium during Pregnancy. J. Reprod. Fert., **16**, 507-509.
13. Parizek, J. and I. Ostadalova (1967): The Protective Effect of Small Amounts of Selenite in Sublimate Intoxication. Experientia, **23**, 142-143.
14. Stoewsand, G.S., C.A. Bache, and D.J. Lisk (1974): Dietary Selenium Protection of Methylmercury Intoxication of Japanese Quail. Bull. Environ. Contam. Toxicol., **11**, 152-156.
15. Wada, O., N. Yamaguchi, T. Ono, M. Nagahashi, and T. Morimura (1976): Inhibitory Effect of Mercury on Kidney Glutathione Peroxidase and Its Prevention by Selenium. Environ. Research, **12**, 75-80.
16. Dulka, J.J., and T.H. Risby (1976): Ultratrace Metals in Some Environmental and

Biological Systems. Anal. Chem., **48**, 640A-653A.
17. Bush, K.W., and G.H. Morrion (1973): Multielement Flame Spectroscopy. Anal. Chem., **45**, 712A-722A.
18. Winefordner, J.D. (1976): Trace Analysis. Spectroscopic Methods for Elements. John Wiley & Sons, New York.
19. Giles, I.S., C. Olivier, and M. Peisach (1977): Recent Developments in the Analytical Application of Prompt Spectrometry. J. Radioanal. Chem., **37**, 141-154.
20. Morrison, G.H. (1965: Trace Analysis—Physical Methods. Interscience, New York, N.Y.
21. Gray, A.L. (1975): Mass-Spectrometric Analysis of Solutions Using an Atmospheric Pressure Ion Source. Analyst, **100**, 298-299.
22. Flato, J.B. (1972): The Renaissance in Polarographic and Voltammetric Analysis. Anal. Chem., **44**, 75A-87A.
23. Bertin, E.P. (1970): Principles and Practices of X-Ray Spectrometric Analysis. Plenum Press, New York, N.Y.
24. Birks, L.S. (1969): X-Ray Spectrochemical Analysis. 2nd Ed., Interscience, New York, N.Y.
25. Campbell, J.L., B.H. Orr, A.W. Herman, L.A. McNelles, J.A. Thomson, and W.B. Cook (1975): Trace Element Analysis of Fluids by Proton-Induced X-Ray Fluorescence Spectrometry. Anal. Chem., **47**, 1542-1553.
26. Fassel, V.A. and R.N. Kniseley (1974): Inductively Coupled Plasma—Optical Emission Spectroscopy. Anal. Chem., **46**, 1110A-1120A.
27. Eckert, H.U. (1974): The Induction Arc: A State-of-the Art Review. High Temp. Sci., **6**, 99-134.
28. McCormack, A.J., S.C. Tong, and W.D. Cooke (1965): Sensitive Selective Gas Chromatography Detector Based on Emission Spectrometry of Organic Compounds. Anal. Chem., **37**, 1470-1476.
29. Beenakker, C.I.M. (1977): Evaluation of a Microwave-induced Plasma in Helium at Atmospheric Pressure as an Element-Selective Detector for Gas Chromatography. Spectrochim. Acta, **32B**, 173-187.
30. Fassel, V.A. and R.N. Kniseley (1974): Inductively Coupled Plasma. Anal. Chem., **46**, 1155A-1164A.
31. Fassel, V.A. (1977): Current and Potential Applications of Inductively Coupled Plasma (ICP)—Atomic Emission Spectroscopy (AES) In the Exploration, Mining, and Processing of Materials. Pure Appl. Chem., **49**, 1533.
32. Mermet, J.M. (1975): Spectroscopic Atomique—Sur les Mécanismes d'Excitation des Éléments Introduits Dans un Plasma HF d'Argon. Note(*) de M. Compt. Rend. Acad. Sci., Ser. B, **281**, 273.
33. Boumans, P.W.J.M. and F.J. de Boer (1977): An Experimental Study of a 1-KW, 50-MHz RF Inductively Coupled Plasma with Pneumatic Nebulizer, and a Discussion of Experimental Evidence for a Non-Thermal Mechanism. Spectrochim. Acta, **32B**, 365-395.
34. Edmonds, T.E. and G. Horlick (1977): Spatial Profiles of Emission from an Inductively Coupled Plasma Source Using a Self-Scanning Photodiode Array. Appl. Spectrosc., **31**, 536-541.
35. Babat, G.I. (1947): Electrodeless Discharges and Some Applied Problems. J. Inst. Elec. Eng. (London), **94**, 27.
36. Reed, T.B. (1961): Induction-Coupled Plasma Torch. J. Appl. Phys., **32**, 821-824.

37. Reed, T.B. (1962): Plasma Torches, Int. Sci. Technol., **6**, 42 .
38. Reed, T.B. (1961): Growth of Refractory Crystals Using the Induction Plasma Torch. J. Appl. Phys., **32**, 2534.
39. Greenfield, S., I.L. Jones, and C.T. Berry (1964): High-pressure Plasma as Spectroscopic Emission Sources. Analyst, **89**, 713-720.
40. Wendt, R.H. and V.A. Fassel (1965): Induction-Coupled Plasma Spectrometric Excitation Source. Anal. Chem., **37**, 920-922.
41. Scott, R.H., V.A. Fassel, R.N. Kniseley and D.E. Nixon (1974): Inductively Coupled Plasma-Optical Emission Analytical Spectrometry. Anal. Chem., **46**, 75-80.
42. Boumans, P.W.J.M. and F.J. de Boer (1975): Studies of an Inductively-Coupled High-Frequency Argon Plasma for Optical Emission Spectrometry—II. Compromise Conditions for Simultaneous Multielement Analysis. Spectrochim. Acta, **30B**, 309-334.
43. Greenfield, S., I.L.W. Jones, C.T. Berry, and L.G. Bunch (1965): The High-frequency Torch: Some Facts, Figures and Thoughts. Proc. Soc. Anal. Chem., **2**, 111.
44. Dickinson, G.W. and V.A. Fassel (1969): Emission Spectrometric Detection of the Elements at the Nanogram per Milliliter Level Using Induction-Coupled Plasma Excitation. Anal. Chem., **41**, 1021-1024.
45. Olson, K.W., W.J. Haas, Jr., and V.A. Fassel (1977): Multielement Detection Limits and Sample Nebulization Efficiencies of an Improved Ultrasonic Nebulizer and a Conventional Preumatic Nebulizer in Inductively Coupled Plasma-Atomic Emission Spectrometry. Anal. Chem., **49**, 632-637.
46. Gaydon, A.G. (1968): Dissociation Energies and Spectra of Diatomic Molecules. 3rd Ed., Chapman & Hall, London.
47. Brody, S.S. and J.E. Chaney (1966): Flame Photometric Detector, The application of a specific detector for phosphorus and for sulfur compounds-sensitive to sub-nanogram quantities. J. Gas Chromat., **4**, 42-46.
48. Pickett, E.E. and S.R. Koirtyohann (1969): Emission Flame Photometry—A New Look at an Old Method. Anal. Chem., **41**, 28A-42A.
49. Christian, G.D., and F.J. Feldman (1971): A Comparison Study of Detection Limits Using Flame-Emission Spectroscopy with the Nitrous Oxide-Acetylene Flame and Atomic-Absorption Spectroscopy. Appl. Spectrosc., **25**, 660-663.
50. Boumans, P.W.J.M. and F.J. de Boer (1972): Studies of Flame and Plasma Torch Emission for Simultaneous Multi-element Analysis—I Preliminary Investigations. Spectrochim. Acta, **27B**, 391-414.
51. Kirkbright, G.F. and A.F. Ward (1974): Atomic-Emission Spectrometry with an Induction-Coupled High-Frequency Plasma Source. Comparison with the inert-gas shielded premixed nitrous oxide acetylene flame for multi-element analysis. Talanta, **21**, 1145-1165.
52. Winefordner, J.D., R. Avni, T.L. Chester, J.J. Fitzgerald, L.P. Hart, D.J. Johnson, and F.W. Plankey (1976): A Comparison of Signal-to-Noise Ratios for Single Channel Methods (Sequential and Multiplex) vs Multichannel Methods in Optical Spectroscopy. Spectrochim. Acta, **31B**, 1-19.
53. Winefordner, J.D., J.J. Fitzgerald, and N. Omenetto (1975): Review of Multielement Atomic Spectroscopic Methods. Appl. Spectrosc., **29**, 369-383.
54. Santini, R.E., M.J. Milano, and H.L. Pardue (1973): Rapid Scanning Spectroscopy: Prelude to a New Era in Analytical Spectroscopy. Anal. Chem., **45**, 915A-927A.
55. Meaburn, J. (1975): Spectrometers Working on the Same Extensive Continuum Source; an estimation of the relative performances of eight instruments. Appl. Opt.,

14, 2521-2526.
56. Johnson, D.J., F.W. Plankey, J.D. Winefordner (1974): Analysis of Wear Metals in Jet Engine Oils via Atomic Fluorescence Flame Spectrometry with a Continuum Source. Can. J. Spectrosc., **19**, 151-152.
57. Furuta, N., H. Haraguchi, and K. Fuwa (1977): Multielement Analysis by Continuum Source Atomic Absorption Spectrometry with the Aid of Analog Data Treatment. Anal. Chem., **49**, 1263-1265.
58. Cordos, E. and H.V. Malmstadt (1973): Programmable Monochromator for Accurate High Speed Wavelength Isolation. Anal. Chem., **45**, 425-433.
59. Spillman, R.W. and H.V. Malmstadt (1976): Computer-Controlled Programmable Monochromator System with Automated Wavelength Calibration and Background Correction. Anal. Chem., **48**, 303-311.
60. Johnson, D.J., F.W. Plankey, and J.D. Winefordner (1975): Multielement Analysis via Computer-Controlled Rapid-Scan Atomic Fluorescence Spectrometer with a Continuum Source. Anal. Chem., **47**, 1739-1743.
61. Kawaguchi, H., M. Okada, T. Ito, and A. Mizuike (1977): Computer-Controlled Programmable Monochromator with Repetitive Optical Scanner for Accurate Peak Detection and Background Correction. Anal. Chem. Acta, **95**, 145-152.
62. Furuta, N., C.W. McLeod, H. Haraguchi and K. Fuwa (1979): Use of a Programmable Monochromator and SIT Detector in Flame Atomic Emission Spectrometry. Bull. Chem. Soc. Japan, **52**, 2913-2917.
63. Furuta, N., C.W. McLeod, H. Haraguchi and K. Fuwa (1980): Evaluation of a SIT Image Detector for Inductively Coupled Plasma Emission Spectrometry. Appl. Spectrosc., in press.
64. Marshall, A.G. and M.B. Comisarow (1975): Fourier and Hadamard Transform Methods in Spectroscopy. Anal. Chem., **47**, 491A-504A.
65. Horlick, G.H. and W.K. Yuen (1975): With a Fourier Transform Spectrometer. Anal. Chem., **47**, 775A-781A.
66. Yuen, W.K. and G. Horlick (1977): Atomic Spectrochemical Measurement with a Fourier Transform Spectrometer. Anal. Chem., **49**, 1446-1448.
67. Horlick, G. and W.K. Yuen (1978): A Modular Michelson Interferometer for Fourier Transform Spectrochemical Measurements from the Mid-infrared to the Ultraviolet. Appl. Spectrosc., **32**, 38-46.
68. Chester, T.L. and J.D. Winefordner (1977): Analytical Capabilities of the Selectively Modulated Interferometric Dispersive Spectrometer. Anal. Chem., **49**, 113-118.
69. Mamiya, M. (1975): Polarization Interferometric Fourier Transform Ultraviolet-Visible-Near Infrared Spectrometer System. Bunseki Kagaku, **24**, 629-635.
70. Plankey, F.W., T.H. Glenn, L.P. Hart, and J.D. Winefordner (1974): Hadmard Spectrometer for Ultraviolet-Visible Spectrometry. Anal. Chem., **46**, 1000-1005.
71. Tai, M.H., D.A. Briotta, Jr., N.S. Kamath, and M. Harwit (1975): Practical Multi-spectrum Hadamard Transform Spectrometer. Appl., Opt., **14**, 2533-2536.
72. Keir, M.J., J.B. Dawson, and D.J. Ellis (1977): Multielement Atomic Absorption Analysis Using Hadamard Transform Spectroscopy with a New Computation and Superposition Procedure. Spectrochim. Acta, **32B**, 59-69.
73. Talmi, Y. (1975): Applicability of TV-Type Multichannel Detectors to Spectroscopy. Anal. Chem., **47**, 658A-670A.
74. Talmi, Y. (1975): TV-Type Multichannel Detectors. Anal. Chem., **47**, 697A-709A.
75. Golightly, D.W., R.N. Kniseley, and V.A. Fassel (1970): The Image-Dissector Photo-

multiplier as a Detector in a Rapid Scanning Approach to Direct-Reading Analytical Emission Spectrometry. Spectrochim. Acta, **25B**, 451-464.
76. Danielsson, A. and P. Lindblom (1972): An Echelle Spectrograph for Image Tubes. Physica Scripta, **5**, 227-231.
77. Danielsson, A., P. Lindblom, and E. Soderman (1974): Image Dissector Echelle Spectrometer System for Spectrochemical Analysis. Chemica Scripta, **6**, 5-9.
78. Felkel, H.L., Jr. and H.L. Pardue (1978): Simultaneous Multielement Determination by Atomic Emission with an Echelle Spectrometer Interfaced to Image Dissector and Silicon Vidicon Tubes. Anal. Chem., **50**, 602-610.
79. Felkel, H.L., Jr. and H.L. Pardue (1978): Evaluation of an Echelle Spectrometer/Image Dissector System for Simultaneous Multielement Determinations by Atomic Absorption Spectroscopy. Clin. Chem., **24**, 602-610.
80. Knapp, D.O., N. Omenetto, L.P. Hart, F.W. Plankey, and J.D. Winefordner (1974): Simultaneous Multi-element Atomic Emission Flame Spectrometry with an Image Vidicon Detector. Anal. Chim. Acta, **69**, 445-460.
81. Wood, D.L., A.B. Dargis, and D.L. Nash (1975): A Computerized Television Spectrometer for Emission Analysis. Appl. Spectrosc., **29**, 310-315.
82. van der Piepen, H., C. Claase, and D.B. de Villiers (1976): A Vidicon Spectrometer and Its Application to the Analysis of Gold. Spectrochim. Acta, **31B**, 389-398.
83. Mitchell, D.G., K.W. Jackson, and K.M. Aldous (1973): Application of a Silicon-Target Vidicon Detector to Simultaneous Multielement Flame Spectrometry. Anal. Chem., **45**, 1215A-1223A.
84. Talmi, Y., D.C. Backer, J.R. Jadamec, and W.A. Saner (1978): Fluorescence Spectrometry with Optoelectronic Image Detector. Anal. Chem., **50**, 936A-952A.
85. Fry, P.W. (1975): Silicon Photodiode Arrays. J. Phys. E, **8**, 337-349.
86. Boumans, P.W.J.M., R.F. Rumphorst, L. Willensen, and F.J. de Boer (1973): Solid State Photodiode System Matched to High-gain Low-noise D.C. and Lock-in Amplifiers for Use in Multichannel Emission Spectrochemical Analysis. Spectrochim. Acta, **28B**, 227-240.
87. Horlick, G. and E.G. Codding (1973): Some Characteristics and Applications of Self-Scanning Linear Silicon Photodiode Arrays as Detector of Spectral Information. Anal. Chem., **45**, 1490-1494.
88. Horlick, G. (1976): Characteristics of Photodiode Arrays for Spectrochemical Measurements. Appl. Spectrosc., **30**, 113-123.
89. Betty, K.R. and G. Gorlick (1978): Correlation Readout System for a Photodiode Array Spectrometer Applied to Inductively Coupled Plasma Emission Spectroscopy. Appl. Spectrosc., **32**, 31-37.
90. Horlick, G. and E.G. Codding (1974): Dye Laser Intra-Cavity Enhanced Absorption Measured Using a Photodiode Array Reading Spectrometer. Anal. Chem., **46**, 133-136.
91. Franklin, M., C. Baber, and S.R. Koirtyohann (1976): Spectral Source Profilling with a Photodiode Array. Spectrochim. Acta, **31B**, 589-597.
92. Ryan, M.A., R.J. Miller, and J.D. Ingle, Jr. (1978): Intensified Diode Array Detector for Molecular Fluorescence and Chemiluminescence Measurements. Anal. Chem., **50**, 1772-1777.
93. Mavrodineanu, R. and R.C. Hughes (1968): A Multichannel Spectrometer for Simultaneous Atomic Absorption and Flame Emission Analysis. Appl. Opt., **7**, 1281-1285.
94. Greenfield, S., I.L. Jones, H.M. McGeachin (1975): Automatic Multi-Sample Simul-

taneous Multi-Element Analysis with a H.F. Plasma Torch and Direct Reading Spectrometer. Anal. Chim. Acta, 74, 225-245.
95. High Resolution Monochromator HR 1000 Operation Instructions. Imprex 833, 76, 62+, Jobin Yvon, Longjumeau, France., (1976).
96. Optical Multichannel Analyzer OMA Operating and Service Manual MDL 1205A; 6/75, Princeton Applied Research Corp., Princeton, N.J., (1975).
97. Osten, D.E. (1975): Transient Analysis: The Optical Multichannel Analyzer quantifies the amount of light of different energies coming from a light source. Industrial Res., 82.
98. Umezawa, Y. (1977): Application of TV Camera in Analytical Chemistry. Bunseki, 12, 767-772, (In Japanese).
99. Boumans, P.W.J.M., G.H. van Gool, J.A.J. Jansen (1976): A Computerised Programmable Monochromator for Flexible Multielement Analysis with Special Reference to the Inductively Coupled Plasma. Analyst, **101**, 585-587.
100. Okada, M., H. Kawaguchi, and A. Mizuike (1976): Signal-to-Noise Ratio Improvement in Emission Spectrometry by Repetitive Optical Scanning and Data Processing with Minicomputer. Bunko Kenkyu, **25**, 194-200, (In Japanese).
101. Hieftje, G.M. and R.J. Sydor (1972): Application of Wave-length Modulation Device to Problems Concerning Spectrometer Misalignment. Appl. Spectrosc., **26**, 624.
102. Dean, J.A. in Flame Emission and Atomic Absorption Spectrometry, Vol. 2 – Components and Techniques. J.A. Dean and T.C. Rains, Ed., Marcel Dekker, New York, N.Y. (1971), p. 140.
103. Jackson, K.W., K.M. Aldous, and D.G. Mitchell (1974): Simultaneous Detemination of Trace Wear Metals in Used Lubrication Oils by Atomic Absorption Spectrometry Using a Silicon-Target Vidicon Detector. Appl. Spectrosc., **28**, 569-573.
104. Aldous, K.M., D.G. Mitchell, and K.W. Jackson (1975): Simultaneous Determination of Seven Trace Metals in Potable Water Using a Vidicon Atomic Absorption Spectrometer. Anal. Chem., **47**, 1034-1037.
105. Fricke, F.L., O. Rose, Jr. and J.A. Caruso (1975): Simultaneous Multielement Determination of Trace Metals By Microwave Induced Plasma Coupled to Vidicon Detector: Carbon Cup Sample Introduction. Anal. Chem., **47**, 2018-2020.
106. Fricke, F.L., O. Rose, Jr., and J.A. Caruso (1976): Microwave-Induced Plasma Coupled to a Tantalum-Strip Vaporization Assembly for Trace Element Analysis. Talanta, **23**, 317-320.
107. Chester, T.L., H. Haraguchi, D.O. Knapp, J.D. Messman, and J.D. Winefordner (1976): Use of a SIT Image Detector for Atomic Emission/Fluorescence Spectrometry. Appl. Spectrosc., **30**, 410-414.
108. Busch, K.W., N.G. Howell, and G.H. Morrison (1974): The Vidicon Tube as a Detector for Multielement Flame Spectrometric Analysis. Anal. Chem., **46**, 575-581.
109. Busch, K.W., N.G. Howell, and G.H. Morrison (1974): Elimination of Interference in Flame Spectrometry Using Spectral Stripping. Anal. Chem., **46**, 2074-2079.
110. Busch, K.W., N.G. Howell, and G.H. Morrison (1974): Simultaneous Determination of Electrolytes in Serum Using a Vidicon Flame Spectrometer. Anal. Chem., **46**, 1231-1236.
111. Howell, N.G., J.D. Ganjei, and G.H. Morrison (1976): Internal-Stadardization in Flame Analyses Using a Vidicon Spectrometer. Anal. Chem., **48**, 319-326.
112. Ganjei, J.D., N.G. Howell, J.R. Roth, and G.H. Morrison (1976): Multielement Atomic Spectrometry with a Computerized Vidicon Detector. Anal. Chem., **48**,

505-510.
113. Howell, N.G. and G.H. Morrison (1971): Evaluation of Silicon Vidicon Detector Sensitivity for Atomic Spectrometry. Anal. Chem., **49**, 106-113.
114. Fassel, V.A. (1978): Quantitative Elemental Analyses by Plasma Emission Spectroscopy: Atomic spectra exicted inductively coupled plasma are used for simultaneous multielement analyses. Science, **202**, 183-191.
115. Fujiwara, K., H. Haraguchi, and K. Fuwa (1975): Profiles of the Distribution of Atoms in the Nitrous Oxide-acetylene Flame. Bull. Chem. Soc. Japan, **48**, 857-862.
116. Greenfield, S., H. M. McGeachin, and P.B. Smith (1976): Talanta Review: Plasma Emission Sources in Analytical Spectoscopy—III. Talanta, **23**, 1-14.
117. Robinson, A.L. (1978): Elemental Analysis: Plasmas Revive Emission Spectroscopy. Science, **199**, 1324-1328.
118. Boumans, P.W.J.M. (1979): ICP Inform. Newslett., **5**, 181-
119. Larson, G.F., V.A.. Fassel, R.H. Scott, and R.N. Kniseley (1975): Inductively Coupled Plasma-Optical Emission Analytical Spectrometry. A Study of Some Interelement Effects. Anal. Chem., **47**, 238-243.
120. Kalnicky, D.J., V.A. Fassel, and R.N. Kniseley (1977): Excitation Temperature and Electron Densities Experienced by Analyte Species in Inductively Coupled Plasmas with and without the Presence of an Easily Ionized Element. Appl. Spectrosc., **31**, 137-150.
121. Winge, R.K., V.A. Fassel, R.N. Kniseley, E. DeKalb, and W.J. Haas, Jr. (1977): Determination of Trace Elements in Soft, Hard, and Saline Waters by the Inductively Coupled Plasma, Multi-element Atomic Emission Spectroscopic (ICP-MAES) Technique. Spectrochim. Acta, **32B**, 327-345.
122. Allemand, C.D. (1976): Unwanted Light in the Jarrell-Ash 90-750 AtomComp. ICP Inform. Newslett., **1**, 238-252.
123. Larson, G.F., V.A. Fassel, R.K. Winge, and R.N. Kniseley (1976): Ultratrace Analyses by Optical Emission Spectroscopy: The Stray Light Problem. Appl. Spectrosc., **30**, 384-389.
124. Nicman, T.A. and C.G. Enke (1976): Development and Characterization of a Computer-Controlled Vidicon Spectrometer. Anal. Chem., **48**, 619-624.
125. Milano, M.J., H.L. Pardue, T.E. Cook, R.E. Santini, D.W. Margerum, and J.M.T. Taycheba (1974): Design and Evaluation of a Vidicon Scanning Spectrometer for Molecular Absorption and Atomic Emission Spectrometry. Anal. Chem., **46**, 374-381.
126. Snellman, W., T.C. Rains, K.W. Yee, H.D. Cook, and O. Menis (1970): Flame Emission Spectrometry with Repetitive Optical Scanning in the Derivative Mode. Anal. Chem., **42**, 394.
127. Skogerboe, R,K., P.J. Lamothe, G.J. Bastiaanes, S.J. Freeland, and G.N. Coleman (1976): A Dynamic Background Correction System for Direct Reading Spectrometry. Appl. Spectrosc., **30**, 495-500.
128. Koirtyohann, S.R., E.D. Glass, D.A. Yates, E.J. Hinderberger, and F.E. Lichte (1977): Effect of Modulation Wave Form on the Utility of Emission Background Corrections Obtained with an Oscillating Refractor Plate. Anal. Chem., **49**, 1121-1126.
129. Fassel, V.A., J.M. Katzenberger, and R.C. Winge (1979): Effectiveness of Interference Filters for Reduction of Stray Light Effects in Atomic Emission Spectrometry. Appl. Spectrosc., **33**, 1-5.

130. Hassell, K.D., D.A. Rase, and J. Warren (1979): Reduction of Calcium and Magnesium Stray Light Effects in Inductively Coupled Plasma–Optical Emission Spectroscopy Using Band Rejection Filters. ICP Inform. Newslett., **4**, 343-347.
131. Koirtyohann, S.R. and F.E. Lichte (1978): A Background Reduction Method in Plasma Emission Spectroscopy Using Flame Atomic Absorption. Can. J. Spectrosc., **23**, 98-101.
132. L.A. Stelmack (1976): MDM-Type Bandpass Filters for the UV and Vacuum UV. ICP Inform. Newslett., **1**, 253-256.

コンピュータ制御装置を利用したフレームおよび誘導結合プラズマ分光法による多元素同時分析

古田直紀*

〔第1章〕

現在の環境基準では、各元素の濃度を汚染の尺度とし、それぞれの元素に対して検定操作が定められている。その定められた別々の検定操作通りに、元素を一つ一つ分析してゆくと、かなりの時間と労力を要する。環境中のサンプルを測定する際、一つの元素を感度良く測定することも必要だが、サンプル中に、どのような元素がどれだけ含まれているかを、同一操作で迅速に測定する必要が指摘されてきた。その多元素同時分析に対する要求は、環境分析に限らず、鉱業、地質学、農学、薬学、医学、生態学など多方面の分野から要求されている。また、リンの欠乏により、アルミニウムの毒性が現れたり、カドミニウムの毒性を、亜鉛が無毒化したり、水銀とセレンが共存すると、水銀の毒性を弱めるというように、元素間に相互作用があり、その複合的な汚染が問題になっている現在、1回の同時操作によってできるだけ多くの元素を測定し、その相対的な値を議論することが必要になってきている。

現在、多元素同時分析として、放射化分析、スパーク質量分析、アノードストリッピング電気化学分析、けい光X線分析、分光分析などがある。より簡単な装置で、しかも感度および精度良く、溶液試料の多元素分析ができる方法として、分光分析を選んだ。

光源として、ラジオ波誘導結合プラズマ（RFICP）を用いた。RFICPは、ダイナミックレンジが広く、同一条件で主要元素から微量元素まで同時測定可能であり、不活性なアルゴンガスプラズマ中で、試料を2msの長い時間、5000Kから8000Kという高温で励起させるので、元素間の干渉およびマトリックス効果が少なく、多元素同時分析用光源としてすぐれている。

測定システムとしては、必要ないくつかの波長のみを逐次掃引し、不必要な波長領域を除いて掃引するSeguential Slew Device方式と、カメラのように受光面に達する光を像として捕える面検出 Image Device 方式とを組み合せた。

〔第2章〕

現在、多元素同時分析装置として、必要な元素の数だけ、幾何学的に光電子増倍管を配列する多点検出 Direct Reading 方式が、ルーチン分析用として市販されている。しかし、Direct Reading 方式は高価であるし、測定する波長が固定してしまっているため、融通性に欠ける。そこで、著者は Sequential Slew Scan 方式を用いたコンピュータ制都分光器を開発した。パルスモータで駆動する回折格子をコンピュータ制御して、できるだけ正確に波長設定しようとしたが、機械的誤差のため±0.025nmの誤差は免れなかった。従来、光路中に挿入した石英板を回転させて、その波長設定誤差を補正していたが、著者は、光電子増倍管の代わりに Silicon Intensified Tar-

* 国立公害研究所 計測技術部 〒305 茨城県筑波郡谷田部町小野川16番2

get（ＳＩＴ）面検出器で、分析波長の近傍５nm 波長領域を同時に測定し、石英板による波長補正操作を省き、迅速に逐次掃引できるシステムを開発した。サンプルと蒸留水とが交互にＩＣＰ光源に自動的に導入されるように、オートサンプラーもコンピュータ制御した。ＳＩＴ検出器で測定したスペクトル（サンプル、〔A〕スペクトル：蒸留水、〔B〕スペクトル）は、積算されてOptical Multichannel Analyzer（ＯＭＡ）に記憶され、オシロスコープ上にディスプレイされる。積算が終わると、ディジタル化されたスペクトルは、ミニコンピュータに転送され、データ処理される。分析結果はテレタイプに出力される。ＳＩＴ検出器で得られたスペクトルは、D／A コンバータを経て、ミニコンピュータよりＸＹレコーダに出力できる。また、ディジタル化されたスペクトルは、紙テープや磁気テープに蓄積でき、中央計算機でデータ処理したり、ＸＹプロッタでプロットすることができる。

ソフトウェアは、CALIBRATE、SET、LIST、RUN(A)、RUN(B)、ENDの六つのコマンドからなっている。

CALIBRATE：水銀ペンレイランプの２本の水銀発光線を光電子増倍管で検知して、その間に要したパルス数より、分光器の波長駆動校正を行う。

SET ：元素名、分析波長、使用する標準溶液の濃度、出力の方法、データ取得方法などを指定する。

LIST ：SETしたパラメータを確認する。

RUN(A)：３点検量法。３種類の標準溶液を用いて、最小自乗法により検量線を求める方法で、多数サンプルの１元素につき、より正確に分析する際に使用する。

RUN(B)：２点検量法。１種類の標準溶液と原点を用いて、検量線を求める方法で、多元素をSlew Scan方式で、迅速に分析する際に有力である。

END ：すべての操作終了。

〔第３，４章〕

笑気－アセチレンフレームを光源に用いて、プログラマブル分光器とＳＩＴ検出器との組み合わせを評価した。フレームの場合、元素によってフレームの最適条件が大きく異なるので、測定位置やガスの流量を、元素ごとに変えてやらないと十分な感度が得られなかった。しかし、SIT-OMAシステムの有用性が明らかになったので、さらに感度を向上させるため、フレームの代わりにＩＣＰ光源を用いた。本システムの利点と欠点を列挙する。

（利　　点）

1. ＩＣＰ光源を用いたので、同一条件のもとで、ng／ml レベルの高感度が得られた。検出限界の50倍から100倍の濃度で、変動係数は３％程度であった。

2. Slew Scan方式のプログラマブル分光器は、Direct Reading方式よりも融通性がある。

3. ＳＩＴ面検出器を用いて、５nm の波長領域が同時に測定できるので、光電子増倍管の場合のような正確な波長設定が必要ない。そこで、迅速に逐次掃引ができ、５分から10分で10元素が定量できる。

4. ５nm の波長領域に、数元素の分析線が観測されるので、多元素同時分析が可能である。

5. ＩＣＰ光源自身のバックグラウンド補正が可能であり、バックグラウンド補正した［A−B］スペクトルを用いると分析操作が容易になる。

6. ［A−B］スペクトルを用いて、さらにサイドバックグラウンドを差し引くことにより、サンプル中の主要成分による、バックグラウンドの変動を補正することができる。

（欠　点）

1. Sequential Slew Scan 方式は、多元素分析するのに、Direct Reading 方式よりも長い時間を要する。

2. ＳＩＴ検出器の、紫外領域の光に対する量子効率が、光電子増倍管に比べ悪い。

3. ＳＩＴ検出器の分解能は、出口スリットを用いた光電子増倍管に比べ悪い。

Multielement analysis studies by flame and inductively coupled plasma spectroscopy utilizing computer-controlled instrumentation

Naoki FURUTA

RESEARCH REPORT FROM
THE NATIONAL INSTITUTE FOR ENVIRONMENTAL STUDIES
No. 12
国立公害研究所研究報告　第12号
(R—12—'80)

昭和55年3月31日発行

編集・発行　国立公害研究所
茨城県筑波郡谷田部町小野川16番2

印　刷　日青工業株式会社
東京都港区西新橋2-5-10

Published by the National Institute for Environmental Studies
Yatabe-machi, Tsukuba, Ibaraki 305, Japan.
March, 1980